

# A Model of Turbulence in Magnetized Plasmas: Implications for the Dissipation Range in the Solar Wind

G. G. Howes,<sup>1</sup> S. C. Cowley,<sup>2, 5</sup> W. Dorland,<sup>3</sup> G. W. Hammett,<sup>4</sup> E. Quataert,<sup>1</sup> and A. A. Schekochihin<sup>5</sup>

**Abstract.** This paper studies the turbulent cascade of magnetic energy in weakly collisional magnetized plasmas. A cascade model is presented, based on the assumptions of local nonlinear energy transfer in wavenumber space, critical balance between linear propagation and nonlinear interaction times, and the applicability of linear dissipation rates for the nonlinearly turbulent plasma. The model follows the nonlinear cascade of energy from the driving scale in the MHD regime, through the transition at the ion Larmor radius into the kinetic Alfvén wave regime, in which the turbulence is dissipated by kinetic processes. The turbulent fluctuations remain at frequencies below the ion cyclotron frequency due to the strong anisotropy of the turbulent fluctuations,  $k_{\parallel} \ll k_{\perp}$  (implied by critical balance). In this limit, the turbulence is optimally described by gyrokinetics; it is shown that the gyrokinetic approximation is well satisfied for typical slow solar wind parameters. Wave phase velocity measurements are consistent with a kinetic Alfvén wave cascade and *not* the onset of ion cyclotron damping. The conditions under which the gyrokinetic cascade reaches the ion cyclotron frequency are established. Cascade model solutions imply that collisionless damping provides a natural explanation for the observed range of spectral indices in the dissipation range of the solar wind. The dissipation range spectrum is predicted to be an exponential fall off; the power-law behavior apparent in observations may be an artifact of limited instrumental sensitivity. The cascade model is motivated by a programme of gyrokinetic simulations of turbulence and particle heating in the solar wind.

## 1. Introduction

In the study of turbulence in magnetized plasmas, the solar wind provides a unique opportunity to characterize the nature of turbulent plasmas by making detailed dynamical measurements through *in situ* satellite observations. But using the solar wind as a turbulence laboratory is complicated by the fact that the solar wind is only weakly collisional, so a kinetic description is necessary [Marsch, 1991; Marsch, 2006]. A useful first step in connecting theoretical ideas to observational data over the range from the large energy-containing scales of the turbulence to the small scales where the turbulence is dissipated is to have a simple model combining our understanding of magnetized turbulence at both fluid and kinetic scales. This paper presents such a model.

This paper follows Howes *et al.* [2006] and Schekochihin *et al.* [2007] as part of a program to study kinetic turbulence in astrophysical plasmas using nonlinear gyrokinetic simulations. Here we attempt to model the observed magnetic energy spectrum in the solar wind using a minimal number of ingredients—namely, finite Larmor radius effects and

kinetic damping via the Landau resonance. A lengthy evaluation of the applicability of the gyrokinetic approximation to the solar wind plasma is presented along with a discussion of the relevant observational data. The gyrokinetic cascade model yields sensible results when compared to the observational data, but much additional physics exists and may prove to be important; nonlinear simulations will play a critical role in unraveling the complex interactions occurring in the turbulent solar wind.

### 1.1. Turbulence in Magnetized Plasmas

The ubiquity of turbulence in space and astrophysical plasmas—e.g., the solar corona and solar wind, accretion disks around black holes, the interstellar medium—has driven a vast effort to understand and characterize turbulence in a magnetized plasma. Progress in the understanding of magnetohydrodynamic (MHD) turbulence has accelerated steadily over the decades. The pioneering work of Iroshnikov [1963] and Kraichnan [1965] identified two key properties of MHD turbulence: first, even in a magnetized plasma with no mean field, the magnetic field of large-scale fluctuations can behave effectively as a mean field for smaller-scale fluctuations; and second, only oppositely directed Alfvén wave packets interact nonlinearly. They assumed weak nonlinear interactions and an isotropic (with respect to the direction of the mean magnetic field) cascade of energy and derived an energy spectrum that scaled as  $k^{-3/2}$ . Measurements of magnetized turbulence in laboratory plasmas [Robinson and Rusbridge, 1971; Zweibel *et al.*, 1979; Montgomery and Turner, 1981] and in the solar wind [Belcher and Davis, 1971] as well as the results of numerical simulations [Shebalin *et al.*, 1983; Oughton *et al.*, 1994] brought attention to the anisotropy inherent in MHD turbulence in the presence of a mean field and inspired the early anisotropic theories of MHD turbulence [Montgomery

<sup>1</sup>Department of Astronomy, University of California, Berkeley, CA, USA.

<sup>2</sup>Department of Physics and Astronomy, UCLA, Los Angeles, CA, USA.

<sup>3</sup>Department of Physics, IREAP, and Center for Scientific Computing and Mathematical Modeling, University of Maryland, College Park, MD, USA.

<sup>4</sup>Princeton Plasma Physics Laboratory, Princeton, NJ, USA.

<sup>5</sup>Department of Physics, Imperial College, London, UK

and Turner, 1981; Montgomery, 1982; Shebalin et al., 1983; Higdon, 1984]. Based on these ideas, Sridhar and Goldreich [1994] constructed a perturbative theory of weak MHD turbulence in which energy cascades only to higher perpendicular wavenumbers; but their neglect of the  $k_{\parallel} = 0$  modes in resonant three-wave couplings provoked criticisms [Montgomery and Matthaeus, 1995; Ng and Bhattacharjee, 1996], and in response refined theories of weak MHD turbulence emerged [Goldreich and Sridhar, 1997; Ng and Bhattacharjee, 1997; Galtier et al., 2000; Lithwick and Goldreich, 2003].

The anisotropic nature of weak turbulence implies that it generates fluctuations that become increasingly strong as the cascade proceeds to higher perpendicular wavenumber; combining this concept with the ideas of Higdon [1984], Goldreich and Sridhar [1995] proposed that a state of strong turbulence is eventually reached that maintains a *critical balance* between the (parallel) linear propagation and (perpendicular) nonlinear interaction timescales. They proceeded to develop a scaling theory of strong turbulence in incompressible MHD, hereafter referred to as the GS theory. Later studies have examined the effects of compressibility [Lithwick and Goldreich, 2001; Cho and Lazarian, 2003; Vestuto et al., 2003], imbalanced Elsässer fluxes [Maron and Goldreich, 2001; Cho et al., 2002; Lithwick et al., 2007], and a host of other refinements [Oughton et al., 2004; Oughton and Matthaeus, 2005; Zhou and Matthaeus, 2005; Boldyrev, 2005; Shaikh and Zank, 2006].

The GS theory for strong, incompressible MHD turbulence rests on two central assumptions: the locality of interactions in the wavenumber space [Kolmogorov, 1941], and the GS conjecture of critical balance. These imply a one-dimensional kinetic energy spectrum  $E_k(k_{\perp}) \propto k_{\perp}^{-5/3}$  (see § 2.1). Using the consequent scaling for the nonlinear frequency  $\omega_{nl} \simeq k_{\perp} v_{\perp} \propto k_{\perp}^{2/3}$  and equating it with the linear frequency for shear Alfvén waves,  $\omega = \pm k_{\parallel} v_A$  (critical balance), one finds  $k_{\parallel} \propto k_{\perp}^{2/3}$ . Therefore, the fluctuations become more anisotropic at high wavenumbers and the turbulence deep in the inertial range consists of nearly perpendicular modes with  $k_{\perp} \gg k_{\parallel}$ . Numerical simulations of MHD turbulence with a dynamically strong mean field appear to support these conclusions [Cho and Vishniac, 2000; Maron and Goldreich, 2001].

In real astrophysical plasmas, although the large scales at which the turbulence is driven may be adequately described by MHD, the turbulent fluctuations at the small-scale end of the inertial range often have parallel wavelengths smaller than the ion mean free path,  $k_{\parallel} \lambda_{mfp_i} \gg 1$ ; therefore, a kinetic description of the plasma is required to capture the turbulent dynamics (a systematic way to do this is given by Schekochihin et al. [2007]). It is, however, possible to show rigorously that Alfvénic fluctuations are essentially fluid in nature, satisfy the Reduced MHD (RMHD) equations [Strauss, 1976], and remain undamped until their cascade reaches the perpendicular scale of the ion Larmor radius,  $k_{\perp} \rho_i \sim 1$  [Quataert, 1998; Lithwick and Goldreich, 2001; Schekochihin et al., 2007]. In contrast, the compressible MHD fluctuations such as the slow, fast, and entropy modes require a kinetic description even at large scales and are damped both collisionally by parallel ion viscosity [Braginskii, 1965] at scales  $k_{\parallel} \lambda_{mfp_i} \sim 1$  and collisionlessly by the ion Landau damping [Barnes, 1966] at scales  $k_{\parallel} \lambda_{mfp_i} \gg 1$ . The cascade of these modes is not fully understood and they will not be considered here (see Schekochihin et al. [2007] for further discussion).

Some fraction of the energy in Alfvénic fluctuations at  $k_{\perp} \rho_i \sim 1$  is expected to launch a kinetic Alfvén wave cascade to smaller scales [Gruzinov, 1998; Quataert and Gruzinov, 1999]. In the limit of anisotropic fluctuations with  $k_{\parallel} \ll k_{\perp}$ , this cascade, in the wavenumber range  $k_{\perp} \rho_i \gg 1$

and  $k_{\perp} \rho_e \ll 1$ , can again be described in fluid-like terms: the governing system of equations is known as Electron Reduced MHD (ERMHD) [Schekochihin et al., 2007]. In the high-beta limit, it coincides with the anisotropic limit of the better known but nonrigorous fluid model called Electron MHD (EMHD) [Kingsep et al., 1990], where the ions are assumed motionless and the current is carried entirely by the electrons. Assuming locality of interactions and a critical balance between the linear and nonlinear timescales is again a plausible route towards a scaling theory of the kinetic Alfvén wave cascade. The outcome of this argument (explained in more detail in § 2.1) is the one-dimensional magnetic energy spectrum  $E_B(k_{\perp}) \propto k_{\perp}^{-7/3}$  and a predicted wavenumber anisotropy that scales as  $k_{\parallel} \propto k_{\perp}^{1/3}$  [Biskamp et al., 1999; Cho and Lazarian, 2004; Krishan and Mahajan, 2004; Shaikh and Zank, 2005; Schekochihin et al., 2007]. Simulations of EMHD turbulence support these predictions [Biskamp et al., 1999; Cho and Lazarian, 2004; Shaikh and Zank, 2005].

The MHD Alfvén wave and kinetic Alfvén wave cascades correspond to a nonlinear flow of energy to higher wavenumbers across the  $(k_{\perp}, k_{\parallel})$  plane, as illustrated in Figure 1. Imposing critical balance constrains the flow of energy to a one-dimensional path on the plane defined by  $\omega = \omega_{nl}$ , delineated on the figure as a solid line. Critical balance effectively defines a relation between  $k_{\perp}$ ,  $k_{\parallel}$ , and the fluctuation amplitude  $\delta B_{\perp}$ ; for strong turbulence [Goldreich and Sridhar, 1995], choosing values for two of these quantities specifies the third. The freedom in this relation is conveniently parameterized by the wavenumber at which the fluctuations are isotropic,  $k_{\perp} = k_{\parallel} \equiv k_0$ . In Figure 1, adjusting the value of the isotropic wavenumber  $k_0 \rho_i$ , or equivalently adjusting the amplitude of the fluctuations at a given value of  $k_{\perp} \rho_i$ , shifts the curve defining critical balance vertically; in this figure, we have chosen  $k_0 \rho_i = 10^{-4}$ , which is the estimated value for the slow solar wind (see § 3.1). Since most treatments of magnetized turbulence assume an isotropic driving mechanism, we call the parameter  $k_0 \rho_i$  the *isotropic driving wavenumber*.<sup>1</sup> We note here that critical balance,  $\omega = \omega_{nl}$ , is not strictly obeyed in MHD turbulence. Numerical simulations [Cho and Vishniac, 2000; Maron and Goldreich, 2001; Cho et al., 2002; Cho and Lazarian, 2003; Oughton et al., 2004] suggest that the turbulent fluctuation energy does not simply reside along the path specified by critical balance but approximately fills the shaded region in Figure 1, where  $\omega \lesssim \omega_{nl}$ . The one-dimensional cascade model presented in this paper can be thought of as integrating vertically over all  $k_{\parallel}$  at each value of  $k_{\perp}$ , and then treating that energy as if it were concentrated on the path of critical balance.

Although the fluid MHD and EMHD treatments provide important insights into turbulence in magnetized plasmas, modeling accurately the nonlinear dynamics, in particular the collisionless damping of turbulent fluctuations, requires a kinetic treatment. The inherently anisotropic nature of magnetized turbulence lends itself to description by an approximation called gyrokinetics [Rutherford and Frieman, 1968; Taylor and Hastie, 1968; Catto, 1978; Antonsen and Lane, 1980; Catto et al., 1981; Frieman and Chen, 1982; Dubin et al., 1983; Hahm et al., 1988; Brizard, 1992; Howes et al., 2006; Brizard and Hahm, 2007; Schekochihin et al., 2007]. Gyrokinetics is a low-frequency expansion of kinetic theory valid in the limit of frequencies small compared to the ion cyclotron frequency  $\omega \ll \Omega_i$ , ion Larmor radius small compared to the length scale of the equilibrium quantities  $\rho_i \ll L$ , wavevectors of electromagnetic fluctuations nearly perpendicular to the mean magnetic field  $k_{\parallel} \ll k_{\perp}$ , and perturbed fields small compared to the mean field  $\delta \mathbf{B} \ll B_0$ . The gyrokinetic equation is derived by averaging over the particle Larmor motion. This averaging eliminates the fast wave and the cyclotron resonances but retains finite Larmor radius effects and collisionless dissipation via the Landau resonance. The averaging procedure also eliminates one of

the dimensions of velocity in phase space, reducing the dimensionality of the distribution function from 6 to 5, enabling numerical studies of nonlinear gyrokinetic turbulence with current computational resources. The validity of the gyrokinetic description for the solar wind is explored in detail in § 3.

## 1.2. Turbulence in the Solar Wind

One of the principal measurements in the study of solar wind turbulence is the magnetic field fluctuation frequency spectrum derived from *in situ* satellite observations. At 1 AU, the one-dimensional energy spectrum in spacecraft-frame frequency typically shows, for low frequencies, a power law with a slope of  $-5/3$ , suggestive of a Kolmogorov-like inertial range [Goldstein *et al.*, 1995]; a spectral break is typically observed at around 0.4 Hz, with a steeper power law at higher frequencies, often denoted the dissipation range in the literature, with a spectral index that varies from  $-2$  to  $-4$  [Leamon *et al.*, 1998b; Smith *et al.*, 2006]. The general consensus is that the  $-5/3$  portion of the spectrum is the inertial range of an MHD Alfvénic turbulent cascade, but the dynamics responsible for the break and steeper portion of the spectrum is not well understood. Various explanations for the location of the break in the spectrum have been proposed: that it is coincident with the ion (proton) cyclotron frequency in the plasma [Denskat *et al.*, 1983; Goldstein *et al.*, 1994; Leamon *et al.*, 1998b; Gary, 1999], or that the fluctuation length scale (adopting Taylor’s hypothesis to convert from temporal frequency to spatial wavenumber [Taylor, 1938]) has reached either the ion Larmor radius [Leamon *et al.*, 1998a, 1999] or the ion inertial length [Leamon *et al.*, 2000; Smith *et al.*, 2001]. The steepening of the spectrum at higher wavenumbers has been attributed to ion cyclotron damping [Coleman, 1968; Denskat *et al.*, 1983; Goldstein *et al.*, 1994; Leamon *et al.*, 1998b; Gary, 1999], Landau damping of kinetic Alfvén waves [Leamon *et al.*, 1998a, 1999; Leamon *et al.*, 2000], or the dispersive nature of whistler waves [Stawicki *et al.*, 2001; Krishan and Mahajan, 2004; Galtier, 2006].

The energy in turbulent fluctuations in the solar wind is not distributed isotropically over wavevector space; Matthaeus *et al.* [1990] demonstrated that, at wavenumbers  $k_{\perp}\rho_i \sim 10^{-3}$ , the distribution of energy is anisotropic with respect to the direction of the mean magnetic field, creating a “Maltese cross” pattern on a contour plot of the magnetic field two-dimensional correlation function. This observation has prompted attempts to quantify the amount of energy split between nearly parallel modes (“slab” modes) and nearly perpendicular modes (“quasi-2-D” modes) [Bieber *et al.*, 1996; Leamon *et al.*, 1998b]; results show that 85–90% of the power resides in the nearly perpendicular modes. Rather than an anisotropic MHD turbulent cascade, Ruderman *et al.* [1999] propose that phase mixing could be responsible for the generation of perpendicular modes. It was recently found that the two components of the MHD-scale fluctuations evident in the Maltese cross inhabit separate environments; Dasso *et al.* [2005] decomposed the Maltese cross into dominantly perpendicular modes within the slow wind and dominantly parallel modes within the fast wind. It is thus crucial to distinguish observations in the slow solar wind from those in the fast.

This is not the only difference between the fast and slow solar wind that serves as a warning that the dynamics underlying the turbulence in each system may be distinct. The fast and slow components of the wind appear to arise from different coronal origins: the steady fast wind originates from funnels of open fields lines in coronal holes [Tu *et al.*, 2005], whereas the unsteady slow wind appears to come from temporarily open streamers and from active regions of closed

magnetic fields [Habbal *et al.*, 1997; Woo *et al.*, 2004; Woo and Habbal, 2005]. The imbalance between anti-sunward and sunward Elsässer spectra can reach nearly two orders of magnitude in the fast wind, while the slow wind has a much smaller imbalance, from a factor of a few to approximate equality [Grappin *et al.*, 1990; Tu *et al.*, 1990]. A detailed study of the electron and ion (proton) temperatures in the solar wind by Newbury *et al.* [1998] revealed a nearly constant mean electron temperature while the mean ion temperature increased monotonically with the solar wind speed. In addition, the sense of the ion temperature anisotropies differ, with  $T_{i\parallel} < T_{i\perp}$  in the fast wind and  $T_{i\parallel} > T_{i\perp}$  in the slow [Kasper *et al.*, 2002; Marsch, 2006]. Horbury [1999] and Marsch [1999] provide reviews of other salient differences between the fast and slow solar wind.

In this paper, we take heed of the warning by Tu and Marsch [1995] of the dangers of averaging measurements over a long time period because of the possibility of mixing systems with different properties. A variation in parameters such as the ion plasma beta  $\beta_i$  and the temperature ratio  $T_i/T_e$  can have a strong effect on the kinetic dynamics of the solar wind, and an imbalance of the sunward and anti-sunward wave fluxes may strongly affect the nonlinear turbulent transfer of energy, so the fast streams of solar wind may evolve quite differently from the slow streams. To provide a concrete example of the effect on kinetic dynamics, we have calculated the kinetic damping of linear waves with  $k_{\perp}\rho_i = 1$  using the gyrokinetic<sup>2</sup> linear collisionless dispersion relation [Howes *et al.*, 2006] over the measured range of temperature ratios  $T_i/T_e$  [Newbury *et al.*, 1998] and ion plasma beta  $\beta_i$  [Leamon *et al.*, 1998b] (note, however, that the  $\beta_i$  range in this paper was not sorted by solar wind speed). Figure 2 presents a contour plot of  $\log(\gamma/\omega)$  on the  $(\beta_i, T_i/T_e)$  plane, where  $\omega$  is the linear frequency and  $\gamma$  the linear damping rate. Marked on this plot are the parameter ranges of the slow (solid shading) and fast (dashed shading) solar wind. Immediately evident is that the Landau damping<sup>3</sup> is significantly stronger in the slow solar wind. It is also clear from Figure 2 that the damping rate varies non-trivially with both ion plasma beta  $\beta_i$  and temperature ratio  $T_i/T_e$ .

## 1.3. Forward Modeling

The complexity of Figure 2 underscores the challenge of unraveling the underlying physical mechanisms at work in the turbulent solar wind from a statistical ensemble of measurements taken over a wide range of the key parameters: the solar wind speed  $V_{sw}$ , ion plasma beta  $\beta_i$ , and temperature ratio  $T_i/T_e$ . Unless two of these parameters can be held fixed while the third is varied—and imposing such a constraint would yield a very small number of selected measurements—extracting meaningful correlations from statistical analyses of data is very difficult. Compounding this difficulty is the fact that—although current and planned missions, such as Cluster, are able to provide simultaneous measurements of the solar wind in multiple spatial locations—most of our knowledge of the nature of turbulence in the solar wind has been gleaned through data streams of single-point measurements in time [Fredricks and Coroniti, 1976; Bruno and Carbone, 2005]. To interpret the data in an attempt to discern the underlying dynamics of the solar wind, a wide range of approaches have been employed, many of which rest upon reasonable but unproven assumptions. The various approaches to interpreting data range from studies of the intrinsic variations of the solar wind parameters as well as their evolution with heliocentric distance, to detailed examination of the characteristics of fluctuation frequency spectra and the anisotropic transfer of energy in wavevector space, to analysis of the fluctuations as linear eigenmodes of the plasma, to indirect investigation of turbulent dissipation through thermodynamic measurements.

Several recent reviews [Tu and Marsch, 1995; Bruno and Carbone, 2005; Marsch, 2006] cover the enormous breadth of knowledge that has been gained through these methods over decades of study. All of these methods fall under the guise of reverse modeling—analyzing observational data in an attempt to divine the underlying mechanisms governing the evolution of turbulence in the solar wind.

Even with the wide reaching characterization of the solar wind that the above methods have achieved, the mechanisms responsible for the ubiquitous break in the magnetic frequency spectrum between the inertial and dissipation ranges or for the varying spectral index in the dissipation range have still not been unequivocally identified [Smith et al., 2006]. Magnetized turbulence and kinetic plasma physics, as well as the starkly contrasting behavior of the fast versus the slow wind, contribute to the overwhelming complexity of the solar wind, making progress through reverse modeling techniques difficult. In light of recent advances in the general understanding of turbulence in magnetized plasmas and of the steady gains in computational resources, this paper pursues the complementary approach of forward modeling [Oughton and Matthaeus, 2005].

A forward modeling approach has been fruitfully employed to study the spatial transport and spectral evolution of large-scale, low-frequency MHD fluctuations in the solar wind [Tu et al., 1984; Tu, 1988; Zhou and Matthaeus, 1990a]; see the review by Tu and Marsch [1995] for an extensive discussion of this well developed field. In addition, the quest to understand MHD turbulence has been spearheaded by forward modeling through detailed numerical simulations [Shebalin et al., 1983; Matthaeus et al., 1996, 1998; Cho and Vishniac, 2000; Müller and Biskamp, 2000; Biskamp and Müller, 2000; Maron and Goldreich, 2001; Cho et al., 2002; Cho and Lazarian, 2003; Vestuto et al., 2003; Oughton et al., 2004; Shaikh and Zank, 2006]. To better understand the turbulent dynamics of the solar wind at frequencies in the neighborhood of the observed break in the magnetic energy spectrum, a kinetic treatment is essential [Marsch, 2006; Schekochihin et al., 2007]. Yet the complexity of this transition regime also affords the opportunity to better constrain the underlying physical mechanisms. Forward modeling through numerical simulation of weakly collisional turbulent plasmas at this transition has just become possible with current computational resources and codes based on gyrokinetic theory. The gyrokinetic framework opens up the opportunity to study not only the dynamics of the turbulence but also its dissipation and the consequent particle heating. We believe that, through detailed nonlinear gyrokinetic simulations of the turbulent cascade of energy through this regime, the mechanisms responsible for the break in the magnetic energy spectrum and for the damping of turbulent fluctuations and particle heating will at last be identified.

To facilitate contact between gyrokinetic numerical simulations, necessarily of limited dynamic range, and the wealth of observational data, we construct a turbulent cascade model. The model combines the heuristic theories of strong turbulence in the MHD Alfvén and kinetic Alfvén wave regimes with the precise predictions of linear wave damping. Although this simple model can account for a number of observations in the turbulent solar wind, we emphasize the importance of nonlinear numerical simulations both in justifying the assumptions made by the model and in enabling detailed comparison to measurements that go beyond its scope.

#### 1.4. Outline of the Paper

In § 2, we first review the theory of critically balanced, magnetized turbulence both in the MHD and kinetic Alfvén wave regimes, constructing an analytical model that

smoothly connects these regimes (§ 2.1). We then proceed to use the model to construct magnetic energy spectra consistent with those observed in the solar wind and to argue that the combination of instrumental effects and linear damping may be sufficient to explain a wide spread in the observed spectral indices in the dissipation range. The validity of gyrokinetics in describing turbulence in the balanced, slow solar wind, the effective driving scale, the degree of anisotropy, evidence of a kinetic Alfvén wave cascade from satellite measurements and the (un)importance of the ion cyclotron resonance are discussed in § 3. The limitations of our approach and related previous work are discussed in § 4. Finally, § 5 summarizes our findings, paving the path for nonlinear gyrokinetic simulations of turbulence in the slow solar wind.

## 2. Magnetic Energy Spectra in the Slow Solar Wind

Here we construct a model that follows the nonlinear transfer of energy from the low driving wavenumber, through the inertial range of the critically balanced MHD Alfvén wave cascade ( $k_{\perp}\rho_i \ll 1$ ), connecting to a critically balanced kinetic Alfvén wave cascade ( $k_{\perp}\rho_i \gg 1$ ), and on to the highest wavenumbers where the turbulent energy is dissipated. To extend the cascade into the kinetic Alfvén wave regime, we choose to follow the magnetic energy rather than the kinetic energy of the turbulent fluctuations because, as the ions decouple from the field fluctuations at scales below the ion Larmor radius, their kinetic energy becomes subdominant. The model assumes that the Alfvén wave energy fluxes along the magnetic field in either direction are balanced; this condition, not generally satisfied in the fast solar wind, is satisfied in at least some intervals of the slow solar wind [Grappin et al., 1990; Tu et al., 1990]. Having set up our model in § 2.1, we solve it numerically and present the resulting spectra in § 2.2–§ 2.5. In this section, we will assume that  $\omega \ll \Omega_i$  and that gyrokinetic theory applies. This assumption will be investigated in detail in § 3, and the limitations of our model are discussed in § 4.

### 2.1. Critically Balanced Turbulence and the Turbulent Cascade Model

Consider a homogeneous magnetized plasma permeated by a mean magnetic field of magnitude  $B_0$  and driven isotropically at an outer scale wavenumber  $k_0$  with velocity  $v_0$ . We assume that both the driving scale and the ion mean free path along the magnetic field are much larger than the ion Larmor radius,  $k_0\rho_i \ll 1$  and  $\lambda_{mfp_i} \gg \rho_i$ .

Following Kolmogorov, we adopt the standard assumption that the flux of turbulent energy (per unit mass and volume) at a given scale is entirely determined by the turbulence at that scale (*locality of interactions*). Note that we make this assumption at *all* scales. We write the energy cascade rate as

$$\epsilon(k_{\perp}) = C_1^{-3/2} k_{\perp} v_k b_k^2. \quad (1)$$

The magnetic field fluctuation is written in velocity units,  $b_k^2 \equiv \delta B_{\perp}^2(k_{\perp})/4\pi n_i m_i$ , where  $\delta B_{\perp}^2(k_{\perp})/8\pi$  is the energy density of the magnetic field fluctuations perpendicular to the mean field integrated over all possible values of  $k_{\parallel}$ . The electron fluid velocity perpendicular to the mean magnetic field is  $v_k \equiv v_{\perp}(k_{\perp})$ , which is equal to the ion velocity in the MHD limit,  $k_{\perp}\rho_i \ll 1$ . All other symbols are defined in Table 1. In principle the dimensionless “Kolmogorov constant”  $C_1$  is a function of all “local” dimensionless numbers—*i.e.*  $T_i/T_e$ ,  $\beta_i$ ,  $k_{\perp}\rho_i$ ,  $k_{\parallel}/k_{\perp}$ ,  $\mathbf{v}_k \cdot \mathbf{b}_k / (v_k b_k)$ , and  $\omega / (k_{\perp} v_{\perp})$ , where  $\omega$  is the local linear frequency. In addition to equation (1), we assume that the linear and nonlinear time scales are equal

at all scales. This is the *critical balance* assumption of Goldreich and Sridhar,

$$\omega = \omega_{nl}(k_{\perp}) = C_2 k_{\perp} v_k. \quad (2)$$

With this second assumption, the two constants,  $C_1$  and  $C_2$ , depend on the slightly reduced set of dimensionless numbers:  $T_i/T_e$ ,  $\beta_i$ ,  $k_{\perp}\rho_i$ ,  $k_{\parallel}/k_{\perp}$ , and  $\mathbf{v}_{\mathbf{k}} \cdot \mathbf{b}_{\mathbf{k}}/(v_k b_k)$ . The critical balance assumption leads, as we have already explained, to the scale dependent anisotropy,  $k_{\parallel} \sim k_{\parallel}(k_{\perp}) \ll k_{\perp}$ . To make further progress we must use the dynamical equations. These are reduced MHD (RMHD) in the Alfvén wave scale range ( $k_{\perp}\rho_i \ll 1$ ) and electron reduced MHD (ERMHD) in the kinetic Alfvén wave range ( $k_{\perp}\rho_i \gg 1$ )—see *Schekochihin et al.* [2007] for a systematic derivation of both sets of equations. Linear theory in both scale ranges relates the magnetic field and the velocity via

$$v_k = \pm \alpha(k_{\perp}) b_k, \quad (3)$$

where the  $\pm$  refers to the direction of wave propagation along  $\mathbf{B}$  and

$$\alpha(k_{\perp}) = \begin{cases} 1, & k_{\perp}\rho_i \ll 1 \\ k_{\perp}\rho_i / \sqrt{\beta_i + 2/(1 + T_e/T_i)}, & k_{\perp}\rho_i \gg 1 \end{cases} \quad (4)$$

We shall assume, in the spirit of the critical balance assumption, that equation (3) holds in the nonlinear cascade. Similarly, the linear frequency in gyrokinetic theory is given by [*Howes et al.*, 2006]

$$\omega = \pm \bar{\omega}(k_{\perp}) k_{\parallel} v_A. \quad (5)$$

where  $\bar{\omega}(k_{\perp}) = \alpha(k_{\perp})$  in both asymptotic ranges  $k_{\perp}\rho_i \ll 1$  and  $k_{\perp}\rho_i \gg 1$  but not in the transition region  $k_{\perp}\rho_i \sim 1$ . The scale invariance of the RMHD and ERMHD equations in their respective scale ranges suggests that  $C_1$  and  $C_2$  are independent of  $k_{\perp}\rho_i$  and  $k_{\parallel}/k_{\perp}$  within each scale range.

The turbulent energy is converted to heat via wave-particle interactions and collisions. In the linear regime, this is manifested as a damping rate, given in the gyrokinetic limit by

$$\gamma = \bar{\gamma}(k_{\perp}) k_{\parallel} v_A. \quad (6)$$

We will assume that the turbulent heating rate per unit mass at each wavenumber  $k_{\perp}$  is  $2\gamma b_k^2$ —in other words, that the linear result persists in the nonlinear regime. This allows us to write a one-dimensional continuity equation for the magnetic energy spectrum in perpendicular wavenumber space, analogous to the standard simplest spectral evolution model used to describe isotropic hydrodynamic turbulence [*Batchelor*, 1953],

$$\frac{\partial b_k^2}{\partial t} = -k_{\perp} \frac{\partial \epsilon(k_{\perp})}{\partial k_{\perp}} + S(k_{\perp}) - 2\gamma b_k^2, \quad (7)$$

where the rate of change of magnetic energy at a given perpendicular wavenumber is given by the three terms on the right-hand side: from left to right they are the flux of energy in wavenumber space, a source term representing the driving of the turbulence (at a low wavenumber  $k_0$ ), and a damping term associated with the linear damping rate at a given perpendicular wavenumber. In steady state, we write

$$k_{\perp} \frac{\partial \epsilon(k_{\perp})}{\partial k_{\perp}} = S(k_{\perp}) - 2C_1^{3/2} C_2 \frac{\bar{\gamma}(k_{\perp})}{\bar{\omega}(k_{\perp})} \epsilon, \quad (8)$$

where we have used equations (1), (2), (5) and (6) to rewrite the damping term. Note that because of dissipation the en-

ergy cascade rate  $\epsilon$  is not constant but depends on  $k_{\perp}$ . Calculating  $\bar{\gamma}(k_{\perp})/\bar{\omega}(k_{\perp})$  from linear gyrokinetic theory [*Howes et al.*, 2006] yields the *gyrokinetic cascade model*. Equation (8) can be integrated if we assume a form for the functions  $C_1$  and  $C_2$ . Assuming the source  $S(k_{\perp})$  is localized at  $k_0$  we have, for  $k_{\perp} > k_0$ ,

$$\epsilon(k_{\perp}) = \epsilon_0 \exp \left\{ - \int_{k_0}^{k_{\perp}} 2C_1^{3/2} C_2 \frac{\bar{\gamma}(k'_{\perp})}{\bar{\omega}(k'_{\perp})} \frac{dk'_{\perp}}{k'_{\perp}} \right\}, \quad (9)$$

where  $\epsilon_0$  is the rate of energy input at  $k_0$ .

Using equations (1) and (3), we obtain the one-dimensional magnetic energy spectrum

$$E_B(k_{\perp}) = \frac{b_k^2}{k_{\perp}} = C_1 \epsilon^{2/3} k_{\perp}^{-5/3} \alpha^{-2/3}. \quad (10)$$

where  $\epsilon$  is obtained from evaluating equation (9). If dissipation were neglected, the energy cascade rate would be constant  $\epsilon = \epsilon_0$  and equations (4) and (10) would lead to the familiar relations:  $E_B(k_{\perp}) = C_1 \epsilon_0^{2/3} k_{\perp}^{-5/3}$  in the MHD Alfvén wave regime and  $E_B(k_{\perp}) = C_1 \epsilon_0^{2/3} k_{\perp}^{-7/3} \rho_i^{-2/3} [\beta_i + 2/(1 + T_e/T_i)]^{1/3}$  in the kinetic Alfvén wave regime. We will assume (as before) isotropic driving at wavenumber  $k_0$ . Thus assuming equations (1), (2), (3), and (5) hold up to the driving scale, where  $k_{\parallel} = k_{\perp} = k_0$  and  $k_0\rho_i \ll 1$ , we obtain  $\epsilon_0 = C_1^{-3/2} C_2^{-3} k_0 v_A^3$ .

Equations (1), (2), (3), and (5) yield the typical parallel wavelength at scale  $k_{\perp}$ ,

$$k_{\parallel}(k_{\perp}) = k_{\perp}^{2/3} k_0^{1/3} \frac{\alpha^{2/3}}{\bar{\omega}} \left( \frac{\epsilon}{\epsilon_0} \right)^{1/3}, \quad (11)$$

where  $\epsilon$  is given by equation (9). Note that the normalized frequency is defined by equation (5) and is calculated from gyrokinetics. It is sufficient, given the brutality of our assumptions, to make the approximation  $\alpha(k_{\perp}) = \bar{\omega}(k_{\perp})$  throughout the scale ranges. Again, if dissipation were neglected,  $\epsilon = \epsilon_0$  and equations (4) and (11) would lead to the familiar relations quoted in the introduction:  $k_{\parallel} = k_0^{1/3} k_{\perp}^{2/3}$  in the MHD Alfvén wave regime and  $k_{\parallel} = k_0^{1/3} k_{\perp}^{1/3} \rho_i^{-1/3} [\beta_i + 2/(1 + T_e/T_i)]^{1/6}$  in the kinetic Alfvén wave regime.

(Gyro)kinetic theory enters the model we have constructed via the computation of the linear frequency  $\bar{\omega}(k_{\perp})$  (assuming also  $\alpha = \bar{\omega}$ ) in equations (10) and (11) and also the linear damping rate  $\bar{\gamma}(k_{\perp})$  in equation (9). The undetermined Kolmogorov constants  $C_1$  and  $C_2$  represent a considerable source of uncertainty, especially because they may depend on the plasma parameters  $\beta_i$  and  $T_i/T_e$  and, around  $k_{\perp}\rho_i \sim 1$ , also on  $k_{\perp}$ . While acknowledging this uncertainty, we believe it is useful to look at the implications of our model with some fiducial values of the constants. We note that  $C_1$  simply normalizes the spectrum, so we only need to specify the product  $C_1^{3/2} C_2$  in equation (9), which parameterizes the overall strength of the collisionless damping. We use the value  $C_1^{3/2} C_2 = 6$ , which was originally inspired by the values of the constants measured in MHD simulations of the Alfvén wave regime ( $C_1 \simeq 2.5$  and  $C_2 \simeq 1.4$  [*Maron*, 1998]; these values were used also in *Quataert and Gruzinov* [1999]). Without similar numerical guidance in the kinetic regime, we take the constants to be the same at all scales. While this guess is expedient it is obviously not entirely satisfactory. Nonetheless, we evaluate equation (9) for  $\epsilon(k_{\perp})$  (numerically) with these assumptions. We will study the sensitivity of our results to the values of  $C_1$  and  $C_2$  in § 2.5. The values of these constants will ultimately be determined by future gyrokinetic simulations.

## 2.2. A Typical Magnetic Energy Spectrum

Let us now present steady-state magnetic fluctuation energy spectra from the numerical solution of the gyrokinetic cascade model constructed in § 2.1. All spectra are normalized such that the spectrum value is 1 at  $k_{\perp} = k_{\perp i} \ll \rho_i^{-1}$ , the lowest plotted perpendicular wavenumber. Thus, we plot

$$\hat{E}_B(k_{\perp}) = E_B(k_{\perp})/E_B(k_{\perp i}) \quad (12)$$

where  $E_B(k_{\perp i}) = (k_0/k_{\perp i})^{2/3} v_A^2/k_{\perp i} C_2^2$ . Note that, given the assumption  $\omega \ll \Omega_i$ , the solution to the model of § 2.1 is formally independent of the value of the driving wavenumber  $k_0\rho_i$ ; this parameter only affects the overall normalization of the spectra plotted here.

In Figure 3 we plot the normalized one-dimensional magnetic fluctuation energy spectrum,  $\hat{E}_B(k_{\perp})$ , as a function of wavenumber  $k_{\perp}\rho_i$  for a plasma with ion plasma beta  $\beta_i = 1$  and temperature ratio  $T_i/T_e = 1$ . A plasma of protons and electrons is assumed for all the steady-state spectra presented in this paper. Two cases are shown: the solution of the gyrokinetic cascade model of § 2.1 using the appropriate gyrokinetic damping rate  $\bar{\gamma}(k_{\perp})$ , and, for comparison, an undamped case with the damping term artificially set to zero,  $\bar{\gamma}(k_{\perp}) = 0$ . The undamped model recovers the spectral indices of  $-5/3$  in the MHD regime and  $-7/3$  in the kinetic Alfvén wave regime, as predicted by the arguments neglecting dissipation in § 2.1. The damping at  $k_{\perp}\rho_i \gtrsim 1$  in the gyrokinetic model is sufficient to cause the spectrum to fall off more steeply than the undamped prediction of  $-7/3$ . The steady-state gyrokinetic spectrum obtained here clearly demonstrates the exponential roll-off characteristic of dissipation [Li *et al.*, 2001].

### 2.3. Effect of Limited Magnetometer Sensitivity

The magnetic fluctuation spectrum at frequencies above the spectral break from *in situ* solar wind measurements is widely interpreted to behave like a power law rather than an exponential decay. We suggest here that the power-law appearance of the spectrum in this range may be an instrumental effect. The power spectrum of magnetic fluctuations from satellite measurements is limited by the fluxgate magnetometer sensitivity; this sensitivity limit can, e.g., be clearly seen in Figure 6 of Leamon *et al.* [1998b] at the high frequency end of the spectrum. The noise floor of a fluxgate magnetometer at frequencies  $f > 1$  Hz is constant in units of nT/ $\sqrt{\text{Hz}}$  [Bale, 2007]; hence, on a plot of the one-dimensional magnetic energy spectrum, this corresponds to a constant noise floor at the high frequency end.

To test the effect of the fluxgate magnetometer noise floor on the appearance of the magnetic fluctuation spectrum from our gyrokinetic cascade model, we mock up the instrumental noise by specifying a constant background value to the one-dimensional energy spectrum. Inspired by the spectra in Figure 6 of Leamon *et al.* [1998b], we choose this noise floor to be approximately two to three orders of magnitude below the spectrum value at the  $k_{\perp}\rho_i = 1$  break. In Figure 4 we plot the spectra for three steady-state solutions of our model with the following parameters, chosen to sample across the range of solar wind parameters depicted in Figure 2: (1)  $\beta_i = 0.5$ ,  $T_i/T_e = 3$ ; (2)  $\beta_i = 3$ ,  $T_i/T_e = 0.6$ ; and (3)  $\beta_i = 0.03$ ,  $T_i/T_e = 0.175$ . All cases include the damping rate calculated gyrokinetically. Panel (a) shows the spectra without the added constant sensitivity limit; panel (b) adds a constant sensitivity level at two (spectrum 1) or three (spectra 2 and 3) orders of magnitude below the spectrum value at  $k_{\perp}\rho_i = 1$ . The behavior of each spectrum in panel (b) in the range  $k_{\perp}\rho_i > 1$  more closely resembles a power law than the exponential roll-off, which would characterize the noiseless spectra; the steady-state solutions are well-fit

by power laws with spectral indices  $-7/3$ ,  $-3$ , and  $-4$ . In summary, the instrumental sensitivity limit may produce spectra that appear to obey a power-law scaling with some effective spectral index even though the underlying spectrum actually has an exponential roll-off.

At present there exists little evidence in the literature to test this prediction. Search coil magnetometers are more sensitive at these high frequencies. Denskat *et al.* [1983] studied the magnetic field power spectra up to 470 Hz using data from both fluxgate and search coil magnetometers. The search coil data shows power-law behavior up to 470 Hz, but the amplitude of the spectral density drops about three orders of magnitude in the gap from the highest frequency fluxgate measurement at 2 Hz to the lowest frequency search coil measurement at 4.7 Hz, suggesting that the higher frequency power law is not a continuation of the lower frequency spectrum. Alternatively, the mismatch may be due to difficulty performing a relative calibration of the instruments, but without an overlap in frequency the difference cannot be resolved. One recent paper [Alexandrova *et al.*, 2008] shows search coil measurements of magnetic field spectra up to 10 Hz, a factor of 20 in frequency above the breakpoint; for the 57-minute interval of the fast solar wind studied, the dissipation range spectrum shows neither an exponential roll-off nor evidence of instrumental noise up to 10 Hz. During one 7-minute interval, the dissipation range index is  $-2.33$ ; during another 7-minute interval, it is  $-2.50$ ; and over the whole 57-minute interval, it is  $-2.6$ . These results are not at odds with our model predictions for weak damping—the dissipation range spectrum is expected to appear as a  $-7/3$  power law to higher frequencies before the damping becomes strong enough to cause the spectrum to roll off exponentially. We must also keep in mind that the fast wind generally does not have a balance of Elsässer energy fluxes, an assumption of the present simple cascade model. An interesting aspect of the measurements in Alexandrova *et al.* [2008] not discussed in their paper is the time variability of the spectral index in the dissipation range. There is a clear need for a detailed study of solar wind turbulence at frequencies above 1 Hz, taking into account the varying plasma parameters, the imbalance in the Elsässer energy fluxes, the sensitivity limits of the various instruments, and the time variability of the dissipation range spectral index.

It is instructive to consider what we will learn if such a study does not find magnetic energy spectra demonstrating a slow, exponential roll-off. The absence of an exponential decay could indicate that using the linear damping rates in a turbulent plasma is incorrect. It is important to emphasize that the predictions of gyrokinetic theory for solar wind turbulence are not equivalent to the predictions of this simple cascade model—nonlinear gyrokinetic simulations of turbulence will play a key role in testing this model, assessing the robustness of the predicted exponential fall-off, and refining the model as necessary.

### 2.4. The Effective Spectral Index in the Dissipation Range

Figure 4 shows that, over the range of the plasma parameters  $\beta_i$  and  $T_i/T_e$  measured in the solar wind, the observed wide spread of the spectral index in the dissipation range from  $-2$  to  $-4$  [Leamon *et al.*, 1998b; Smith *et al.*, 2006] can be explained by the damping of kinetic Alfvén waves via the Landau resonance. If the Landau damping is negligible, the spectral index is expected to be  $-7/3$ , close to the observed upper limit; over the range of parameters relevant to the solar wind, our cascade model gives a lower limit to the (effective) spectral index of about  $-4$ , consistent with observations. The measured effective spectral index for  $k_{\perp}\rho_i > 1$  is a complicated function of the parameters  $\beta_i$ ,  $T_i/T_e$ , and

$k_0\rho_i$  as well as of the sensitivity limit of the magnetometer. If it is indeed the linear damping that explains the wide spread in the measured values, the complexity of this parameter dependence is a natural outcome of the nontrivial behavior of the collisionless damping as a function of  $\beta_i$  and  $T_i/T_e$  over the range of parameters in the slow and fast solar wind depicted in Figure 2. Plots of the measured spectral index versus a single plasma parameter are unlikely to reveal strong correlations due to variation in the other parameters within the data set. To make headway here, a forward modeling approach may prove more fruitful. One needs to incorporate all of the measured parameters to determine the predicted spectral index for an interval of solar wind data.

## 2.5. Uncertainty in the Kolmogorov Constants

The spectrum derived from our cascade model depends on the values of the Kolmogorov constants in the theory. As we noted above, while  $C_1$  merely normalizes the spectrum, the product  $C_1^{3/2}C_2$  affects the competition of the nonlinear transfer of energy with the linear damping [see equation (9)]. If this product is increased (decreased), this effectively makes the linear dissipation stronger (weaker) relative to the nonlinear transfer. These order unity constants must be determined from nonlinear simulations or experimental data. To judge the effect of varying these constants on the steady-state solution, Figure 6 presents the gyrokinetic spectrum for  $\beta_i = 1$  and  $T_i/T_e = 1$ , with this product taken to be  $C_1^{3/2}C_2 = 3, 6$ , and  $12$ . The resulting variation in the effective spectral index is  $+1/3$  or  $-2/3$ , so all of our steady-state spectra suffer this systematic uncertainty. In the rest of this paper we use the fiducial value  $C_1^{3/2}C_2 = 6$ .

## 3. Applicability of Gyrokinetics to the Slow Solar Wind

In this section, we argue that gyrokinetics is applicable to the dynamics of the turbulence in the balanced, slow solar wind at the dissipation scale. Gyrokinetics is *not*, of course, applicable at the driving scale  $L = 2\pi/k_0$ , where the magnetic field fluctuations are of the order of the mean field and are relatively isotropic. Formally, as described in § 1.1, a number of conditions must *all* be met for the gyrokinetic approach to be valid:  $\rho_i \ll L$ ,  $k_{\parallel} \ll k_{\perp}$ ,  $\delta\mathbf{B} \ll B_0$ , and  $\omega \ll \Omega_i$ . Let us consider whether each of these conditions is satisfied in the solar wind. In § 3.1 we estimate the effective driving scale ( $\rho_i \ll L$ ). An estimate of the anisotropy  $k_{\parallel} \ll k_{\perp}$  at the dissipation scale  $k_{\perp}\rho_i \sim 1$  follows in § 3.2. The observed amplitude of the fluctuations  $\delta\mathbf{B} \ll B_0$  is discussed in § 3.3. In § 3.4 we present wave phase velocity evidence from satellite measurements that is consistent with a kinetic Alfvén wave cascade but inconsistent with the onset of ion cyclotron damping—indirect evidence for  $\omega \ll \Omega_i$ . In § 3.5 we show (in some detail) that the turbulent frequencies are usually less than the cyclotron frequency ( $\omega \ll \Omega_i$ ). Finally, in § 3.6, we explain what happens if the cyclotron resonance is reached in the dissipation range.

### 3.1. Turbulence Driving Scale

The nature of the turbulent fluctuations in the dissipation range of the solar wind depends on the driving scale  $L$  at which energy is injected into the turbulent cascade. The anisotropy predicted by the critically balanced Alfvén wave cascade in GS theory is scale dependent, so this raises two questions: is the solar wind driven isotropically or anisotropically, and what is the effective driving scale  $L$ ? Unfortunately, the mechanisms responsible for driving turbulence in the solar wind are unknown; the matter is further complicated by the radial expansion of the solar wind as it travels outward from the sun and the measured imbalance of anti-sunward vs. sunward directed Alfvén wave flux [Grappin

*et al.*, 1990; Tu *et al.*, 1990; Tu and Marsch, 1990]. Nevertheless, we can make some headway on this complex problem if we ignore the specific details of the driving mechanism and the radial expansion and simply estimate the anisotropy of the balanced, slow solar wind turbulence from *in situ* measurements at 1 AU.

As discussed in § 1.1, determining the isotropic driving wavenumber  $k_0\rho_i = 2\pi/L$  fixes the path of the critically balanced cascade as depicted in Figure 1. Equivalently, a measurement of the wavenumber anisotropy at any scale in the solar wind can also be used to fix the critical balance relation; here we use this measurement to estimate the resulting effective value of  $k_0\rho_i$ . From measurements of the anisotropy of the spatial correlation of magnetic field fluctuations in the slow solar wind, presented in the left panel of Figure 1 from Dasso *et al.* [2005], we estimate the anisotropy  $k_{\perp}/k_{\parallel} = r_{\parallel}/r_{\perp} \simeq 1.5$  at an average scale  $2\pi/k_{\perp} = 6 \times 10^{10}$  cm. If we assume that the turbulence is strong at the isotropic driving scale and that the energy cascade rate is a constant  $\epsilon = \epsilon_0$  between the driving and the observed scales (a reasonable assumption given that observed spectra consistently show a spectral index of  $-5/3$  [Smith *et al.*, 2006] and that the damping rate for Alfvén waves is small,  $\gamma \ll \omega$ , at these scales), we can estimate the driving scale from which the observed turbulence arose using equation (11),

$$k_0\rho_i = \left(\frac{k_{\parallel}}{k_{\perp}}\right)^3 k_{\perp}\rho_i. \quad (13)$$

which applies for scales in the MHD Alfvén wave regime  $k_{\perp}\rho_i \ll 1$ . Using a mean ion (proton) temperature for the slow wind  $T_i \simeq 4.5 \times 10^4$  K [Newbury *et al.*, 1998] and the geometric mean of the range of magnetic field magnitude in Leamon *et al.* [1998b] of  $B_0 \simeq 10^{-4}$  G, we obtain the ion Larmor radius  $\rho_i \simeq 3 \times 10^6$  cm. Hence, we find  $k_0\rho_i \simeq 10^{-4}$ , or an isotropic driving scale  $L \simeq 2 \times 10^{11}$  cm.

This value is consistent with the estimate by Matthaeus *et al.* [2005] of the mean magnetic field correlation length in the solar wind (over all solar wind speeds) of  $L \simeq 1.2 \times 10^{11}$  cm. Figure 3 of Tu and Marsch [1990] presents spectra of the outward directed Elsässer flux of Alfvén waves measured by the Helios spacecraft missions which show, for the slow solar wind at 0.9 AU,<sup>4</sup> the beginning of the  $-5/3$  spectrum at a reduced wavenumber  $k/2\pi \simeq 10^{-7}$  km<sup>-1</sup>, corresponding to a driving scale of  $L = 10^{12}$  cm. Finally, an estimate of the correlation length of the anti-sunward Elsässer field at 0.3 AU is  $L = 1.6 \times 10^{11}$  cm [Tu and Marsch, 1995]; scaling this length for radial expansion to 1 AU gives a value of  $L = 5 \times 10^{11}$  cm. These four independent determinations of the driving scale, at which we assume the fluctuations are isotropic, are consistent to within an order of magnitude. This suggests that the driving is at least approximately isotropic and that  $k_0\rho_i = 10^{-4}$  is a good choice for a fiducial value of the isotropic driving wavenumber.

It is perhaps appropriate to discuss why this number is physically sensible. The simplest interpretation of solar wind turbulence is that energy resides in large-scale, energy containing modes driven in the solar corona, and those modes are subsequently left to decay freely in the wind within the inner heliosphere. A reasonable estimate for the decay time of turbulent energy characterized by a velocity  $v_{\perp}$  at scale  $k_{\perp}$  is the eddy turnover time  $\tau \sim (k_{\perp}v_{\perp})^{-1}$ . For the driving scale estimated above,  $L = 2\pi/k_{\perp} = 2 \times 10^{11}$  cm, and a turbulent velocity estimated from the slow solar wind Elsässer spectra in Figure 4 of Grappin *et al.* [1990] of  $v_{\perp} = 2$  km/s, this decay time is  $\tau \sim 50$  h. The travel time for slow solar wind with a velocity  $V_{sw} \sim 350$  km/s to reach  $R = 1$  AU is  $t = R/v_{sw} \sim 10$  h. If there is energy

in much larger scales than our estimated value for  $L$ , those larger scale fluctuations will not have had time to transfer their energy in the nonlinear cascade. On the other hand, energy in modes much smaller than  $L$  in the solar corona would have already cascaded to the dissipation scale and would not be observed at 1 AU. Indeed the near agreement between the estimated turbulent decay time,  $\tau \sim 50$  h, and the travel time of the slow solar wind to 1 AU,  $t \sim 100$  h, is probably not coincidental. It suggests that, within 1 AU, the turbulence in the slow solar wind is freely decaying and that we are seeing the energy injected at the largest scale that can cascade on the travel time.

### 3.2. Anisotropy at the Ion Larmor Radius Scale

Assuming an ion number density in the slow solar wind of  $n_i \simeq 20 \text{ cm}^{-3}$  (Leamon *et al.* [1998b]) and an electron temperature of  $T_e \simeq 1.3 \times 10^5 \text{ K}$  [Newbury *et al.*, 1998], we find the ion plasma beta  $\beta_i \simeq 0.3$  and temperature ratio  $T_i/T_e \simeq 0.35$ ; for these parameters, the normalized frequency from the gyrokinetic dispersion relation at  $k_\perp \rho_i = 1$  is  $\bar{\omega} \simeq 1.45$ . Substituting these values, along with our fiducial isotropic driving wavenumber  $k_0 \rho_i = 10^{-4}$ , into equation (11) and taking for simplicity  $\epsilon = \epsilon_0$ , we obtain the estimate  $k_\parallel/k_\perp \simeq 0.04$  at  $k_\perp \rho_i = 1$ . As will be demonstrated in Figure 8, by neglecting dissipation, this estimate represents an upper limit on the value of  $k_\parallel/k_\perp$ .

### 3.3. Fluctuation Amplitude in the Dissipation Range

One might be concerned that gyrokinetics requires a strong mean magnetic field in order for the gyroaveraging procedure to be valid, and that the solar wind does not contain such a strong mean field. At the driving scale  $L$  of the turbulence in the solar wind, the magnetic field has fluctuations of the same order as the mean field,  $\delta \mathbf{B} \sim B_0$ . However, as was realized by Kraichnan [1965], even in a plasma with no mean magnetic field, the magnetic field of the large-scale fluctuations can serve as an effective mean field for smaller-amplitude fluctuations on smaller scales. Raw magnetometer data, for instance Figure 3-5a of Tu and Marsch [1995] or Figure 1 of Bale *et al.* [2005], show order one fluctuations of the magnetic field vector components, corresponding to large changes in the direction of the mean magnetic field (the magnitude of the field has much smaller fractional fluctuations) on timescales from 15 minutes to 1 hour. On shorter timescales, however, the field direction remains relatively constant with small amplitude, short-timescale fluctuations about the mean. This is in agreement with Kraichnan's hypothesis, showing fluctuations of both small amplitude and scale about a mean magnetic field arising from the larger scale fluctuations—these small fluctuations are precisely those which are well-described by gyrokinetics. Once the cascade has progressed to scales a couple of orders of magnitude smaller than the driving scale, the amplitude of the fluctuations becomes small compared to the local mean field amplitude and the fluctuations become significantly anisotropic,  $\delta \mathbf{B}/B_0 \ll 1$  and  $k_\parallel \ll k_\perp$ . Gyrokinetics then becomes a valid description of the fluctuations, and the deeper one goes into the inertial range, the better it works. From equation (10), taking  $\epsilon = \epsilon_0$ , we have

$$\frac{|\delta \mathbf{B}|_k}{B_0} = \frac{b_k}{v_A} = \frac{1}{C_2} \left( \frac{k_0}{k_\perp} \right)^{1/3} \alpha^{-1/3}. \quad (14)$$

Thus, for our estimated  $k_0$  we have  $\delta \mathbf{B}/B_0 \lesssim 0.03$  for  $k_\perp \rho_i \gtrsim 1$ .

### 3.4. Evidence against the Cyclotron Resonance

There exists evidence from *in situ* satellite measurements consistent with the existence of a kinetic Alfvén wave cas-

cade, at least in some cases. Wave phase velocity information in the region of the spectral break can be used to distinguish the characteristics of the underlying wave modes. Bale *et al.* [2005] have produced the first simultaneous measurements of the fluctuating electric and magnetic fields, demonstrating that the wave phase velocity above the spectral breakpoint increases, as shown in panel (b) of Figure 3 in Bale *et al.* [2005]. Using the Taylor hypothesis to convert the frequency spectrum to a wavenumber spectrum, the spectral breakpoint occurs near the ion Larmor radius,  $k \rho_i \sim 1$ .

Using the full Vlasov-Maxwell linear dispersion relation for a hot collisionless plasma (see Quataert [1998] for a description of the code that we use to solve it), we plot in Figure 7 the normalized wave phase velocity  $\omega/k_\parallel v_A$  vs. the normalized wavenumber  $k \rho_i$ . Plasma parameters are chosen to be  $\beta_i = 1$  and  $T_i/T_e = 1$ . Although in the gyrokinetic theory  $\omega/k_\parallel v_A = \bar{\omega}(k_\perp)$  is a function of  $k_\perp$  alone, in hot plasma theory  $\omega/k_\parallel v_A$  depends also on  $k_\parallel$ . The parallel wavenumber needed for this calculation is determined by using equation (11) with no dissipation,  $\epsilon = \epsilon_0$ . The change in wave phase velocity is plotted for driving scales  $k_0 \rho_i = 10^{-6}$ ,  $10^{-4}$ ,  $10^{-2}$ , and 1. The wave phase velocity increases until the ion cyclotron frequency is reached; then, the frequency asymptotes  $\omega \rightarrow \Omega_i$  as ion cyclotron damping becomes important (see Appendix A), so  $\omega/k_\parallel v_A$  decreases due to the increasing  $k_\parallel(k_\perp)$  [see equation (11)]. The measured wave phase velocity in Figure 3 of Bale *et al.* [2005] does not show this downturn, suggesting that the ion cyclotron damping remains unimportant below the highest wavenumber measured,  $k_\perp \rho_i \simeq 10$ . In the limit  $k_\parallel \ll k_\perp$ , the upturn of the wave phase velocity above the breakpoint in the magnetic fluctuation spectrum is consistent with underlying wave modes consisting of kinetic Alfvén waves with  $\omega \ll \Omega_i$ . We do note, however, that this increase of phase velocity may also be consistent with fast MHD/whistler mode of Vlasov-Maxwell kinetic theory for certain wavevector anisotropies. For either case, though, it appears that the break is not due to the onset of ion cyclotron damping.

### 3.5. Conditions for Reaching the Ion Cyclotron Resonance

Although the Bale *et al.* [2005] measurements of the electric fields in the solar wind are consistent with kinetic Alfvén waves with frequencies  $\omega \ll \Omega_i$ , there is also indirect evidence that fluctuations at or above the cyclotron frequency are present in the solar corona and solar wind. For example, minor ions such as  $\text{O}^{+5}$  are selectively heated to high perpendicular temperatures [Kohl *et al.*, 1997, 1998]. Also, the adiabatic invariant  $\mu \propto T_\perp/B$  for ions and alpha particles is observed to increase with heliocentric distance [Marsch *et al.*, 1983], indicating some mechanism for perpendicular heating of these species, particularly in the fast wind. Since (the collisionless part of) gyrokinetics preserves the adiabatic invariant  $\mu$ , it cannot describe such heating. This heating may come from fast wave fluctuations [Chandran, 2006] or velocity-space instabilities [Scarf *et al.*, 1967; Evitar and Schulz, 1970; Gary *et al.*, 1976; Kasper *et al.*, 2002; Hellinger *et al.*, 2006; Marsch, 2006] rather than the Alfvén wave cascade, but it is nevertheless important to know where in  $(k_\perp, k_\parallel)$  space the turbulent cascade may start to be affected by the cyclotron resonance. In this section we employ the steady-state solutions of the turbulent cascade model presented in § 2 to estimate the perpendicular wavenumber at which the cascade reaches the cyclotron frequency—this is the same wavenumber at which a gyrokinetic treatment fails to be valid.

From equation (5) and equation (11) we obtain

$$\frac{\omega}{\Omega_i} = \frac{k_\parallel \rho_i}{\sqrt{\beta_i}} \bar{\omega}(k_\perp) = (k_\perp \rho_i)^{2/3} (k_0 \rho_i)^{1/3} \frac{\bar{\omega}^{2/3}}{\sqrt{\beta_i}} \left( \frac{\epsilon}{\epsilon_0} \right)^{1/3}, \quad (15)$$

where  $\epsilon/\epsilon_0$  is given by equation (9) and we have assumed  $\alpha = \varpi(k_\perp)$  for all  $k_\perp$ . In Figure 8, we plot  $\omega/\Omega_i$  and  $k_\parallel\rho_i$  for both the undamped and gyrokinetic cascade models with  $\beta_i = 1$ ,  $T_i/T_e = 1$ , and  $k_0\rho_i = 10^{-4}$ . It is unknown if the linear damping rates are a good estimate of the damping of nonlinear turbulent fluctuations, but the undamped model certainly provides upper limits for the frequency and parallel wavenumber. Figure 8 shows that the undamped model reaches the cyclotron frequency at  $k_\perp\rho_i \simeq 12$ , whereas the model using the linear gyrokinetic damping rates never reaches the cyclotron frequency. The plot of  $k_\parallel\rho_i$  vs.  $k_\perp\rho_i$  for the gyrokinetic model in Figure 8 reaches a maximum at  $k_\perp\rho_i \simeq 5$  and then  $k_\parallel\rho_i$  begins decreasing. In this typical case, it is clear that, *if the cyclotron frequency is reached*, it is only after the fluctuations have already cascaded to a high perpendicular wavenumber,  $k_\perp\rho_i \gg 1$ , at which point most of the energy in the cascade has already been dissipated. Consequently, the gyrokinetic treatment will be valid over a large part, if not all, of the dissipation range.

The decrease in  $k_\parallel\rho_i$  seen in the solution of the gyrokinetic model in Figure 8 is likely an unphysical result arising from the imposition of critical balance, a condition requiring that the turbulence remains strong. The kinetic damping of the turbulent fluctuations becomes significant at this point, so the nonlinear frequency begins to fall below the linear frequency. Instead of  $k_\parallel\rho_i$  decreasing, it is more likely that the turbulence becomes weak, a condition not treated within our simple cascade model. The realm of weak turbulence,  $\omega > \omega_{nl}$ , exists above the line of critical balance as depicted in Figure 1. In weak turbulence theory, the cascade to higher parallel wavenumber is suppressed [Goldreich and Sridhar, 1997; Ng and Bhattacharjee, 1997; Galtier et al., 2000; Lithwick and Goldreich, 2003], so a more physical result is that the value of  $k_\parallel\rho_i$  should remain constant, rather than decrease, as the cascade progresses to higher  $k_\perp\rho_i$ . Adjusting the model to prevent the value of  $k_\parallel\rho_i$  from decreasing results in a sharper cutoff in the magnetic energy spectrum at the high wavenumbers where the parallel wavenumber is held constant—this is the result of a decrease in the ratio of the nonlinear transfer frequency to the linear damping rate as the turbulence weakens. The simplicity of our cascade model limits our ability to determine the correct physical behavior in this regime; nonlinear simulations are necessary to determine accurately the behavior of the turbulent cascade as the kinetic damping becomes significant.

Analogous to our gyrokinetic cascade model, we can construct a *hot plasma cascade model* using the frequencies and damping rates from the linear hot plasma dispersion relation [Stix, 1992; Quataert, 1998] instead of the gyrokinetic values. In hot plasma theory, however, the normalized wave frequency  $\omega/(k_\parallel v_A)$  is no longer a function of  $k_\perp$  alone, but depends also on  $k_\parallel$ . Since the linear hot plasma and gyrokinetic theories agree when the gyrokinetic approximation is valid, we will continue to use the solution of the gyrokinetic model to specify the path of the cascade in the  $(k_\perp, k_\parallel)$  plane. This is probably at least qualitatively correct because cyclotron damping does not in fact become large.

To quantify the conditions where the cyclotron resonance terms becomes important we define a threshold value of  $k_\perp$  to be the value along the cascade path at which the solutions of the gyrokinetic and hot plasma dispersion relations diverge by 10%. This threshold is plotted (solid line) in Figure 9 for a range of  $\beta_i$  with parameters  $T_i/T_e = 1$  and  $k_0\rho_i = 10^{-4}$ . We probe the sensitivity of the threshold  $k_\perp$  to our assumptions by plotting the same 10% threshold for the path in the  $(k_\perp, k_\parallel)$  plane calculated from the gyrokinetic model with *no* damping (dashed line). The dotted line is an estimate of this threshold determined by solving the  $k_\perp\rho_i \gg 1$  limit of equation (15) with  $\omega/\Omega_i = 1$  and  $\epsilon = \epsilon_0$  to find

$$k_\perp\rho_i \simeq (k_0\rho_i)^{-1/4} \beta_i^{5/8} \left[ 1 + \frac{2}{\beta_i(1 + T_e/T_i)} \right]^{1/4} \quad (16)$$

(this rough estimate is only plotted over the typical range of  $\beta_i$  in the solar wind near Earth).

The solid line in Figure 9 represents our best estimate of the threshold at which the cyclotron resonance becomes important and the gyrokinetic approximation fails. If the effective damping of the fluctuations in the nonlinear turbulence is less than the linear damping rates, the true threshold will fall within the vertically shaded region. This region is bounded from below by the short-dashed line—our estimate of the threshold with no damping—and represents the most conservative estimate of the limit of applicability of gyrokinetics. Thus, throughout the diagonally shaded region, gyrokinetics is certainly a valid description of the turbulent dynamics in the plasma, and this region covers a substantial part of the parameter range of interest in the study of turbulence in the solar wind.

The cyclotron resonance has a strong effect on the cascade only when it is reached at a relatively low wavenumber,  $k_\perp\rho_i \lesssim 1$ ; otherwise, the cascade is likely to be rather heavily damped before reaching the cyclotron frequency, leaving little energy available for perpendicular heating. Equation (16) provides a rough estimate of how the wavenumber threshold in the undamped case scales with the plasma and system parameters. This *undamped* threshold has little dependence on the temperature ratio  $T_i/T_e$ . Thus, the cyclotron resonance occurs early on in the dissipation range only in plasmas with  $\beta_i \lesssim 0.01$  or when the isotropic driving wavenumber is much larger than our fiducial estimate  $k_0\rho_i \gg 10^{-4}$ .

### 3.6. Effect of the Ion Cyclotron Resonance

Let us now discuss what happens if the cyclotron resonance is reached in the dissipation range ( $k_\perp\rho_i > 1$ ) and before the kinetic Alfvén wave cascade is converted into heat by Landau damping ( $k_\perp\rho_e < 1$ ). The idealized asymptotic version of the appropriate linear theory (the case  $k_\perp\rho_i \gg 1$ ,  $k_\perp\rho_e \ll 1$  at the cyclotron resonance) can be worked out analytically from the general hot plasma dispersion relation—this is done in Appendix A. The key points that this calculation demonstrates are

- the cyclotron effects only matter when the frequency of the fluctuations is very close to one of the resonances: for integer  $n \geq 1$ ,  $(\omega - n\Omega_i)/(|k_\parallel|v_A k_\perp\rho_i) \sim 1/\sqrt{k_\perp\rho_i}$ ;
- away from the resonances, the ions effectively have a Boltzmann response and kinetic Alfvén waves (weakly damped by the electron Landau resonance) exist both below the ion cyclotron frequency ( $\omega < \Omega_i$ ) and between the resonances ( $n\Omega_i < \omega < (n+1)\Omega_i$ );
- at the resonances, there is a conversion between kinetic Alfvén waves and ion Bernstein waves—electrostatic waves whose frequencies are close to  $n\Omega_i$  [cf. Li and Habbal, 2001];
- because  $k_\perp\rho_i \gg 1$ , the ion cyclotron damping is exponentially weak ( $\sim e^{-k_\perp\rho_i}$ ) and very localized in frequency.

These points are illustrated in Figure 10. Together, they imply that the effect of passing through the cyclotron resonance on the kinetic Alfvén wave cascade is unlikely to be drastic: in order to be subjected to even a weak cyclotron damping, the fluctuations have to couple nonlinearly into a rather narrow frequency band around  $\Omega_i$ ; it appears more likely that most of the turbulent energy would leapfrog the resonance altogether and continue as a kinetic Alfvén wave cascade, until converted into heat by electron Landau damping (at  $k_\perp\rho_e \sim 1$ ). However, it is probably prudent to acknowledge that linear calculations such as the one presented in Appendix A may have limited utility in predicting nonlinear behavior.

It is important to understand that the calculation in Appendix A considers an idealized asymptotic solution. It is known that the precise mode conversion and damping properties at the cyclotron resonances depend rather sensitively on the plasma parameters: such behavior at oblique ( $k_{\perp} > k_{\parallel}$ ) propagation was explored in detail by *Li and Habbal* [2001]. To demonstrate some of the non-asymptotic possibilities that may be present in the solar wind, it is perhaps useful to consider here a rather extreme low- $\beta_i$  example in which the ion cyclotron resonance is reached quite close to the beginning of the dissipation range.

In Figure 11, we present the cascade path on the  $(k_{\perp}, k_{\parallel})$  plane (solid) and the frequencies along that path calculated by numerically solving both the linear gyrokinetic (dashed) and hot plasma (dotted) dispersion relations for plasma parameters  $\beta_i = 0.03$ ,  $T_i/T_e = 3$ , and  $k_0\rho_i = 2 \times 10^{-4}$  (chosen to highlight mode conversion features). Two branches of the hot plasma dispersion relation are plotted: in the MHD limit  $k_{\perp}\rho_i \ll 1$ , these correspond to the MHD Alfvén wave and MHD fast wave. As discussed in § 1.1, the MHD Alfvén wave transitions to a kinetic Alfvén wave at  $k_{\perp}\rho_i > 1$ . The corresponding solution of the gyrokinetic dispersion relation, which does not include the cyclotron resonance, continues right through  $\omega = \Omega_i$ . The effect of the cyclotron resonance on the Alfvén branch of the hot plasma solution is that, as  $\omega \rightarrow \Omega_i$ , the kinetic Alfvén wave converts into an ion Bernstein wave at  $k_{\perp}\rho_i \simeq 3$ . The fast wave has a similarly interesting behavior in this example. At  $k_{\perp}\rho_i \simeq 0.3$ , the fast wave converts to an ion Bernstein wave; eventually this same branch, at  $k_{\perp}\rho_i \simeq 5$  connects onto a continuation of the kinetic Alfvén wave in the range  $\Omega_i < \omega < 2\Omega_i$  before becoming an  $n = 2$  ion Bernstein wave at  $k_{\perp}\rho_i \simeq 8$ .

In a turbulent cascade, different wave modes can couple nonlinearly, but if the nonlinear transfer is local in wavenumber, the coupling will be strong only when those modes have similar wavevectors and frequencies. Thus, in our example, at  $k_{\perp}\rho_i \simeq 0.1$ , the two branches (the fast and Alfvén modes) have frequencies that differ by an order of magnitude, so the coupling is likely to be weak; but, at  $k_{\perp}\rho_i \simeq 4$ , their frequencies differ by only a factor of 2, so the coupling may be much more efficient. In this case, the coupling may enable the turbulent energy of the kinetic Alfvén wave on the low-frequency branch to cascade nonlinearly to the continuation of the kinetic Alfvén wave on the high-frequency branch. The efficiency of such a process and the amount of perpendicular cyclotron heating that can occur as the cascade passes through the resonance is likely to depend on the damping rates of the modes involved. In Figure 12 we plot the damping rates onto ions and electrons for the solutions of the gyrokinetic (dashed) and hot plasma (dotted) dispersion relations for the same parameters as in Figure 11. In the gyrokinetic case, the ion Landau damping falls below the plotted range, while the electron Landau damping is significant (indeed, it is this damping that served as the primary kinetic input in our cascade model). For the low-frequency (Alfvén) branch (upper panel), there is a rise of ion cyclotron damping at  $k_{\perp}\rho_i \simeq 3$  and a slight decrease in the electron Landau damping. For the high-frequency (fast) branch (lower panel), there is a narrow peak of ion cyclotron damping at  $k_{\perp}\rho_i \simeq 0.16$ , the point where the fast wave frequency crosses  $\omega = \Omega_i$ . Two more ion cyclotron damping peaks occur in wavenumber ranges where the fast branch takes on the characteristics an ion Bernstein wave. (Similar cyclotron damping peaks for the low- and high-frequency branches are seen in the more asymptotic case considered in Appendix A; see Figure 10). Thus, if the kinetic Alfvén wave cascade reaches the ion cyclotron frequency, it is possible for some of the energy to go into perpendicular ion heating via coupling to the ion Bernstein wave modes. However, for parameters typical of the slow solar wind, and even for the rather extreme low- $\beta_i$  example considered here, the ion cyclotron damping is weak because it only sets in at  $k_{\perp}\rho_i \gtrsim 1$ ;

in Figure 12 it remains at least an order of magnitude below the electron Landau damping.

As noted above, when the cascade reaches the ion cyclotron frequency, the path of the cascade on the  $(k_{\perp}, k_{\parallel})$  plane, calculated using the gyrokinetic cascade model, is unlikely to be quantitatively correct. Nonetheless, we can tentatively examine the differences in the resulting magnetic energy spectra between the gyrokinetic and hot plasma cascade models (defined in § 3.5). These are plotted in Figure 13 for the same parameters as the example in Figures 11 and 12. Because the ion cyclotron resonance does not significantly alter the total damping rates (see the upper panel of Figure 12), the resulting spectra differ very little, both producing an effective dissipation range spectral index near  $-4$ . This suggests that the effect of the ion cyclotron resonance cannot be identified based solely on the magnetic fluctuation energy spectrum; an examination of the underlying dynamics in concert with a forward modeling approach, like the wave phase velocity study in § 3.4, is necessary if one hopes to distinguish between ion cyclotron and electron Landau damping and, consequently, between ion and electron heating.

## 4. Discussion

The gyrokinetic cascade model developed in this paper is meant to describe in a simple way the physical mechanism—the nonlinear cascade through the MHD Alfvén wave and kinetic Alfvén wave regimes—by which the vast reservoir of energy contained in large-scale turbulent eddies in the solar wind cascades to high wavenumber and frequency and ultimately dissipates due to collisionless damping. Our aim is to reconcile observational data with theoretical ideas about the energy transfer to the small dissipative scales, and eventually to thermal energy of the plasma particles. In that light, this section contains a lengthy discussion of the limitations of our model, followed by a discussion of its relation to previous work.

### 4.1. Limitations of Our Model

One of the key assumptions of our model is that the turbulence can be treated as if it were driven isotropically at some large scale, characterized by an effective isotropic driving wavenumber  $k_0\rho_i$ . Two exceptions can be made to this assumption: the turbulence may not be driven isotropically, and it may be driven at more than one scale.

**Possibility of Anisotropic Driving:** To dispense with this question, we recall that, as we noted in § 1.1, our model does not strictly require that the turbulence is driven isotropically. The critical balance path in the  $(k_{\perp}, k_{\parallel})$  plane, as plotted in Figure 1, simply requires a single point to fix the relation—we use the parameter  $k_0\rho_i$  as a convenient characterization of that point. The anisotropy of the slow solar wind turbulence at  $k_{\perp}\rho_i \sim 10^{-3}$ , measured by *Dasso et al.* [2005], supplies the necessary data point to pin down the scale-dependent anisotropy of the GS theory; we determine the characteristic value of  $k_0\rho_i$  based on that point. A strong test of this model would be a measurement of the anisotropy, similar to that in *Matthaeus et al.* [1990], at a smaller scale around  $k_{\perp}\rho_i \sim 0.1$ . At this wavenumber the anisotropy is predicted to be much stronger with  $k_{\perp}/k_{\parallel} \sim 10$ .

A note is, perhaps, necessary regarding our use of frequencies and damping rates from the gyrokinetic dispersion relation for the entire turbulent cascade even though gyrokinetics is obviously not valid at the isotropic driving scale. While our model undoubtedly does not describe the driving scale well, the effect of driving is probably well modeled by the simple idea of a constant energy input: the damping rate

is negligible at the driving scale and the Alfvén frequency gives a good order-of-magnitude approximation to the nonlinear cascade rate, so the values from the gyrokinetic theory are satisfactory. As we noted in § 3, the assumptions behind the gyrokinetic theory are ever better satisfied as we proceed deeper into the inertial range.

**Possibility of Small-Scale Driving:** The second exception is that energy may be injected at multiple scales. In § 3.1, we argued that our estimated effective driving scale was consistent with the turbulence driven at the Sun and then decaying in transit to 1 AU. It is unlikely that there are large-scale energy sources affecting the turbulence during this transit. It has, however, been suggested that Kelvin-Helmholtz instabilities arising from shear between fast and slow solar wind streams could continually drive turbulence in the solar wind [Coleman, 1968; Roberts *et al.*, 1987; Roberts *et al.*, 1991; Roberts *et al.*, 1992; Zank *et al.*, 1996]; such a mechanism could inject energy at scales smaller than our estimated isotropic driving scale. However, magnetic fluctuation frequency spectra for the slow solar wind typically show a very clean  $-5/3$  spectrum all the way to the low frequencies associated with our fiducial driving wavenumber  $k_0\rho_i \simeq 10^{-4}$  [Tu and Marsch, 1990; Grappin *et al.*, 1990; Tu and Marsch, 1995], suggesting a continuous inertial range below the energy injection scale. If significant energy were injected at smaller scales, one would expect to see structure in the magnetic energy spectrum at the associated frequencies. The lack of such structure argues against significant energy injection at smaller scales. Hence, we conclude that a single effective isotropic driving wavenumber  $k_0\rho_i$  is a reasonable assumption.

**Plasma Instabilities:** Another potential source of small-scale energy injection neglected in our model is the possible presence of temperature anisotropy instabilities, e.g., the mirror or firehose instabilities. Adiabatic expansion of the solar wind drives ions towards  $T_{i\perp} < T_{i\parallel}$ , which should trigger firehose instabilities [Scarf *et al.*, 1967]; indeed, there exists observational evidence that the solar wind ion temperature anisotropies are constrained by the firehose marginal stability criterion [Eviatar and Schulz, 1970; Kasper *et al.*, 2002]. These instabilities may inject energy into the cascade at  $k_{\parallel}\rho_i \sim 1$  and  $\omega \sim \Omega_i$ . It is not possible yet to determine whether such energy injection is present in the data. The role of kinetic instabilities will be investigated in future studies.

Besides the presence of a single isotropic driving scale, two other key assumptions were made in the construction of our model:

**Critical Balance:** We followed Goldreich and Sridhar [1995] in assuming that the turbulent cascade maintains a state of critical balance,  $\omega = \omega_{nl}$ . Imposing critical balance and choosing a driving wavenumber  $k_0\rho_i$  enables one to determine the frequency of the cascade with respect to the ion cyclotron frequency. Critical balance is used to approximate the energy flow on the  $(k_{\perp}, k_{\parallel})$  plane as a one-dimensional path, as shown by the solid line in Figure 1; the turbulent energy is, however, expected not to be restricted to this line but to fill the shaded region for which  $\omega \lesssim \omega_{nl}$  (the hydro-like modes in the nomenclature of Oughton *et al.* [2004]); simulations of MHD turbulence support this notion [Cho and Vishniac, 2000; Maron and Goldreich, 2001; Cho *et al.*, 2002; Cho and Lazarian, 2003; Oughton *et al.*, 2004]. An extension of this cascade model to two dimensions, allowing energy to fill modes throughout the  $(k_{\perp}, k_{\parallel})$  plane, is required to relax this assumption; we do not believe such a treatment would substantially alter the conclusions of this paper. Ultimately, the premise of critical balance will be evaluated by the nonlinear gyrokinetic simulations of magnetized turbulence.

**Linear Damping Rates for Nonlinear Cascade:** We assumed that the damping rates for linear eigenmodes are appropriate for the nonlinear turbulent cascade in which the

energy in a wave mode is transferred to higher wavenumbers within a single wave period. Li *et al.* [2001] call into question the validity of this linear damping approach, citing results in contrast to observation; for a more detailed comparison of this paper to their work, see § 4.2. We find that our results are consistent with a range of observations, but we must leave the final judgment to nonlinear gyrokinetic simulations.

Finally, we ignored a number of potentially significant physical effects. One of them was the possible presence of small-scale plasma instabilities briefly mentioned above. Some of the others are discussed below.

**Radial Expansion of the Solar Wind:** Not only does this have the effect of altering the parameters of the plasma—for example, the plasma transits from the low  $\beta_i$  corona to the order unity  $\beta_i$  solar wind at 1 AU—but the expansion may also affect the turbulent fluctuations. We focus here on the properties of the slow solar wind at 1 AU, but admit a possible influence of this expansion on our results. There exists a substantial literature focusing on the spatial transport and evolution of the solar wind throughout the heliosphere [see Tu and Marsch, 1995, for a review]. The turbulence in these models is usually specified locally by prescription. Our model is also local, so the effect of the expansion on the turbulence is not addressed.

**Imbalanced Turbulence:** Early measurements of the fast solar wind at large scale suggested it was dominated by anti-sunward propagating Alfvén waves [Belcher and Davis, 1971]. Subsequent measurements in the fast solar wind found that anti-sunward Elsässer energy fluxes can exceed sunward fluxes by more than an order of magnitude; in the slow wind, the imbalance is reduced, sometimes showing equal energy in both directions [Tu *et al.*, 1990; Tu and Marsch, 1990; Grappin *et al.*, 1990; Tu and Marsch, 1995]. Our model only had one flux quantity  $\epsilon$ , i.e., it assumed a balance of Elsässer energy. An imbalanced turbulence requires a somewhat more complicated treatment [Dobrowolny *et al.*, 1980; Grappin *et al.*, 1983; Politano *et al.*, 1989; Hossein *et al.*, 1995; Lithwick and Goldreich, 2003; Lithwick *et al.*, 2007]; thus, a more general cascade model would need to include an additional parameter to account for the imbalance between the fluxes. While this means that our model is likely not appropriate for the fast solar wind, we believe that it is applicable to the slow solar wind when the Elsässer energy fluxes are balanced.

Note also that our model does not address the implications of the conservation of magnetic and cross helicities in MHD.

**Compressive Modes:** Compressive fluctuations, such as the MHD slow, entropy, and fast modes, or, more generally, the density and field strength fluctuations, are left out of our model. Observational evidence suggests less than 10% of the power resides in compressive modes [Belcher and Davis, 1971]. Linear theory predicts that these modes are damped when  $k_{\parallel}\lambda_{mfpi} \gtrsim 1$  in the weakly collisional solar wind [Braginskii, 1965; Barnes, 1966]. However, it has been suggested that a fast wave cascade may be able to transfer energy to high frequencies where it can heat ions perpendicular to the magnetic field [Chandran, 2006]. The cascade of slow and entropy modes is also under investigation [Schekochihin *et al.*, 2007]—it is not clear that the parallel cascade of these modes is similar to the Alfvén wave cascade. If a cascade of compressive fluctuations carries a significant amount of energy to the ion Larmor radius scale, this can contribute to the kinetic Alfvén wave cascade in the dissipation range, thus altering somewhat the energetics of our model.

**Kinetic Entropy Cascade:** We have referred to collisionless kinetic damping of electromagnetic fluctuations as the mechanism that leads to plasma heating. The way this

heating occurs is, in fact, quite complex. Collisionless damping is an energy conversion mechanism that transfers the electromagnetic energy of the MHD and kinetic Alfvén wave cascades into purely kinetic cascades of ion and electron entropy fluctuations—cascades that occur in phase space and that take the energy to sufficiently small spatial and velocity scales for the collisions to render the “collisionless” damping irreversible and to effect the heating. How these cascades work is explained in *Schekochihin et al.* [2007]. An important point here is that these cascades should have observational signatures, in particular, steep power-law spectra of low-frequency electric and magnetic fluctuations [*Schekochihin et al.*, 2007]. A superposition of these kinetically induced fluctuations with the kinetic Alfvén wave cascade may contribute to the wide spread in the observed spectral index in the dissipation range.

#### 4.2. Relation to Previous Work

The cascade model proposed here is similar to that constructed by *Zhou and Matthaeus* [1990b] and later used by *Li et al.* [2001] in a study of the dissipation of solar wind turbulence. The *Zhou and Matthaeus* [1990b] model employed a diffusion operator for the nonlinear cascade of energy in wavenumber space [*Leith*, 1967] to develop an *isotropic* model for turbulence in the MHD regime. This model was used by *Li et al.* [2001] to determine the characteristics of the resulting energy spectrum in the dissipation range when collisionless damping by the cyclotron and Landau resonances was considered; they concluded that these mechanisms could only cause a steep cutoff in wavenumber rather than the power-law seen in observations. We come to a different conclusion for reasons that we shall now explain.

First, the *Li et al.* [2001] model did not assume that the cascade frequency was determined by critical balance, so the change of dynamics leading to a faster cascade beginning at  $k_{\perp}\rho_i \sim 1$  was neglected. Second, they followed the cascade along constant angles in  $(k_{\perp}, k_{\parallel})$  plane of  $\theta = 0^\circ$ ,  $30^\circ$ ,  $45^\circ$ , and  $60^\circ$ , effectively assuming either isotropy or a scale-independent anisotropy. On the other hand, our critically balanced model predicts that at  $k_{\perp}\rho_i \sim 1$ —where collisionless damping first becomes significant—the anisotropy should be  $k_{\parallel}/k_{\perp} \sim 0.1$ , leading to an angle  $\theta \gtrsim 85^\circ$ . For these nearly perpendicular modes, the frequency remains low,  $\omega \ll \Omega_i$ , so the Alfvén wave cascade is damped only by the Landau resonance, and the damping is less vigorous. Hence, we find a cutoff due to collisionless damping that is much less sharp than that found by *Li et al.* [2001], and that is consistent with *in situ* measurements.

In a related work, *Gary and Borovsky* [2004] also found that ion cyclotron damping produced a steep damping inconsistent with observations. Furthermore, they noted that, in the limit that  $k_{\parallel} < k_{\perp}$ , electron Landau damping would dominate collisionless damping with a more gradual onset. They suggested a qualitative picture that, in this case, the location of the spectral break between the inertial and dissipation ranges would be dependent on the turbulent energy cascade rate. We agree with their prediction of the more gradual onset of Landau damping, but believe the spectral break is most often caused by a change in dynamics at  $k_{\perp}\rho_i \sim 1$ , a feature not included in their paper.

*Smith et al.* [2001] investigated an unusual period of solar wind turbulence with  $\beta_i \ll 1$ , a condition in which the ion inertial length and the ion Larmor radius are well separated; they concluded that the dissipation processes occur at the ion inertial length and that this finding is inconsistent with dissipation due to the ion cyclotron resonance. Here we compare our hot plasma cascade model predictions directly to interval (c) of *Smith et al.* [2001]. From Figure 1 of their paper, we estimate the following mean

values of the parameters over interval (c):  $B_0 \simeq 6$  nT,  $V_{sw} \simeq 350$  km/s,  $T_i \simeq 6 \times 10^4$  K, and  $\beta_i \simeq 0.01$ . We employ our fiducial driving wavenumber  $k_0\rho_i = 10^{-4}$ , and take the mean electron temperature for the slow solar wind as  $T_e \simeq 1.3 \times 10^5$  K [*Newbury et al.*, 1998], giving a temperature ratio  $T_i/T_e = 0.5$ . For these parameters, the ion Larmor radius is  $\rho_i \simeq 5.5 \times 10^6$  cm. As presented in the upper panel of Figure 14, the steady-state magnetic energy spectrum from the hot plasma cascade model breaks from the  $-5/3$  spectral index at a value of  $k_{\perp}\rho_i \simeq 0.25$ ; we transform from the wavenumber spectrum generated by our model to a frequency spectrum in the satellite frame by the Taylor hypothesis, using  $f = (k_{\perp}\rho_i)v_{sw}/(2\pi\rho_i)$  to find a breakpoint frequency of  $f \simeq 0.25$  Hz. *Smith et al.* [2001] measure the breakpoint frequency to be  $f \simeq 0.168$  Hz; the hot plasma cascade model therefore predicts a breakpoint frequency that is roughly consistent with the observations. In the lower panel of Figure 14, it is shown that electron Landau damping is responsible for the break. In this case, the damping is sufficient to prevent the cascade from reaching the ion cyclotron frequency; thus, ion cyclotron damping is negligible, falling below the plotted range of the lower panel. We note here that the gyrokinetic cascade model gives results nearly indistinguishable from those presented in Figure 14 for the hot plasma cascade model; this is not surprising since the cyclotron resonance plays a negligible role. It is worth noting that the wavenumber associated with the breakpoint, when cast in terms of the ion inertial length, is  $k_{\perp}d_i \simeq 2.5$ , so we agree with the *Smith et al.* [2001] conclusion that the breakpoint occurs at the ion inertial length scale. The salient point here is that, although the magnetic energy spectrum breakpoint often occurs at  $k_{\perp}\rho_i \sim 1$  due to the change in linear physics from the MHD to the kinetic Alfvén wave regime, strong damping may shift the breakpoint to a lower value of  $k_{\perp}\rho_i$ .

#### 4.3. Application to the Solar Corona

Although this paper has focused on anisotropic turbulence in the solar wind, such turbulence is also expected to be present in the solar corona. One of the key problems for the solar corona is the identification of the mechanism by which the coronal plasma is heated to yield the observed minority ion temperatures higher than proton temperatures  $T_{ion} > T_p$  and large ion and proton temperature anisotropies  $T_{\perp} \gg T_{\parallel}$  [*Kohl et al.*, 1997, 1998; *Antonucci et al.*, 2000; *Kohl et al.*, 2006]. In the spirit of a long line of previous investigations [*Hollweg*, 1986; *Isenberg*, 1990; *Li et al.*, 1999; *Matthaeus et al.*, 1999; *Dmitruk et al.*, 2001, 2002; *Cranmer and van Ballegoijen*, 2003, 2005; *Cranmer et al.*, 2007], we briefly address what our cascade model predicts for ion heating in the solar corona.

The first caveat is that the cascade model described in this paper assumes a balance of the oppositely-directed Elsässer energy fluxes along the magnetic field line. Therefore, the predictions of this simple model cannot be applied to the coronal hole regions in which the field lines are open and the anti-sunward Alfvén wave energy flux dominates; the conclusions here will only apply to regions of closed field lines in which the turbulence demonstrates balanced energy fluxes. For the solar corona at a heliocentric radius  $r = 2R_{\odot}$ , we take the following plasma parameters: magnetic field magnitude  $B_0 = 0.8$  G, number density  $n = 3.7 \times 10^5$  cm $^{-3}$ , electron temperature  $T_e = 8 \times 10^5$  K, and proton temperature  $T_p = 2 \times 10^6$  K. These plasma conditions give an ion Larmor radius  $\rho_i = 2.4 \times 10^3$  cm, an ion cyclotron frequency  $\Omega_i = 7.7 \times 10^3$  rad/s, an ion plasma beta  $\beta_i = 0.004$ , and a temperature ratio  $T_i/T_e = 2.5$ .

In addition to these parameters, for the hot plasma cascade model we must also specify the driving by supplying the characteristic isotropic driving wavenumber  $k_0\rho_i$ . From the model of *Cranmer and van Ballegoijen* [2005], we find

that, at a radius of  $r = 2R_\odot$ , the driving energy due to photospheric motions peaks at a period of  $P = 120$  s. Using the dispersion relation for Alfvén waves  $\omega = k_\parallel v_A$ , this gives a parallel driving length scale  $L_\parallel = 3.4 \times 10^{10}$  cm. At this radius, the *Cranmer and van Ballegoijen* [2005] model estimates the perpendicular driving scale  $L_\perp = 1.3 \times 10^9$  cm (using their best value of  $\Lambda = 0.35$  in their equation [51]); for the period  $P = 120$  s, this implies a perpendicular velocity of  $v_\perp = 110$  km/s. The effective isotropic driving wavenumber can be found using equation (13), giving the result  $k_0 \rho_i = 7 \times 10^{-10}$ . Note that, although the length scale associated with  $k_0$  is  $L_0 = 2 \times 10^{13}$  cm, there are no motions at this scale; the driving occurs anisotropically at  $L_\parallel > L_\perp$  and the value of  $k_0 \rho_i$  calculated here is simply a convenient way to specify the critical balance relation determined by the driving mechanism, as explained in § 1.1.

The heating resulting from the damping of the turbulence can occur via either the Landau or cyclotron resonances in the hot plasma cascade model; Landau damping leads to an increase of the parallel temperature, cyclotron damping to an increase of the perpendicular temperature. For the low  $\beta_i$  conditions in the solar corona, Landau damping onto the ions is negligible, so all heating is due to either electron Landau damping or ion cyclotron damping. Using equation (15) to estimate the frequency of the cascade at  $k_\perp \rho_i = 1$  (and neglecting damping by taking  $\epsilon = \epsilon_0$ ), we find  $\omega/\Omega_i = 1.7 \times 10^{-2}$ ; this suggests ion cyclotron damping will be negligible in this case. The steady-state solution of the hot plasma cascade model for these parameters confirms that the Alfvén wave cascade driven by photospheric motions results in only parallel electron heating via the Landau resonance. In fact, for all values of  $k_0 \rho_i < 10^{-5}$ , the turbulent cascade fails to reach the ion cyclotron frequency and therefore no ion heating occurs. Significant perpendicular ion heating via the balanced, Alfvén wave cascade requires an isotropic driving scale  $L_0 \leq 1.5 \times 10^7$  cm, a condition not satisfied in the solar corona. In conclusion, this turbulent cascade model cannot account for the perpendicular ion heating observed in the solar corona.

## 5. Conclusions

In the study of solar wind turbulence, a central issue is to understand the mechanisms by which the energy contained in large-scale turbulent motions is transferred to smaller scales and higher frequencies where it is eventually deposited as thermal energy in the plasma. In § 2.1 we develop a simple model that traces the anisotropic cascade of Alfvén wave energy from the MHD to the kinetic Alfvén wave regime. The model is based on the assumption of locality of energy transfer in wavenumber space, the conjecture of a critical balance between the nonlinear interaction and linear propagation timescales, and the premise that the linear kinetic damping rates determine heating rates even in the presence of the nonlinear cascade. It provides a guide for the interpretation of observational data in the balanced, slow solar wind and will be useful in connecting these observations to nonlinear gyrokinetic simulations of turbulence.

The anisotropic cascade model makes several predictions about the turbulent magnetic energy spectrum measured in the balanced, slow solar wind—these are presented in § 2.2–§ 2.5. The cascade is weakly damped in the Alfvén wave regime  $k_\perp \rho_i \ll 1$  and the spectrum has the familiar  $k^{-5/3}$  slope. In the dissipation range, at wavenumbers above the observed break, the magnetic energy spectrum undergoes a slow exponential cut-off. We show that the measured power-law behavior of the spectrum in the dissipation range may be an artifact of limited magnetometer sensitivity (except in the case of very weak damping) and that over the typical range of parameters  $\beta_i$  and  $T_i/T_e$  in the solar wind, the varying strength of Landau damping naturally reproduces

the observed variation of the effective spectral index in the dissipation range from  $-7/3$  to  $-4$  (§ 2.3–§ 2.4). The spectral break between the inertial range and dissipation range power laws occurs at the ion Larmor radius  $k_\perp \rho_i \simeq 1$  in plasmas with weak damping due to the dispersive nature of the kinetic Alfvén wave; in the presence of strong damping, it may occur at  $k_\perp \rho_i \lesssim 1$  due to damping by the Landau resonance and/or the ion cyclotron resonance. See Figure 2 for a plot of the damping rate as a function of plasma parameters at  $k_\perp \rho_i = 1$ .

In § 3 we examine the applicability of gyrokinetics to turbulence in the balanced, slow solar wind. At scales somewhat below the driving scale, the anisotropy of the turbulence,  $k_\parallel < k_\perp$ , is supported by observations [*Dasso et al.*, 2005] in the slow solar wind. Given the observed anisotropy, we find that a gyrokinetic description becomes valid from a scale a couple of orders of magnitude below the driving scale up to the point where the fluctuation frequency approaches the cyclotron frequency,  $\omega \simeq \Omega_i$ . The driving scale of the turbulence in the slow solar wind is estimated to be  $L \simeq 2 \times 10^{11}$  cm (§ 3.1), in agreement with three other independent determinations. For typical solar wind parameters, we find that  $k_\parallel \ll k_\perp$  and  $\omega \ll \Omega_i$  at a perpendicular wavenumber  $k_\perp \rho_i \sim 1$  (§ 3.2); therefore, this transition regime is well described by gyrokinetics. Wave phase velocity evidence from *in situ* observations [*Bale et al.*, 2005] argues for the existence of a kinetic Alfvén wave cascade in the dissipation range (which is captured in our model); the measurements are inconsistent with the onset of ion cyclotron damping (§ 3.4).

The gyrokinetic cascade and the resultant particle heating through Landau damping, however, cannot be the whole story. The selective perpendicular heating of minor ions and the breaking of adiabatic invariance for ions implied by observational data, particularly in the fast wind, indicate that fluctuations at or above the cyclotron frequency are present in the solar corona and solar wind. Although a mechanism not incorporated into our model may be responsible—for example, heating by fast waves [*Chandran*, 2006] or velocity-space instabilities that transfer energy from the parallel to the perpendicular direction [*Scarf et al.*, 1967; *Eviatar and Schulz*, 1970; *Kasper et al.*, 2002; *Marsch*, 2006]—we may employ our model to determine under what conditions the gyrokinetic cascade reaches the ion cyclotron frequency. For plasma parameters typical of the solar wind and the driving scale estimate  $L \simeq 2 \times 10^{11}$  cm, the gyrokinetic cascade model generally reaches the ion cyclotron frequency at  $k_\perp \rho_i \gg 1$ , by which point Landau damping has removed much of the cascade energy. In addition, damping of the cascade can slow the increase of the frequency with perpendicular wavenumber, possibly preventing the cyclotron frequency from being reached at all, as shown in Figure 8. A strong constraint on the wavenumber threshold at which the cyclotron resonance becomes important—the same threshold at which the gyrokinetic approximation is violated—is determined by a comparison of the gyrokinetic and hot plasma cascade models. The regime of validity for gyrokinetics is given by the shaded region in Figure 9 and covers most of the parameter range of interest in the study of turbulence in the solar wind. In the range of parameters relevant to the solar wind, this threshold roughly scales as  $k_\perp \rho_i \sim (k_0 \rho_i)^{-1/4} \beta_i^{5/8}$  (§ 3.5). Therefore, the cyclotron resonance can have a significant effect on the dissipation-range dynamics only in plasmas with  $\beta_i < 0.01$  or in systems driven isotropically at scales  $L \ll 2 \times 10^{11}$  cm. If the cyclotron resonance is reached within the dissipation range before the electron Landau damping becomes dominant, there is a conversion between kinetic Alfvén waves and ion Bernstein waves in the narrow frequency band around the resonance. However, the amount of cyclotron damping

associated with this conversion is quite small and the narrowness of the resonance suggests that the kinetic Alfvén wave cascade may in fact continue virtually unimpeded even at  $\omega > \Omega_i$  (see § 3.6 and Appendix A).

In § 4.3, we apply this cascade model to the problem of ion heating in the solar corona. For the low  $\beta_i$  conditions of the corona, the dissipation of turbulence can cause parallel heating of the electrons via the Landau resonance or perpendicular heating of the ions via the ion cyclotron resonance. We conclude, however, that the highly anisotropic driving due to photospheric motions results in only parallel electron heating via the Landau resonance; only for an effective isotropic driving scale  $L_0 \leq 1.5 \times 10^7$  cm, a condition not satisfied in the corona, will the Alfvén wave cascade as modeled here lead to substantial perpendicular ion heating.

Although our simple cascade model allows us to produce plausible predictions for magnetic-energy spectra, reaching a definitive understanding of turbulence in the solar wind will require nonlinear simulations of magnetized plasma turbulence in the weakly collisional regime. A program of gyrokinetic simulations is currently underway [Howes et al., 2008; Howes, 2008]. These simulations will both test the validity of the ideas that underpin the approach taken in this paper and probe the physics beyond the scope of our simple model, in particular the complicated dynamics at the scale of the ion Larmor radius  $k_\perp \rho_i \sim 1$ . To provide detailed information for comparison to *in situ* measurements, gyrokinetic simulations will calculate particle heating rates, magnetic and cross helicities, and nonlinear energy transfer rates in imbalanced cascades. The cascade model proposed in this paper is a first step in connecting the results of nonlinear gyrokinetic simulations to the observations in the solar wind and in assessing the applicability of gyrokinetics to this problem.

**Acknowledgments.** We thank S. Bale for useful discussions. G.G.H. was supported by the DOE Center for Multiscale Plasma Dynamics, Fusion Science Center Cooperative Agreement ER54785. G.G.H., S.C.C., and W.D. thank the Aspen Center for Physics for their hospitality. E.Q. and G. G. H. were supported in part by the David and Lucille Packard Foundation. A. A. S. was supported by an STFC Advanced Fellowship and an RCUK Academic Fellowship.

## Appendix A: Plasma Dispersion Relation, Mode Conversion and Damping at the Ion Cyclotron Resonance

The general eigenvalue problem for linear perturbations of a thermal plasma is

$$\hat{\mathbf{D}} \cdot \delta \mathbf{E} = 0. \quad (\text{A1})$$

where, if we choose the coordinate frame so that  $z$  is the direction of the mean magnetic field and  $x$  is the direction of  $\mathbf{k}_\perp$ , the components of the dielectric tensor are (see, e.g., Stix 1992)

$$D_{xx} = -k_\parallel^2 + \frac{\omega^2}{c^2} + \sum_s \frac{\omega_{ps}^2}{c^2} \sum_{n=-\infty}^{+\infty} \frac{n^2 I_n(\alpha_s) e^{-\alpha_s}}{\alpha_s} \zeta_{0s} Z(\zeta_{ns}), \quad (\text{A2})$$

$$D_{yy} = D_{xx} - k_\perp^2 - \sum_s \frac{\omega_{ps}^2}{c^2} \sum_{n=-\infty}^{+\infty} 2\alpha_s \frac{\partial [I_n(\alpha_s) e^{-\alpha_s}]}{\partial \alpha_s} \zeta_{0s} Z(\zeta_{ns}), \quad (\text{A3})$$

$$D_{zz} = -k_\perp^2 + \frac{\omega^2}{c^2} - \sum_s \frac{\omega_{ps}^2}{c^2} \sum_{n=-\infty}^{+\infty} I_n(\alpha_s) e^{-\alpha_s} \zeta_{0s} \zeta_{ns} Z'(\zeta_{ns}), \quad (\text{A4})$$

$$D_{xy} = -D_{yx} = i \sum_s \frac{\omega_{ps}^2}{c^2} \sum_{n=-\infty}^{+\infty} n \frac{\partial [I_n(\alpha_s) e^{-\alpha_s}]}{\partial \alpha_s} \zeta_{0s} Z(\zeta_{ns}), \quad (\text{A5})$$

$$D_{xz} = D_{zx} = k_\parallel k_\perp - \sum_s \frac{\omega_{ps}^2}{c^2} \sum_{n=-\infty}^{+\infty} \frac{n I_n(\alpha_s) e^{-\alpha_s}}{\sqrt{2\alpha_s}} \zeta_{0s} Z'(\zeta_{ns}), \quad (\text{A6})$$

$$D_{yz} = -D_{zy} = i \sum_s \frac{\omega_{ps}^2}{c^2} \sum_{n=-\infty}^{+\infty} \sqrt{\frac{\alpha_s}{2}} \frac{\partial [I_n(\alpha_s) e^{-\alpha_s}]}{\partial \alpha_s} \zeta_{0s} Z'(\zeta_{ns}), \quad (\text{A7})$$

where  $\alpha_s = k_\perp^2 \rho_s^2$ ,  $\zeta_{ns} = (\omega - n\Omega_s)/|k_\parallel|v_{\text{th}s}$ ,  $I_n$  are modified Bessel functions, and  $Z$  is the plasma dispersion function.

We now consider the general hot plasma dispersion  $\det \hat{\mathbf{D}} = 0$ , or

$$D_{xx} D_{yy} D_{zz} + 2D_{xy} D_{yz} D_{xz} - D_{xz}^2 D_{yy} + D_{yz}^2 D_{xx} + D_{xy}^2 D_{zz} = 0, \quad (\text{A8})$$

in the asymptotic limits that we believe to be appropriate for the dissipation range of the solar wind:  $k_\perp \rho_i \gg 1$ ,  $k_\perp \rho_e \ll 1$ , and  $k_\parallel \ll k_\perp$ . Then we may expand the Bessel and plasma dispersion functions in the above expressions for  $D_{ij}$ , taking  $k_\parallel \ll k_\perp$ ,  $\alpha_e \ll 1$ ,  $\zeta_{0e} \ll 1$ ,  $\zeta_{ne} \gg 1$  for  $n \neq 0$ ,  $\alpha_i \gg 1$ ,  $\zeta_{ni} \gg 1$ . After straightforward algebra, we get

$$D_{xx} = -k_\parallel^2 [1 - 2\tilde{\omega}^2 (1 - C)], \quad (\text{A9})$$

$$D_{yy} = -k_\perp^2 \left(1 - \beta_i \frac{T_e}{T_i} L\right), \quad (\text{A10})$$

$$D_{zz} = -k_\perp^2 \left[1 - 2 \frac{T_i}{T_e} \tilde{\omega}^2 (1 + L)\right], \quad (\text{A11})$$

$$D_{xy} = ik_\parallel k_\perp \tilde{\omega} \sqrt{\beta_i}, \quad (\text{A12})$$

$$D_{xz} = k_\parallel k_\perp, \quad (\text{A13})$$

$$D_{yz} = ik_\perp^2 \tilde{\omega} \sqrt{\beta_i} (1 + L), \quad (\text{A14})$$

where  $\tilde{\omega} = \omega/|k_\parallel|v_A k_\perp \rho_i$ . The (small) terms containing

$$L = i\tilde{\omega} k_\perp \rho_i \sqrt{\frac{\pi T_i m_e}{\beta_i T_e m_i}} \quad (\text{A15})$$

are responsible for electron Landau damping of the kinetic Alfvén waves, while the effect of the cyclotron resonance is (to lowest order) contained only in the matrix element  $D_{xx}$  (corresponding to perpendicular electrostatic fluctuations):

$$C = \frac{2}{\sqrt{\pi} k_\perp \rho_i} \sum_{n=1}^{\infty} \frac{\tilde{\omega}^2}{\tilde{\omega}^2 - n^2 \tilde{\Omega}_i^2} - \frac{i}{\sqrt{\beta_i}} \sum_{n=1}^{\infty} \frac{n^2 \tilde{\Omega}_i^2}{\tilde{\omega}} \left(e^{-\zeta_{ni}^2} + e^{-\zeta_{-ni}^2}\right), \quad (\text{A16})$$

where  $\tilde{\Omega}_i = \Omega_i/(|k_\parallel|v_A|k_\perp \rho_i)$  and, in terms of the normalized frequencies  $\tilde{\omega}$  and  $\tilde{\Omega}_i$ ,  $\zeta_{ni} = (\tilde{\omega} - n\tilde{\Omega}_i)k_\perp \rho_i/\sqrt{\beta_i}$ . The dispersion relation (A8) can then be written as follows:

$$\begin{aligned} & \tilde{\omega}^2 \left[2 + \left(1 + \frac{T_e}{T_i}\right) \beta_i + (2 + \beta_i)L\right] - \left(1 + \frac{T_e}{T_i}\right) \\ & \quad - \left[1 - \frac{T_e}{T_i} \left(1 + \frac{T_e}{T_i}\right) \beta_i\right] L \\ & = C \left[\tilde{\omega}^2 \left(2 + \frac{T_e}{T_i} \beta_i + 2L\right) - \frac{T_e}{T_i} \left(1 - \frac{T_e}{T_i} \beta_i L\right)\right]. \quad (\text{A17}) \end{aligned}$$

If we set  $C = 0$  here, we recover the gyrokinetic dispersion relation (in the limit  $k_{\perp}\rho_i \gg 1$ ,  $k_{\perp}\rho_e \ll 1$ ), whose solutions are the weakly Landau-damped kinetic Alfvén waves (see section 2.6.2 of *Howes et al.* [2006]). The normalized frequency and damping rate of these waves in our notation are

$$\tilde{\omega} = \tilde{\omega}_{\text{KAW}} = \frac{1}{\sqrt{\beta_i + 2/(1 + T_e/T_i)}}, \quad (\text{A18})$$

$$\tilde{\gamma} = -\tilde{\gamma}_{\text{KAW}} = -\frac{k_{\perp}\rho_i}{2} \sqrt{\frac{\pi T_e m_e}{\beta_i T_i m_i}} \times \left\{ 1 - 2 \frac{1 + (1 + T_e/T_i)\beta_i}{[2 + (1 + T_e/T_i)\beta_i]^2} \right\}. \quad (\text{A19})$$

The kinetic Alfvén waves will be affected by the ion cyclotron resonance when their frequency is close the cyclotron frequency, i.e.,  $\tilde{\Omega}_i \sim \tilde{\omega}_{\text{KAW}}$ , or

$$\frac{k_{\parallel}}{k_{\perp}} (k_{\perp}\rho_i)^2 \sim 1. \quad (\text{A20})$$

For the highly anisotropic fluctuations in the kinetic Alfvén wave cascade, we have  $k_{\parallel}/k_{\perp} \ll 1$ , so condition (A20) is reached deep in the dissipation range,  $k_{\perp}\rho_i \gg 1$ —where exactly depends on the degree of anisotropy of the fluctuations and can be estimated using the critical balance assumption to relate  $k_{\parallel}$  and  $k_{\perp}$  (see equation (16), which also includes the dependence on  $\beta_i$  and  $T_e/T_i$ ). Note that gyrokinetics breaks down at this point.

Let us consider what happens in the region of the wavenumber space where the condition (A20) is satisfied. Define  $\Delta_n \equiv \tilde{\omega}_{\text{KAW}} - n\tilde{\Omega}_i$  and assume  $\Delta_n \ll n\tilde{\Omega}_i \sim \tilde{\omega}_{\text{KAW}} \sim 1$ . We now look for solutions of the dispersion relation (A17) in the form  $\tilde{\omega} = \tilde{\omega}_{\text{KAW}} + \delta\tilde{\omega}$ , where  $\delta\tilde{\omega} \sim \Delta_n \ll \tilde{\omega}_{\text{KAW}}$  (the validity of this assumption will be confirmed shortly). In the dispersion relation (A17), we neglect the Landau damping terms (they are controlled by an independent small parameter,  $L \propto \sqrt{m_e/m_i}$ ) and get

$$\tilde{\omega}_{\text{KAW}}\delta\tilde{\omega} = \frac{C}{[2 + (1 + T_e/T_i)\beta_i]^2}, \quad (\text{A21})$$

$$C \simeq n\tilde{\Omega}_i \left[ \frac{1}{\sqrt{\pi}k_{\perp}\rho_i(\Delta_n + \delta\tilde{\omega})} - \frac{i}{\sqrt{\beta_i}} e^{-\zeta_{ni}^2} \right]. \quad (\text{A22})$$

We shall see that the imaginary part of  $C$  is exponentially small, so to lowest order, equations (A21) and (A22) combine into a quadratic equation for  $\delta\tilde{\omega}$ . The solutions of this equation are

$$\delta\tilde{\omega} = -\frac{\Delta_n}{2} \pm \sqrt{\frac{\Delta_n^2}{4} + \frac{1}{\sqrt{\pi}k_{\perp}\rho_i[2 + (1 + T_e/T_i)\beta_i]^2}}. \quad (\text{A23})$$

When the kinetic Alfvén wave frequency is not too close to the cyclotron resonance, namely  $|\Delta_n| \gg 1/\sqrt{k_{\perp}\rho_i}$ , the “+” solution corresponds to the kinetic Alfvén wave

$$\tilde{\omega} \simeq \tilde{\omega}_{\text{KAW}} + \frac{1}{\sqrt{\pi}k_{\perp}\rho_i\Delta_n[2 + (1 + T_e/T_i)\beta_i]^2} \quad (\text{A24})$$

and the “−” solution to an approximately electrostatic wave called the ion Bernstein wave (see, e.g., *Stix* 1992), whose frequency is close to  $n\tilde{\Omega}_i$ :

$$\tilde{\omega} \simeq n\tilde{\Omega}_i - \frac{1}{\sqrt{\pi}k_{\perp}\rho_i\Delta_n[2 + (1 + T_e/T_i)\beta_i]^2}. \quad (\text{A25})$$

(this solution is high frequency and is not captured by gyrokinetics).

When  $|\Delta_n| \sim 1/\sqrt{k_{\perp}\rho_i}$ , the more general formula (A23) describes the conversion of the kinetic Alfvén wave into the ion Bernstein wave below the cyclotron resonance ( $\tilde{\omega}_{\text{KAW}} <$

$\tilde{\Omega}_i$ ) and of the ion Bernstein wave into the kinetic Alfvén wave above the resonance ( $\tilde{\omega}_{\text{KAW}} > \tilde{\Omega}_i$ ). This transition is illustrated in Figure 10 for the  $n = 1$  resonance. The behavior at  $n > 1$  is similar.

The damping rate can now be calculated perturbatively: restoring the Landau term  $L$  and the imaginary part of  $C$  and replacing  $\delta\tilde{\omega} \rightarrow \delta\tilde{\omega} + i\tilde{\gamma}$  in equations (A21) and (A22) with  $\delta\tilde{\omega}$  given by equation (A23), we get (keeping only the lowest order terms for  $k_{\perp}\rho_i \gg 1$ )

$$\tilde{\gamma} = -\frac{\Delta_n + \delta\tilde{\omega}}{\Delta_n + 2\delta\tilde{\omega}} \left[ \tilde{\gamma}_{\text{KAW}} + \frac{1}{\sqrt{\beta_i}[2 + (1 + T_e/T_i)\beta_i]^2} e^{-\zeta_{ni}^2} \right], \quad (\text{A26})$$

where  $\tilde{\gamma}_{\text{KAW}}$  is the electron Landau damping rate given by equation (A19) and  $\zeta_{ni} = (\Delta_n + \delta\tilde{\omega})k_{\perp}\rho_i/\sqrt{\beta_i}$ . Since  $\delta\tilde{\omega} \sim \Delta_n \sim 1/\sqrt{k_{\perp}\rho_i}$ , we find that  $\zeta_{ni} \sim \sqrt{k_{\perp}\rho_i}$ , so the cyclotron damping remains exponentially small and we have thus confirmed *a posteriori* that the expansion of  $Z(\zeta_{ni})$  in large argument was justified. The electron Landau damping rate (the first term in equation (A26)) and the ion cyclotron damping rate (the second term in equation (A26)) are plotted in Figure 10. Note that the ion cyclotron damping is quite weak both in absolute terms and in comparison with the electron Landau damping.

The main points that we have demonstrated by the above calculation are itemized at the beginning of § 3.6, where they are followed by a discussion of a somewhat less asymptotic case. That discussion and a much more detailed numerical study by *Li and Habbal* [2001] demonstrate some of the possibilities for mode conversion and damping at the ion cyclotron resonances that are beyond the scope of a simple asymptotic calculation like the one presented in this Appendix.

## Notes

1. Note that, although we parameterize the cascade in terms of the isotropic driving wavenumber  $k_{0\rho_i}$ , this parameterization does not require that the cascade be driven isotropically. A cascade driven both *in critical balance* and anisotropically, with  $k_{\perp} \neq k_{\parallel}$ , can be characterized by an effective value of  $k_{0\rho_i}$  along the extrapolated cascade path at which  $k_{\perp} = k_{\parallel}$ .
2. The Vlasov-Maxwell dispersion relation for a hot plasma agrees with the gyrokinetic results in the limit  $k_{\parallel} \ll k_{\perp}$  and  $\omega \ll \Omega_i$ , precisely the anisotropic and low-frequency fluctuations anticipated by the GS theory for MHD turbulence.
3. The Landau resonance includes both Landau damping by the parallel electric field perturbation and transit-time, or *Barnes* [1966], damping by the parallel magnetic field perturbation; in this paper, we refer to the collective damping effect of these mechanisms as Landau damping.
4. There is a typo in the legend of this figure: the spectrum at 0.9 AU is for the slow solar wind (L), not the fast (H).

## References

- Alexandrova, O., V. Carbone, P. Veltri, and L. Sorriso-Valvo, Small scale energy cascade of the solar wind turbulence, *Astrophys. J.*, apJ preprint doi:10.1086/524056, 2008.
- Antonsen, T. M., Jr., and B. Lane, Kinetic equations for low frequency instabilities in inhomogeneous plasmas, *Physics of Fluids*, 23, 1205–1214, 1980.
- Antonucci, E., M. A. Doderio, and S. Giordano, Fast Solar Wind Velocity in a Polar Coronal Hole during Solar Minimum, *Sol. Phys.*, 197, 115–134, 2000.
- Bale, S. D., private communication, 2007.
- Bale, S. D., P. J. Kellogg, F. S. Mozer, T. S. Horbury, and H. Reme, Measurement of the Electric Fluctuation Spectrum of Magnetohydrodynamic Turbulence, *Physical Review Letters*, 94(21), 215,002–+, doi:10.1103/PhysRevLett.94.215002, 2005.

- Barnes, A., Collisionless Damping of Hydromagnetic Waves, *Phys. Fluids*, *9*, 1483–1495, 1966.
- Batchelor, G. K., *The Theory of Homogeneous Turbulence*, The Theory of Homogeneous Turbulence, Cambridge: Cambridge University Press, 1953, 1953.
- Belcher, J. W., and L. Davis, Large-Amplitude Alfvén Waves in the Interplanetary Medium, *2*, *J. Geophys. Res.*, *76*, 3534–3563, 1971.
- Bieber, J. W., W. Wanner, and W. H. Matthaeus, Dominant two-dimensional solar wind turbulence with implications for cosmic ray transport, *J. Geophys. Res.*, *101*, 2511–2522, doi:10.1029/95JA02588, 1996.
- Biskamp, D., and W.-C. Müller, Scaling properties of three-dimensional isotropic magnetohydrodynamic turbulence, *Phys. Plasmas*, *7*, 4889–4900, doi:10.1063/1.1322562, 2000.
- Biskamp, D., E. Schwarz, A. Zeiler, A. Celani, and J. F. Drake, Electron magnetohydrodynamic turbulence, *Phys. Plasmas*, *6*, 751–758, 1999.
- Boldyrev, S., On the Spectrum of Magnetohydrodynamic Turbulence, *Astrophys. J. Lett.*, *626*, L37–L40, doi:10.1086/431649, 2005.
- Braginskii, S. I., Transport Processes in a Plasma, *Rev. Plasma Phys.*, *1*, 205–+, 1965.
- Brizard, A., Nonlinear gyrofluid description of turbulent magnetized plasmas, *Physics of Fluids B*, *4*, 1213–1228, 1992.
- Brizard, A. J., and T. S. Hahm, Foundations of nonlinear gyrokinetic theory, *Reviews of Modern Physics*, *79*, 421–468, doi:10.1103/RevModPhys.79.421, 2007.
- Bruno, R., and V. Carbone, The Solar Wind as a Turbulence Laboratory, *Living Reviews in Solar Physics*, *2*, 4, 2005.
- Catto, P. J., Linearized gyro-kinetics, *Plasma Physics*, *20*, 719–722, 1978.
- Catto, P. J., W. M. Tang, and D. E. Baldwin, Generalized gyrokinetics, *Plasma Physics*, *23*, 639–650, 1981.
- Chandran, B. D. G., Weak compressible magnetohydrodynamic turbulence in the solar corona, *Phys. Rev. Lett.*, *95*, 265,004/1–4, 2006.
- Cho, J., and A. Lazarian, Compressible magnetohydrodynamic turbulence: mode coupling, scaling relations, anisotropy, viscosity-damped regime and astrophysical implications, *Mon. Not. Roy. Astron. Soc.*, *345*, 325–339, doi:10.1046/j.1365-8711.2003.06941.x, 2003.
- Cho, J., and A. Lazarian, The Anisotropy of Electron Magnetohydrodynamic Turbulence, *Astrophys. J. Lett.*, *615*, L41–L44, doi:10.1086/425215, 2004.
- Cho, J., and E. T. Vishniac, The anisotropy of magnetohydrodynamic alfvénic turbulence, *Astrophys. J.*, *539*, 273–282, 2000.
- Cho, J., A. Lazarian, and E. T. Vishniac, Simulations of Magnetohydrodynamic Turbulence in a Strongly Magnetized Medium, *Astrophys. J.*, *564*, 291–301, doi:10.1086/324186, 2002.
- Coleman, P. J., Jr., Turbulence, Viscosity, and Dissipation in the Solar-Wind Plasma, *Astrophys. J.*, *153*, 371, 1968.
- Cranmer, S. R., and A. A. van Ballegoijen, Alfvénic Turbulence in the Extended Solar Corona: Kinetic Effects and Proton Heating, *Astrophys. J.*, *594*, 573–591, doi:10.1086/376777, 2003.
- Cranmer, S. R., and A. A. van Ballegoijen, On the Generation, Propagation, and Reflection of Alfvén Waves from the Solar Photosphere to the Distant Heliosphere, *Astrophys. J. Supp.*, *156*, 265–293, doi:10.1086/426507, 2005.
- Cranmer, S. R., A. A. van Ballegoijen, and R. J. Edgar, Self-consistent Coronal Heating and Solar Wind Acceleration from Anisotropic Magnetohydrodynamic Turbulence, *Astrophys. J. Supp.*, *171*, 520–551, doi:10.1086/518001, 2007.
- Dasso, S., L. J. Milano, W. H. Matthaeus, and C. W. Smith, Anisotropy in Fast and Slow Solar Wind Fluctuations, *Astrophys. J. Lett.*, *635*, L181–L184, doi:10.1086/499559, 2005.
- Denskat, K. U., H. J. Beinroth, and F. M. Neubauer, Interplanetary magnetic field power spectra with frequencies from 2.4 X 10 to the -5th HZ to 470 HZ from HELIOS-observations during solar minimum conditions, *Journal of Geophysics Zeitschrift Geophysik*, *54*, 60–67, 1983.
- Dmitruk, P., L. J. Milano, and W. H. Matthaeus, Wave-driven Turbulent Coronal Heating in Open Field Line Regions: Non-linear Phenomenological Model, *Astrophys. J.*, *548*, 482–491, doi:10.1086/318685, 2001.
- Dmitruk, P., W. H. Matthaeus, L. J. Milano, S. Oughton, G. P. Zank, and D. J. Mullan, Coronal Heating Distribution Due to Low-Frequency, Wave-driven Turbulence, *Astrophys. J.*, *575*, 571–577, doi:10.1086/341188, 2002.
- Dobrowolny, M., A. Mangeney, and P. Veltri, Fully Developed Anisotropic Hydromagnetic Turbulence in Interplanetary Space, *Phys. Rev. Lett.*, *45*, 144–147, 1980.
- Dubin, D. H. E., J. A. Krommes, C. Oberman, and W. W. Lee, Nonlinear gyrokinetic equations, *Physics of Fluids*, *26*, 3524–3535, 1983.
- Eviatar, A., and M. Schulz, Ion-temperature anisotropies and the structure of the solar wind, *Planet. Space Sci.*, *18*, 321–+, 1970.
- Fredricks, R. W., and F. V. Coroniti, Ambiguities in the deduction of rest frame fluctuation spectrums from spectrums computed in moving frames, *J. Geophys. Res.*, *81*, 5591–5595, 1976.
- Frieman, E. A., and L. Chen, Nonlinear gyrokinetic equations for low-frequency electromagnetic waves in general plasma equilibria, *Physics of Fluids*, *25*, 502–508, 1982.
- Galtier, S., Wave turbulence in incompressible hall magnetohydrodynamics, *J. Plasma Phys.*, *72*, 721–769, 2006.
- Galtier, S., S. V. Nazarenko, A. C. Newell, and A. Pouquet, A weak turbulence theory for incompressible magnetohydrodynamics, *J. Plasma Phys.*, *63*, 447–488, 2000.
- Gary, S. P., Collisionless dissipation wavenumber: Linear theory, *J. Geophys. Res.*, *104*, 6759–6762, doi:10.1029/1998JA900161, 1999.
- Gary, S. P., and J. E. Borovsky, Alfvén-cyclotron fluctuations: Linear Vlasov theory, *Journal of Geophysical Research (Space Physics)*, *109*, 6105–+, doi:10.1029/2004JA010399, 2004.
- Gary, S. P., M. D. Montgomery, W. C. Feldman, and D. W. Forslund, Proton temperature anisotropy instabilities in the solar wind, *J. Geophys. Res.*, *81*, 1241–1246, 1976.
- Goldreich, P., and S. Sridhar, Toward a theory of interstellar turbulence ii. strong alfvénic turbulence, *Astrophys. J.*, *438*, 763–775, 1995.
- Goldreich, P., and S. Sridhar, Magnetohydrodynamic turbulence revisited, *Astrophys. J.*, *485*, 680–688, 1997.
- Goldstein, M. L., D. A. Roberts, and C. A. Fitch, Properties of the fluctuating magnetic helicity in the inertial and dissipation ranges of solar wind turbulence, *J. Geophys. Res.*, *99*, 11,519–11,538, doi:10.1029/94JA00789, 1994.
- Goldstein, M. L., D. A. Roberts, and W. H. Matthaeus, Magnetohydrodynamic Turbulence In The Solar Wind, *Ann. Rev. Astron. Astrophys.*, *33*, 283–326, doi:10.1146/annurev.aa.33.090195.001435, 1995.
- Grappin, R., J. Leorat, and A. Pouquet, Dependence of MHD turbulence spectra on the velocity field-magnetic field correlation, *Astron. Astrophys.*, *126*, 51–58, 1983.
- Grappin, R., A. Mangeney, and E. Marsch, On the origin of solar wind MHD turbulence - HELIOS data revisited, *J. Geophys. Res.*, *95*, 8197–8209, 1990.
- Gruzinov, A. V., Radiative Efficiency of Collisionless Accretion, *Astrophys. J.*, *501*, 787–+, doi:10.1086/305845, 1998.
- Habbal, S. R., R. Woo, S. Fineschi, R. O’Neal, J. Kohl, G. Noci, and C. Korendyke, Origins of the Slow and the Ubiquitous Fast Solar Wind, *Astrophys. J. Lett.*, *489*, L103+, doi:10.1086/310970, 1997.
- Hahm, T. S., W. W. Lee, and A. Brizard, Nonlinear gyrokinetic theory for finite-beta plasmas, *Physics of Fluids*, *31*, 1940–1948, 1988.
- Hellinger, P., P. Trávníček, J. C. Kasper, and A. J. Lazarus, Solar wind proton temperature anisotropy: Linear theory and WIND/SWE observations, *Geophys. Res. Lett.*, *33*, 9101–+, doi:10.1029/2006GL025925, 2006.
- Higdon, J. C., Density fluctuations in the interstellar medium: Evidence for anisotropic magnetogasdynamic turbulence i. model and astrophysical sites, *Astrophys. J.*, *285*, 109–123, 1984.
- Hollweg, J. V., Transition region, corona, and solar wind in coronal holes, *J. Geophys. Res.*, *91*, 4111–4125, 1986.
- Horbury, T. S., Waves and Turbulence in the Solar Wind – an Overview, in *Plasma Turbulence and Energetic Particles in Astrophysics, Proceedings of the International Conference, Cracow (Poland), 5-10 September 1999*, Eds.: Michał Ostrowski, Reinhard Schlickeiser, Obserwatorium Astronomiczne, Uniwersytet Jagielloński, Kraków 1999, p. 115–134., edited by M. Ostrowski and R. Schlickeiser, pp. 115–134, 1999.

- Hossain, M., P. C. Gray, D. H. Pontius, Jr., W. H. Matthaeus, and S. Oughton, Phenomenology for the decay of energy-containing eddies in homogeneous MHD turbulence, *Phys. Fluids*, **7**, 2886–2904, 1995.
- Howes, G. G., Inertial range turbulence in kinetic plasmas, *Phys. Plasmas*, submitted, arXiv:0711.4358, 2008.
- Howes, G. G., S. C. Cowley, W. Dorland, G. W. Hammett, E. Quataert, and A. A. Schekochihin, Astrophysical Gyrokinetics: Basic Equations and Linear Theory, *Astrophys. J.*, **651**, 590–614, doi:10.1086/506172, 2006.
- Howes, G. G., W. Dorland, S. C. Cowley, G. W. Hammett, E. Quataert, A. A. Schekochihin, and T. Tatsuno, Kinetic Simulations of Magnetized Turbulence in Astrophysical Plasmas, *Phys. Rev. Lett.*, accepted, arXiv:0711.4355, 2008.
- Iroshnikov, R. S., The turbulence of a conducting fluid in a strong magnetic field, *Astron. Zh.*, **40**, 742, English Translation: *Sov. Astron.*, **7** 566 (1964), 1963.
- Isenberg, P. A., Investigations of a turbulence-driven solar wind model, *J. Geophys. Res.*, **95**, 6437–6442, 1990.
- Kasper, J. C., A. J. Lazarus, and S. P. Gary, Wind/SWE observations of firehose constraint on solar wind proton temperature anisotropy, *Geophys. Res. Lett.*, **29**, 20–1, 2002.
- Kingsep, A. S., K. V. Chukbar, and V. V. Yankov, Collisionless Heating of the Solar-Wind Plasma. II. Application of the Theory of Plasma Heating by Hydromagnetic Waves, *Rev. Plasma Phys.*, **16**, 243, 1990.
- Kohl, J. L., G. Noci, E. Antonucci, G. Tondello, M. C. E. Huber, L. D. Gardner, P. Nicolosi, L. Strachan, S. Fineschi, J. C. Raymond, M. Romoli, D. Spadaro, A. Panasyuk, O. H. W. Siegmund, C. Benna, A. Ciaravella, S. R. Cranmer, S. Giordano, M. Karovska, R. Martin, J. Michels, A. Modigliani, G. Naletto, C. Pernechele, G. Poletto, and P. L. Smith, First Results from the SOHO Ultraviolet Coronagraph Spectrometer, *Sol. Phys.*, **175**, 613–644, doi:10.1023/A:1004903206467, 1997.
- Kohl, J. L., G. Noci, E. Antonucci, G. Tondello, M. C. E. Huber, S. R. Cranmer, L. Strachan, A. V. Panasyuk, L. D. Gardner, M. Romoli, S. Fineschi, D. Dobrzycka, J. C. Raymond, P. Nicolosi, O. H. W. Siegmund, D. Spadaro, C. Benna, A. Ciaravella, S. Giordano, S. R. Habbal, M. Karovska, X. Li, R. Martin, J. G. Michels, A. Modigliani, G. Naletto, R. H. O’Neal, C. Pernechele, G. Poletto, P. L. Smith, and R. M. Suleiman, UVCS/SOHO Empirical Determinations of Anisotropic Velocity Distributions in the Solar Corona, *Astrophys. J. Lett.*, **501**, L127+, doi:10.1086/311434, 1998.
- Kohl, J. L., G. Noci, S. R. Cranmer, and J. C. Raymond, Ultraviolet spectroscopy of the extended solar corona, *Astron. Astrophys. Rev.*, **13**, 31–157, doi:10.1007/s00159-005-0026-7, 2006.
- Kolmogorov, A. N., The local structure of turbulence in incompressible viscous fluid for very large Reynolds numbers, *Dokl. Akad. Nauk SSSR*, **30**, 9–, English Translation: *Proc. Roy. Soc. London A*, **434**, 9 (1991), 1941.
- Kraichnan, R. H., Inertial range spectrum of hydromagnetic turbulence, *Phys. Fluids*, **8**, 1385–1387, 1965.
- Krishan, V., and S. M. Mahajan, Magnetic fluctuations and Hall magnetohydrodynamic turbulence in the solar wind, *J. Geophys. Res.*, **109**, 11,105+, doi:10.1029/2004JA010496, 2004.
- Leamon, R. J., W. H. Matthaeus, C. W. Smith, and H. K. Wong, Contribution of cyclotron-resonant damping to kinetic dissipation of interplanetary turbulence, *Astrophys. J.*, **507**, L181–L184, 1998a.
- Leamon, R. J., C. W. Smith, N. F. Ness, W. H. Matthaeus, and H. K. Wong, Observational constraints on the dynamics of the interplanetary magnetic field dissipation range, *J. Geophys. Res.*, **103**, 4775–4787, 1998b.
- Leamon, R. J., C. W. Smith, N. F. Ness, and H. K. Wong, Dissipation range dynamics: Kinetic Alfvén waves and the importance of  $\beta_e$ , *J. Geophys. Res.*, **104**, 22,331–22,344, 1999.
- Leamon, R. J., W. H. Matthaeus, C. W. Smith, G. P. Zank, D. J. Mullan, and S. Oughton, MHD-driven Kinetic Dissipation in the Solar Wind and Corona, *Astrophys. J.*, **537**, 1054–1062, doi:10.1086/309059, 2000.
- Leith, C. E., Diffusion approximation to inertial energy transfer in isotropic turbulence, *Phys. Fluids*, **10**, 1409–1416, 1967.
- Li, H., S. P. Gary, and O. Stawicki, On the dissipation of magnetic fluctuations in the solar wind, *Geophys. Res. Lett.*, **28**, 1347–1350, doi:10.1029/2000GL012501, 2001.
- Li, X., and S. R. Habbal, Damping of fast and ion cyclotron oblique waves in the multi-ion fast solar wind, *J. Geophys. Res.*, **106**, 10,669–10,680, doi:10.1029/2000JA000420, 2001.
- Li, X., S. R. Habbal, J. V. Hollweg, and R. Esser, Heating and cooling of protons by turbulence-driven ion cyclotron waves in the fast solar wind, *J. Geophys. Res.*, **104**, 2521–2536, doi:10.1029/1998JA900126, 1999.
- Lithwick, Y., and P. Goldreich, Compressible magnetohydrodynamic turbulence in interstellar plasmas, *Astrophys. J.*, **562**, 279–296, 2001.
- Lithwick, Y., and P. Goldreich, Imbalanced weak magnetohydrodynamic turbulence, *Astrophys. J.*, **582**, 1220–1240, 2003.
- Lithwick, Y., P. Goldreich, and S. Sridhar, Imbalanced Strong MHD Turbulence, *Astrophys. J.*, **655**, 269–274, doi:10.1086/509884, 2007.
- Maron, J., private communication, 1998.
- Maron, J., and P. Goldreich, Simulations of incompressible magnetohydrodynamic turbulence, *Astrophys. J.*, **554**, 1175–1196, 2001.
- Marsch, E., Kinetic Physics of the Solar Wind Plasma, in *Physics of the Inner Heliosphere II. Particles, Waves and Turbulence.*, edited by E. Schwenn, R. and Marsch, pp. 45–133, Springer-Verlag, Berlin, 1991.
- Marsch, E., Solar Wind Models from the Sun to 1 AU: Constraints by in Situ and Remote Sensing Measurements, *Space Science Reviews*, **87**, 1–24, doi:10.1023/A:1005137311503, 1999.
- Marsch, E., Kinetic physics of the solar corona and solar wind, *Living Reviews in Solar Physics*, **3**(1), 2006.
- Marsch, E., K. H. Muehlhaeuser, H. Rosenbauer, and R. Schwenn, On the equation of state of solar wind ions derived from HELIOS measurements, *J. Geophys. Res.*, **88**, 2982–2992, 1983.
- Matthaeus, W. H., M. L. Goldstein, and D. A. Roberts, Evidence for the presence of quasi-two-dimensional nearly incompressible fluctuations in the solar wind, *J. Geophys. Res.*, **95**, 20,673–20,683, 1990.
- Matthaeus, W. H., S. Ghosh, S. Oughton, and D. A. Roberts, Anisotropic three-dimensional MHD turbulence, *J. Geophys. Res.*, **101**, 7619–7630, doi:10.1029/95JA03830, 1996.
- Matthaeus, W. H., S. Oughton, S. Ghosh, and M. Hossain, Scaling of Anisotropy in Hydromagnetic Turbulence, *Phys. Rev. Lett.*, **81**, 2056–2059, 1998.
- Matthaeus, W. H., G. P. Zank, S. Oughton, D. J. Mullan, and P. Dmitruk, Coronal Heating by Magnetohydrodynamic Turbulence Driven by Reflected Low-Frequency Waves, *Astrophys. J. Lett.*, **523**, L93–L96, doi:10.1086/312259, 1999.
- Matthaeus, W. H., S. Dasso, J. M. Weygand, L. J. Milano, C. W. Smith, and M. G. Kivelson, Spatial Correlation of Solar-Wind Turbulence from Two-Point Measurements, *Phys. Rev. Lett.*, **95**(23), 231,101+, doi:10.1103/PhysRevLett.95.231101, 2005.
- Montgomery, D., Major disruptions, inverse cascades, and the Strauss equations, *Physica Scripta*, **T2A**, 83–88, 1982.
- Montgomery, D., and W. H. Matthaeus, Anisotropic Modal Energy Transfer in Interstellar Turbulence, *Astrophys. J.*, **447**, 706+, doi:10.1086/175910, 1995.
- Montgomery, D., and L. Turner, Anisotropic magnetohydrodynamic turbulence in a strong external magnetic field, *Phys. Fluids*, **24**, 825–831, 1981.
- Müller, W.-C., and D. Biskamp, Scaling properties of three-dimensional magnetohydrodynamic turbulence, *Phys. Rev. Lett.*, **84**(3), 475–478, doi:10.1103/PhysRevLett.84.475, 2000.
- Newbury, J. A., C. T. Russell, J. L. Phillips, and S. P. Gary, Electron temperature in the ambient solar wind: Typical properties and a lower bound at 1 AU, *J. Geophys. Res.*, **103**, 9553–9566, doi:10.1029/98JA00067, 1998.
- Ng, C. S., and A. Bhattacharjee, Interaction of Shear-Alfvén Wave Packets: Implication for Weak Magnetohydrodynamic Turbulence in Astrophysical Plasmas, *Astrophys. J.*, **465**, 845–+, doi:10.1086/177468, 1996.
- Ng, C. S., and A. Bhattacharjee, Scaling of anisotropic spectra due to the weak interaction of shear-Alfvén wave packets, *Phys. Plasmas*, **4**, 605–610, 1997.
- Oughton, S., and W. H. Matthaeus, Parallel and perpendicular cascades in solar wind turbulence, *Nonlin. Proc. Geophys.*, **12**, 299–310, 2005.
- Oughton, S., E. R. Priest, and W. H. Matthaeus, The influence of a mean magnetic field on three-dimensional magnetohydrodynamic turbulence, *Journal of Fluid Mechanics*, **280**, 95–117, 1994.

- Oughton, S., P. Dmitruk, and W. H. Matthaeus, Reduced magnetohydrodynamics and parallel spectral transfer, *Phys. Plasmas*, *11*, 2214–2225, doi:10.1063/1.1705652, 2004.
- Politano, H., A. Pouquet, and P. L. Sulem, Inertial ranges and resistive instabilities in two-dimensional magnetohydrodynamic turbulence, *Phys. Fluids B*, *1*, 2330–2339, 1989.
- Quataert, E., Particle Heating by Alfvénic Turbulence in Hot Accretion Flows, *Astrophys. J.*, *500*, 978–+, doi:10.1086/305770, 1998.
- Quataert, E., and A. Gruzinov, Turbulence and Particle Heating in Advection-dominated Accretion Flows, *Astrophys. J.*, *520*, 248–255, doi:10.1086/307423, 1999.
- Roberts, D. A., M. L. Goldstein, L. W. Klein, and W. H. Matthaeus, Origin and evolution of fluctuations in the solar wind - HELIOS observations and Helios-Voyager comparisons, *J. Geophys. Res.*, *92*, 12,023–12,035, 1987.
- Roberts, D. A., S. Ghosh, M. L. Goldstein, and W. H. Matthaeus, Magnetohydrodynamic simulation of the radial evolution and stream structure of solar-wind turbulence, *Phys. Rev. Lett.*, *67*(27), 3741–3744, doi:10.1103/PhysRevLett.67.3741, 1991.
- Roberts, D. A., M. L. Goldstein, W. H. Matthaeus, and S. Ghosh, Velocity shear generation of solar wind turbulence, *J. Geophys. Res.*, *97*, 17,115–+, 1992.
- Robinson, D. C., and M. G. Rusbridge, Structure of turbulence in the zeta plasma, *Phys. Fluids*, *14*, 2499–2511, 1971.
- Ruderman, M. S., M. L. Goldstein, D. A. Roberts, A. Deane, and L. Ofman, Alfvén wave phase mixing driven by velocity shear in two-dimensional open magnetic configurations, *J. Geophys. Res.*, *104*, 17,057–17,068, doi:10.1029/1999JA900144, 1999.
- Rutherford, P. H., and E. A. Frieman, Drift Instabilities in General Magnetic Field Configurations, *Physics of Fluids*, *11*, 569–585, 1968.
- Scarf, F. L., J. H. Wolfe, and R. W. Silva, A Plasma Instability Associated with Thermal Anisotropies in the Solar Wind, *J. Geophys. Res.*, *72*, 993–+, 1967.
- Schekochihin, A. A., S. C. Cowley, W. Dorland, G. W. Hammett, G. G. Howes, E. Quataert, and T. Tatsuno, Kinetic and Fluid Turbulent Cascades in Magnetized Weakly Collisional Astrophysical Plasmas, *Astrophys. J. Supp.*, submitted, arXiv:0704.0044, 2007.
- Shaikh, D., and G. P. Zank, Driven dissipative whistler wave turbulence, *Phys. Plasmas*, *12*, 2310–+, doi:10.1063/1.2146957, 2005.
- Shaikh, D., and G. P. Zank, The Transition to Incompressibility from Compressible Magnetohydrodynamic Turbulence, *Astrophys. J. Lett.*, *640*, L195–L198, doi:10.1086/503833, 2006.
- Shebalin, J. V., W. H. Matthaeus, and D. Montgomery, Anisotropy in mhd turbulence due to a mean magnetic field, *J. Plasma Phys.*, *29*, 525–547, 1983.
- Smith, C. W., D. J. Mullan, N. F. Ness, R. M. Skoug, and J. Steinberg, Day the solar wind almost disappeared: Magnetic field fluctuations, wave refraction and dissipation, *J. Geophys. Res.*, *106*, 18,625–18,634, doi:10.1029/2001JA000022, 2001.
- Smith, C. W., K. Hamilton, B. J. Vasquez, and R. J. Leamon, Dependence of the Dissipation Range Spectrum of Interplanetary Magnetic Fluctuations on the Rate of Energy Cascade, *Astrophys. J. Lett.*, *645*, L85–L88, doi:10.1086/506151, 2006.
- Sridhar, S., and P. Goldreich, Toward a theory of interstellar turbulence I. weak alfvénic turbulence, *Astrophys. J.*, *433*, 612–621, 1994.
- Stawicki, O., S. P. Gary, and H. Li, Solar wind magnetic fluctuation spectra: Dispersion versus damping, *J. Geophys. Res.*, *106*, 8273–8282, doi:10.1029/2000JA000446, 2001.
- Stix, T. H., *Waves in Plasmas*, New York: American Institute of Physics, 1992, 1992.
- Strauss, H. R., Nonlinear, three-dimensional magnetohydrodynamics of noncircular tokamaks, *Phys. Fluids*, *19*, 134–140, 1976.
- Taylor, G. I., The Spectrum of Turbulence, *Proc. Roy. Soc. A*, *164*, 476–490, 1938.
- Taylor, J. B., and R. J. Hastie, Stability of general plasma equilibria - I formal theory, *Plasma Physics*, *10*, 479–494, 1968.
- Tu, C.-Y., The damping of interplanetary Alfvénic fluctuations and the heating of the solar wind, *J. Geophys. Res.*, *93*, 7–20, 1988.
- Tu, C.-Y., and E. Marsch, Evidence for a 'background' spectrum of solar wind turbulence in the inner heliosphere, *J. Geophys. Res.*, *95*, 4337–4341, 1990.
- Tu, C.-Y., and E. Marsch, MHD structures, waves and turbulence in the solar wind: Observations and theories, *Space Science Reviews*, *73*, 1–2, 1995.
- Tu, C.-Y., Z.-Y. Pu, and F.-S. Wei, The power spectrum of interplanetary Alfvénic fluctuations Derivation of the governing equation and its solution, *J. Geophys. Res.*, *89*, 9695–9702, 1984.
- Tu, C.-Y., E. Marsch, and H. Rosenbauer, The dependence of MHD turbulence spectra on the inner solar wind stream structure near solar minimum, *Geophys. Res. Lett.*, *17*, 283–286, 1990.
- Tu, C.-Y., C. Zhou, E. Marsch, L.-D. Xia, L. Zhao, J.-X. Wang, and K. Wilhelm, Solar Wind Origin in Coronal Funnel, *Science*, *308*, 519–523, doi:10.1126/science.1109447, 2005.
- Vestuto, J. G., E. C. Ostriker, and J. M. Stone, Spectral Properties of Compressible Magnetohydrodynamic Turbulence from Numerical Simulations, *Astrophys. J.*, *590*, 858–873, doi:10.1086/375021, 2003.
- Woo, R., and S. R. Habbal, Origin and Acceleration of the Slow Solar Wind, *Astrophys. J. Lett.*, *629*, L129–L132, doi:10.1086/447767, 2005.
- Woo, R., S. R. Habbal, and U. Feldman, Role of Closed Magnetic Fields in Solar Wind Flow, *Astrophys. J.*, *612*, 1171–1174, doi:10.1086/422799, 2004.
- Zank, G. P., W. H. Matthaeus, and C. W. Smith, Evolution of turbulent magnetic fluctuation power with heliospheric distance, *J. Geophys. Res.*, *101*, 17,093–17,108, doi:10.1029/96JA01275, 1996.
- Zhou, Y., and W. H. Matthaeus, Transport and turbulence modeling of solar wind fluctuations, *J. Geophys. Res.*, *95*, 10,291–10,311, 1990a.
- Zhou, Y., and W. H. Matthaeus, Models of inertial range spectra of interplanetary magnetohydrodynamic turbulence, *J. Geophys. Res.*, *95*, 14,881–14,892, 1990b.
- Zhou, Y., and W. H. Matthaeus, Phenomenology treatment of magnetohydrodynamic turbulence with nonequipartition and anisotropy, *Phys. Plasmas*, *12*, 6503–+, doi:10.1063/1.1887187, 2005.
- Zweibel, S. J., C. R. Menyuk, and R. J. Taylor, Small-scale magnetic fluctuations inside the macro-tokamak, *Phys. Rev. Lett.*, *42*, 1270–1274, 1979.

---

G. G. Howes, Department of Astronomy, University of California, 601 Campbell Hall, Berkeley, CA 94720, USA. (ghowes@astro.berkeley.edu)

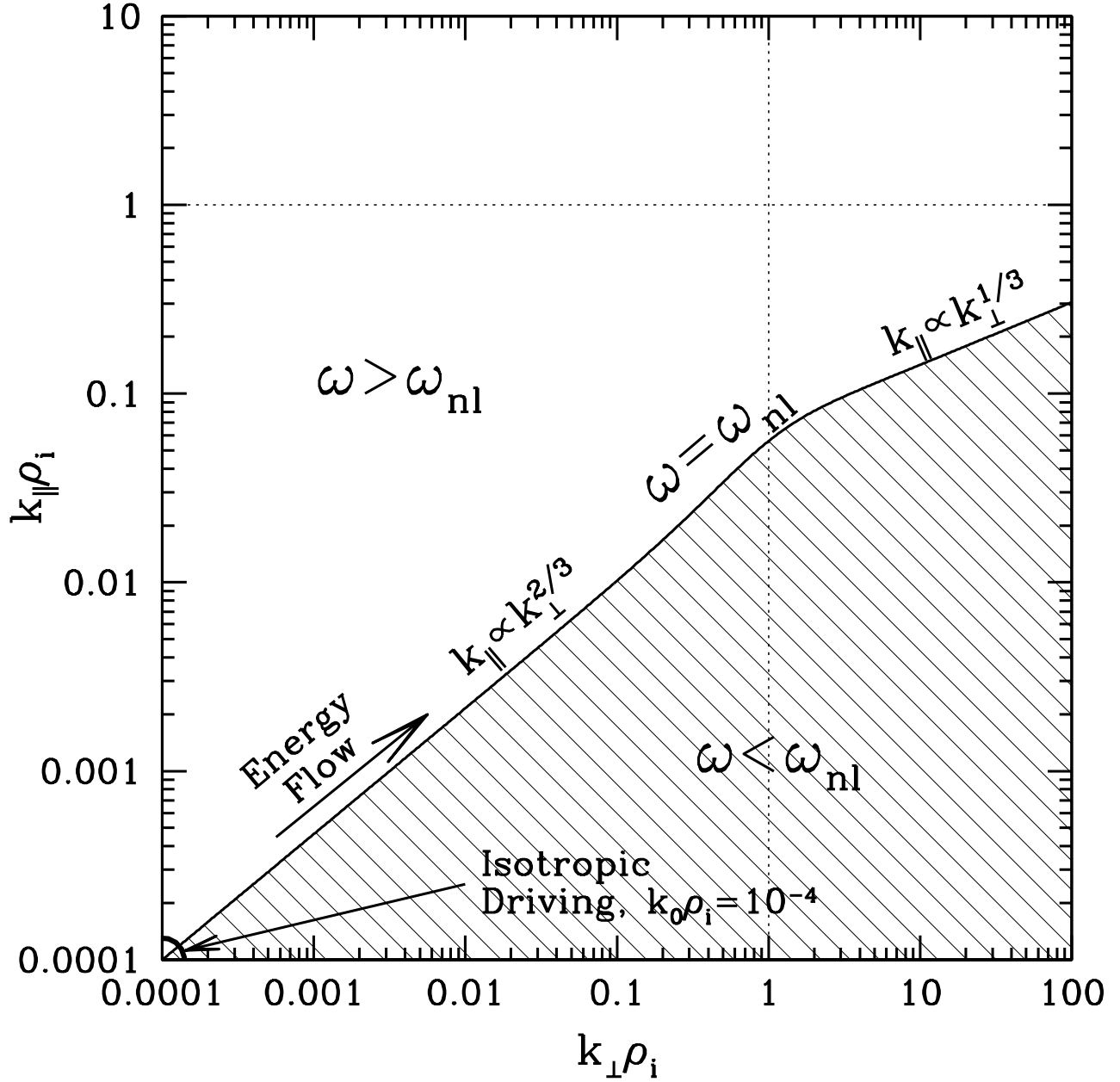


**Figure 1.** Schematic diagram of the nonlinear transfer of energy across the  $(k_{\perp}, k_{\parallel})$  plane from the low driving wavenumber to high wavenumbers where the turbulence is dissipated by kinetic processes. Driving is chosen to be isotropic at a wavenumber  $k_0\rho_i = 10^{-4}$ . Critical balance,  $\omega = \omega_{nl}$ , defines a one-dimensional path for the turbulent cascade of energy on the  $(k_{\perp}, k_{\parallel})$  plane denoted by the solid line. Numerical simulations show turbulent energy over the entire shaded region, in which  $\omega \leq \omega_{nl}$ . The cascade model constructed in this paper can be thought of as describing energy integrated over all  $k_{\parallel}$  at each value of  $k_{\perp}$ .

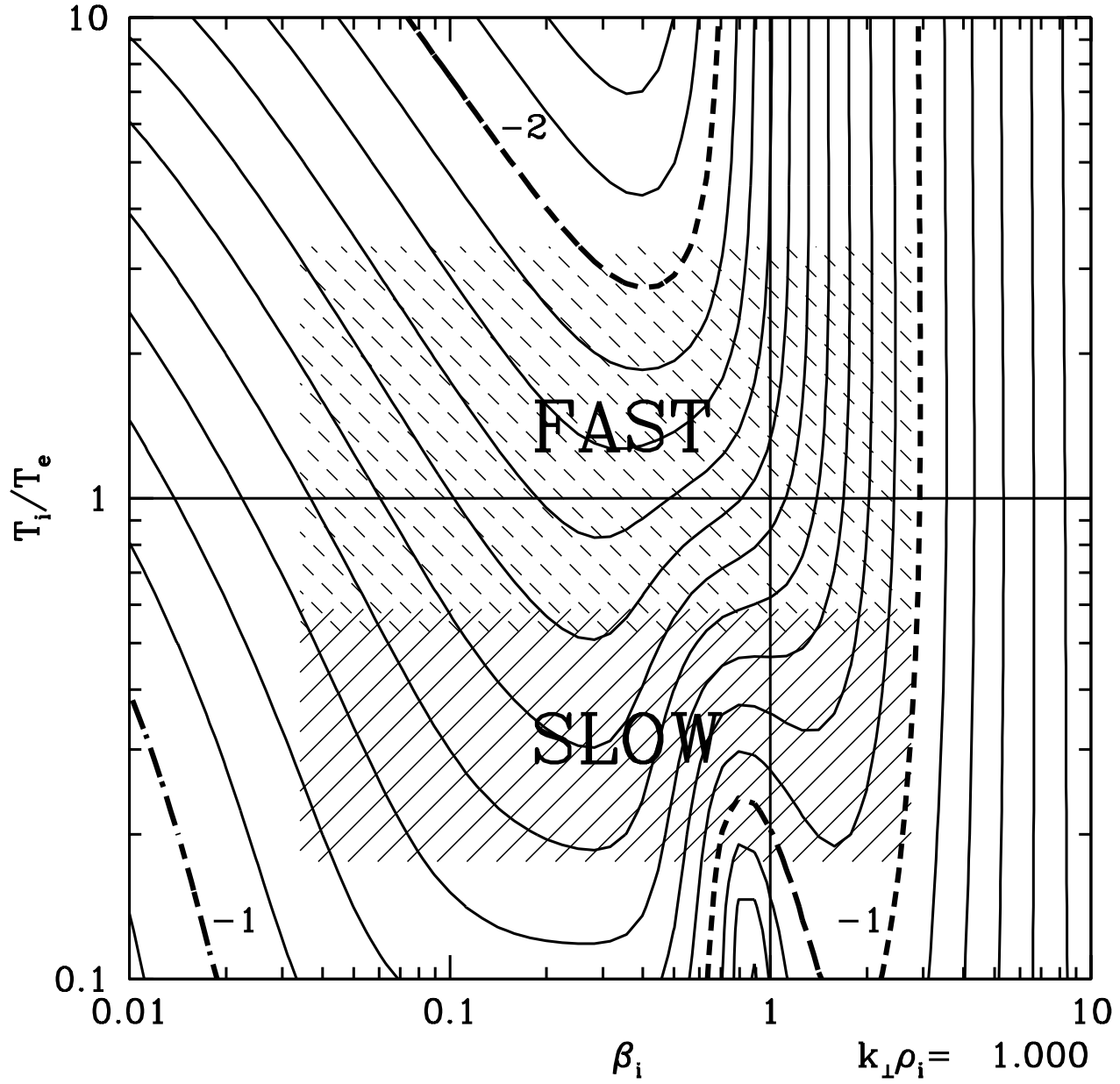


**Figure 2.** Contours of  $\log(\gamma/\omega)$  on the plane  $(\beta_i, T_i/T_e)$  for  $k_{\perp}\rho_i = 1$ . The solid shading corresponds to the range of parameters in the slow solar wind, the dashed shading to the fast solar wind. Contours are spaced at  $\Delta \log(\gamma/\omega) = 0.1$  with thick dashed lines at each unit of the logarithm; contour values for each logarithmic unit are denoted.

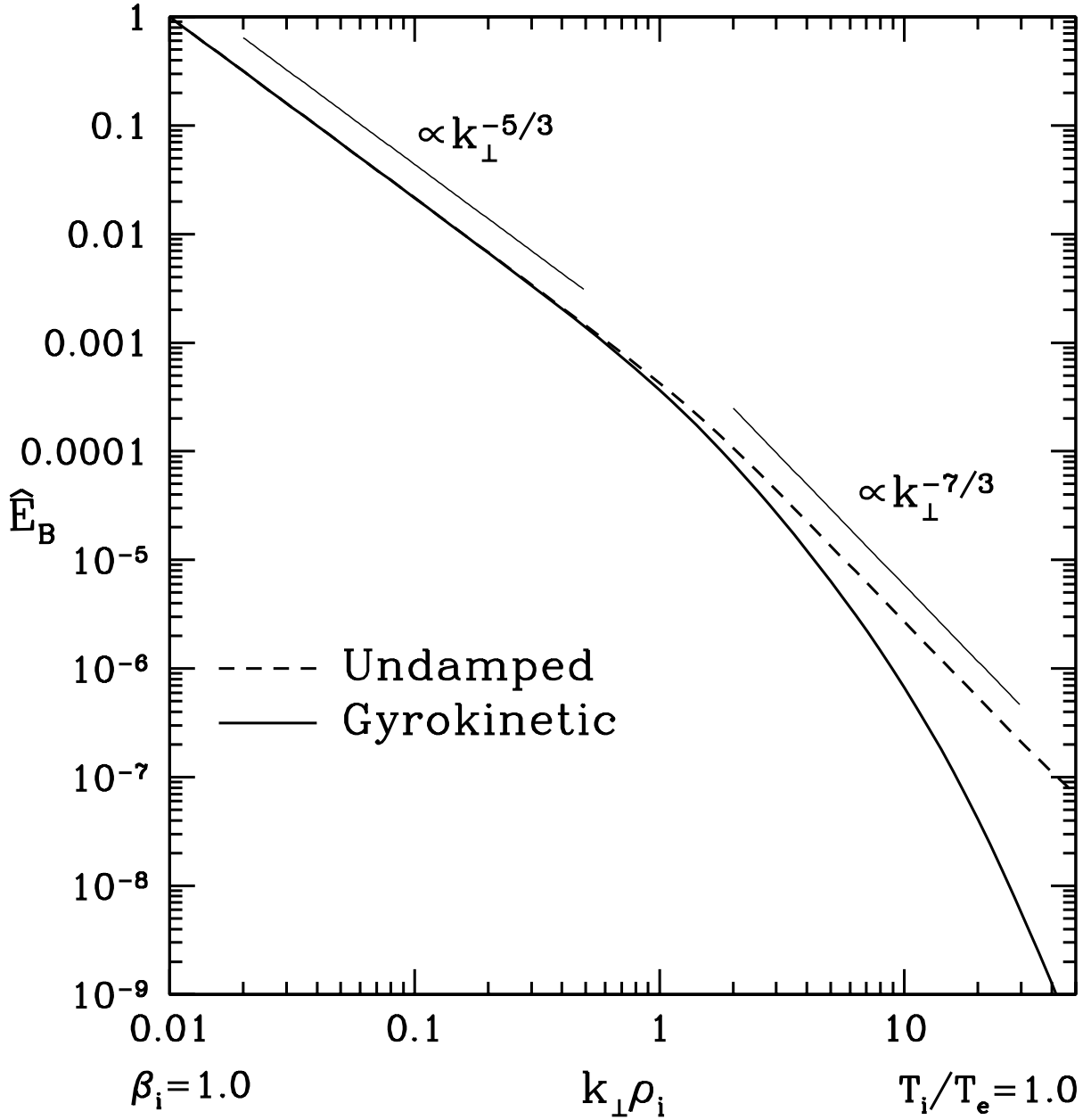


**Figure 3.** One-dimensional magnetic energy spectra for the turbulent cascade from the MHD to the kinetic Alfvén wave regime. The chosen parameters are  $\beta_i = 1$  and  $T_i/T_e = 1$ . Solutions of our cascade model with no damping (dashed) and with the gyrokinetic damping rate (solid) are shown.

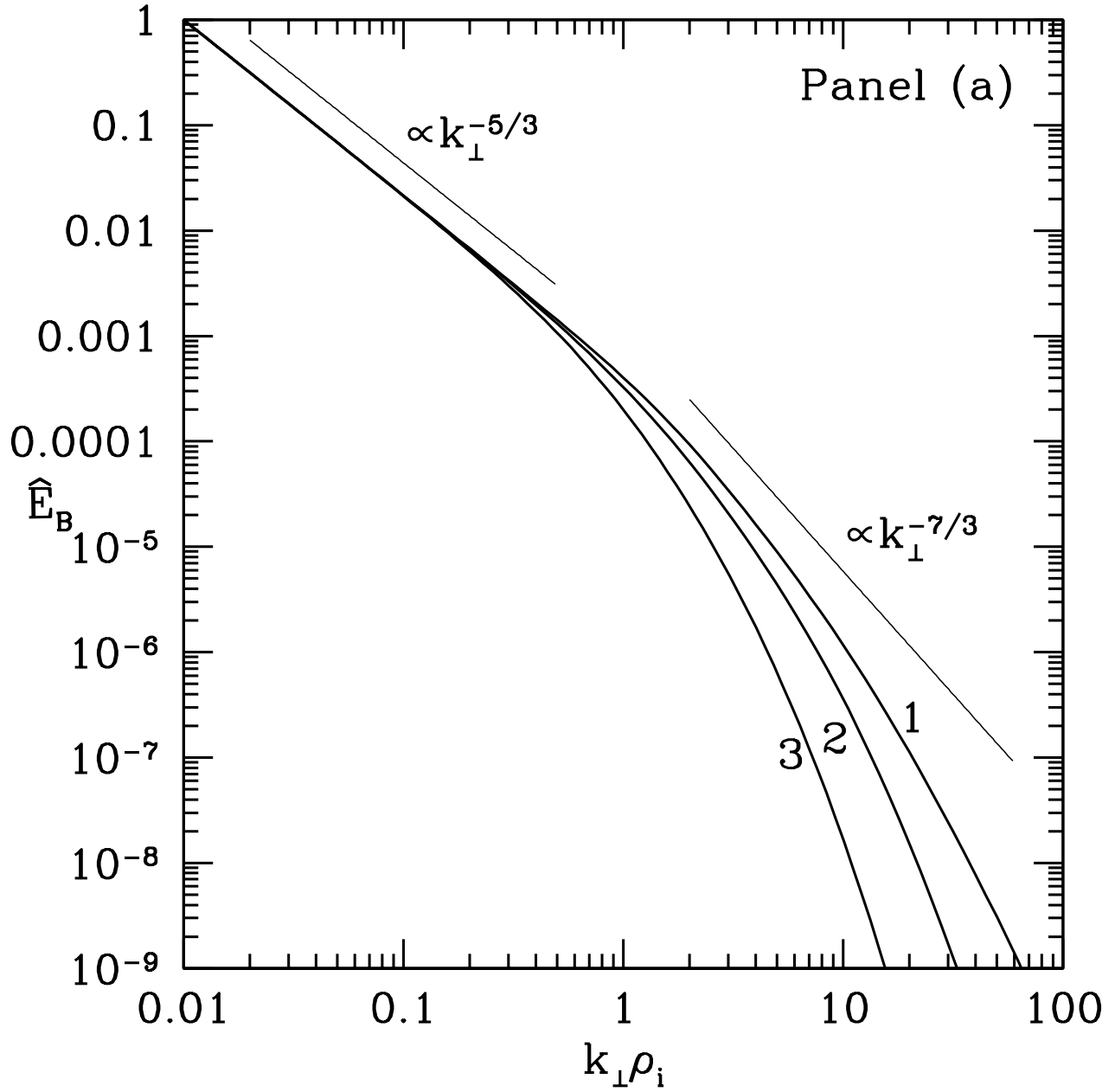


**Figure 4.** One-dimensional magnetic energy spectra for three gyrokinetic models: (1)  $\beta_i = 0.5$ ,  $T_i/T_e = 3$ , (2)  $\beta_i = 3$ ,  $T_i/T_e = 0.6$ , (3)  $\beta_i = 0.03$ ,  $T_i/T_e = 0.175$ . Panel (a) shows that all three spectra demonstrate a dissipative roll-off that cannot be fit by a single spectral index  $k_{\perp}\rho_i > 1$  (consistent with an exponential roll-off).

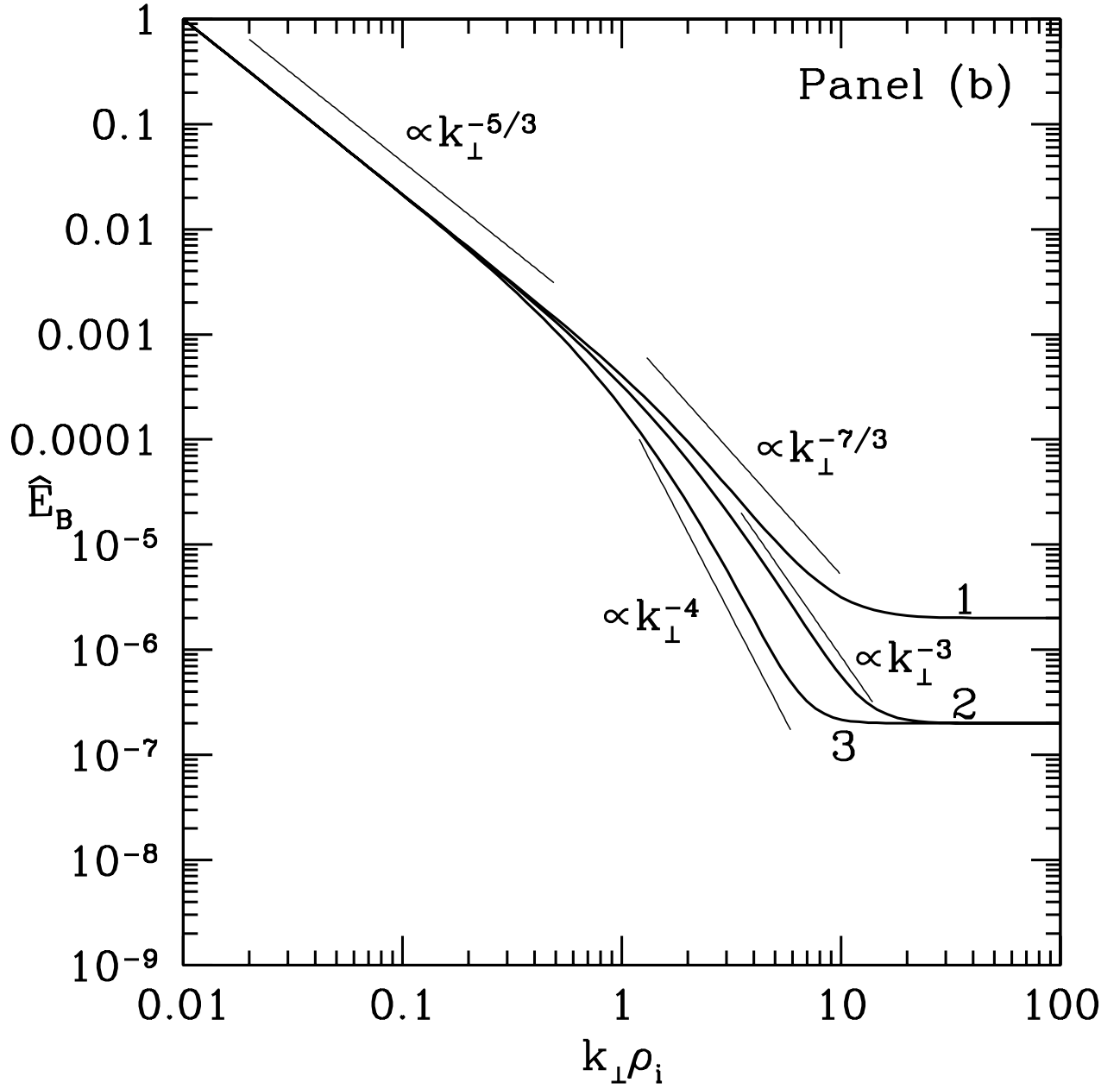


**Figure 5.** One-dimensional magnetic energy spectra for three gyrokinetic models: (1)  $\beta_i = 0.5$ ,  $T_i/T_e = 3$ , (2)  $\beta_i = 3$ ,  $T_i/T_e = 0.6$ , (3)  $\beta_i = 0.03$ ,  $T_i/T_e = 0.175$ . Panel (b) shows the same spectra as panel (a) with an added constant sensitivity limit, which causes resulting the spectra to resemble power laws. The sensitivity limit is two orders of magnitude below the value of the spectrum at  $k_\perp \rho_i = 1$  for spectrum 1, three for spectra 2 and 3.

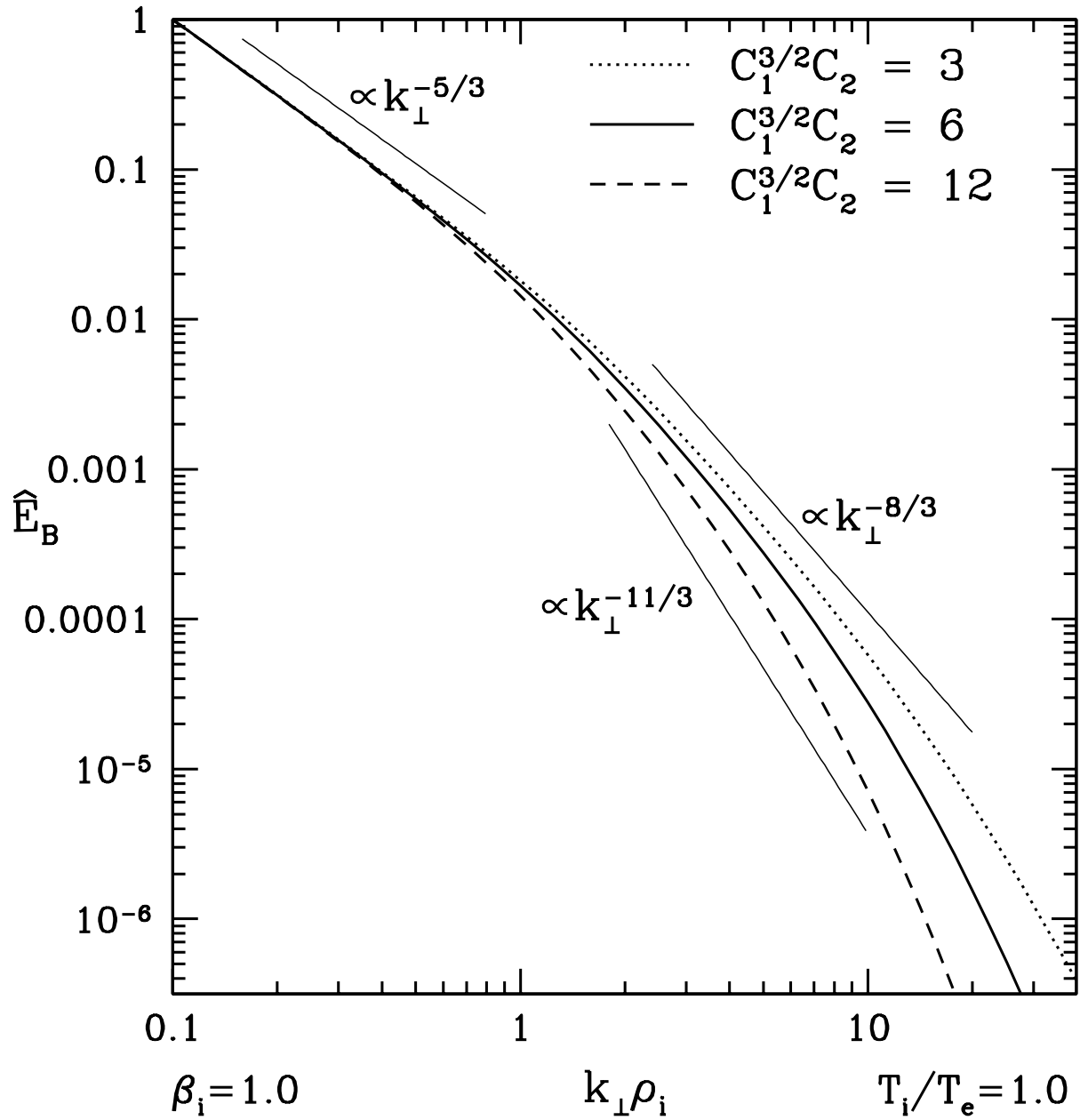


**Figure 6.** The effect of changing the Kolmogorov constants over a range of values  $C_1^{3/2}C_2 = 3, 6,$  and  $12$ . The measured effective spectral index in the dissipation range varies by  $+1/3$  or  $-2/3$ .

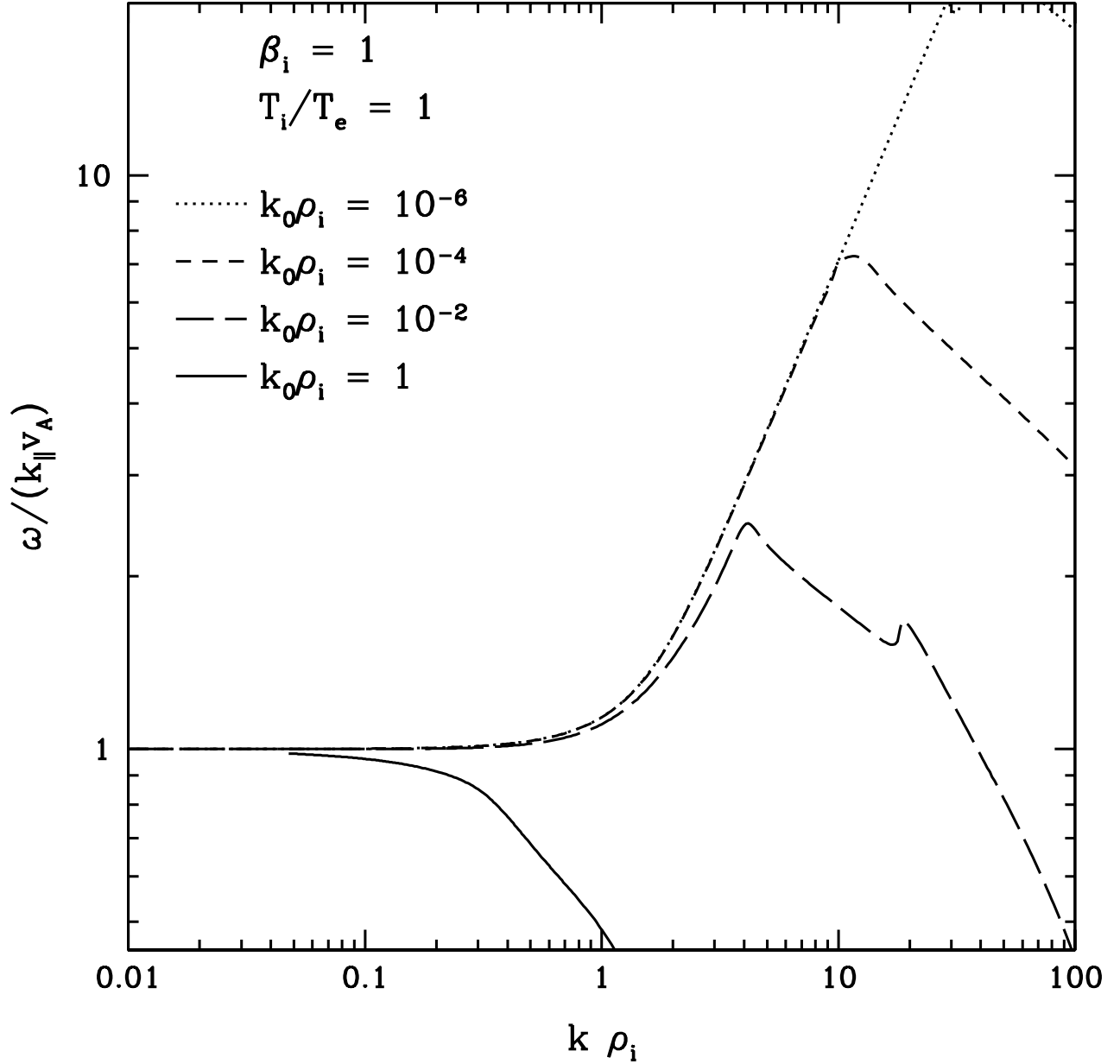


**Figure 7.** The normalized wave phase velocity  $\omega/(k_{\parallel} v_A)$  vs. wavenumber  $k \rho_i$  for models with different assumptions about the anisotropy of the fluctuations. The calculations use the full linear plasma dispersion relation for a collisionless plasma with  $\beta_i = 1$  and  $T_i/T_e = 1$ . We assume a critically balanced cascade with the parallel wavenumber governed by equation (11) with no dissipation,  $\epsilon = \epsilon_0$ , and driving scales  $k_0 \rho_i = 10^{-6}, 10^{-4}, 10^{-2}$ , and 1. The rise in wave phase velocity at  $k \rho_i \sim 1$  for  $k_0 \rho_i \ll 1$  is due to the transition to kinetic Alfvén waves; this is consistent with the *in situ* measurements by [Bale *et al.*, 2005]. The turn-down in wave phase velocity, due to the onset of ion cyclotron damping, is not observed.

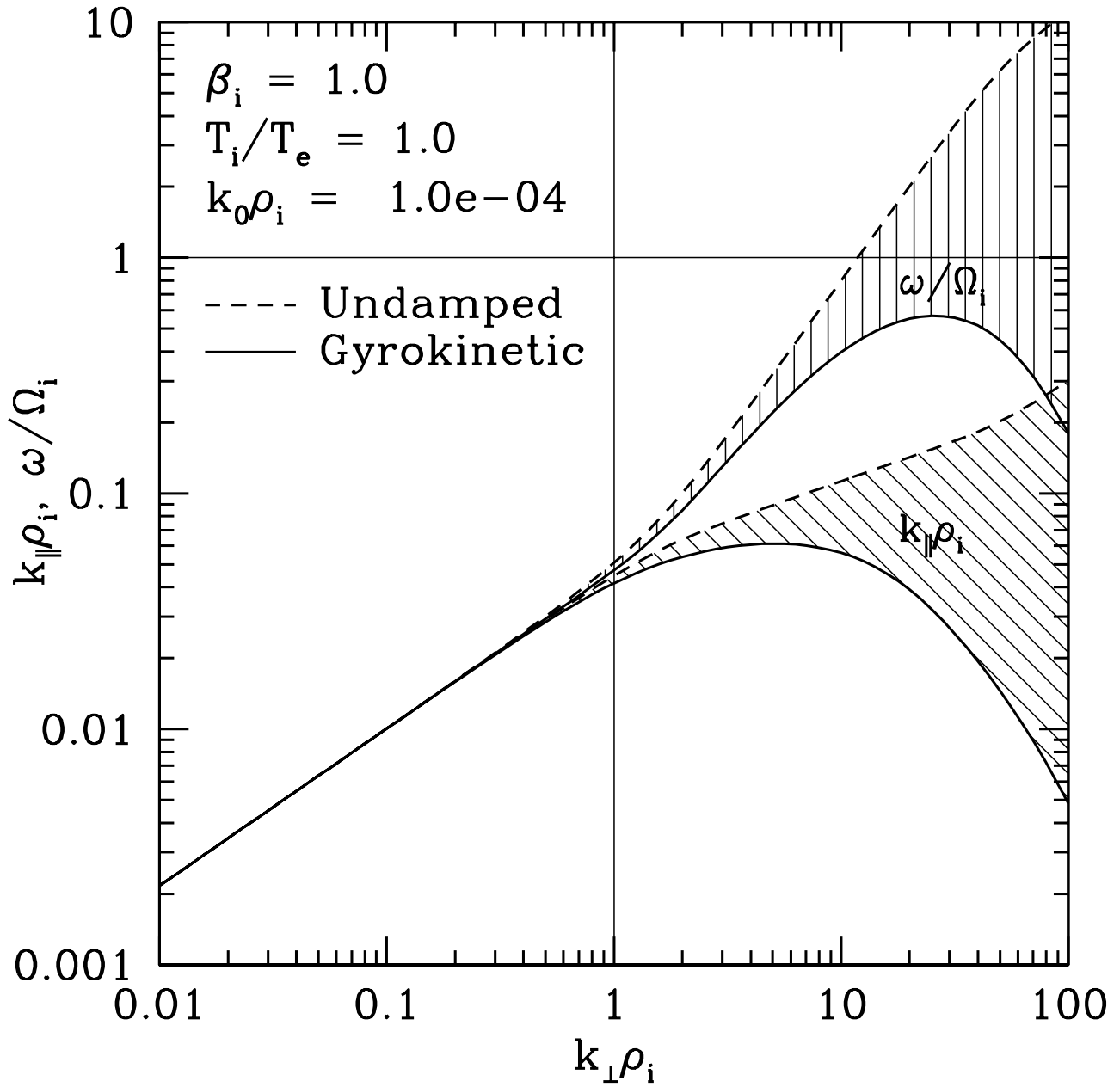


**Figure 8.** The frequency  $\omega/\Omega_i$  [equation (15)] and parallel wavenumber  $k_{\parallel}\rho_i$  vs.  $k_{\perp}\rho_i$  [equation (11)] for undamped (dashed) and gyrokinetic (solid) steady-state solutions of the gyrokinetic cascade model. If the damping of nonlinear turbulent fluctuations is less than or equal to the linear gyrokinetic damping rates, then the nonlinear frequency should lie within the vertically shaded region and the parallel wavenumber within the diagonally shaded region. The effective damping clearly plays a strong role in determining whether the turbulent fluctuations reach the cyclotron frequency,  $\omega/\Omega_i \simeq 1$ .

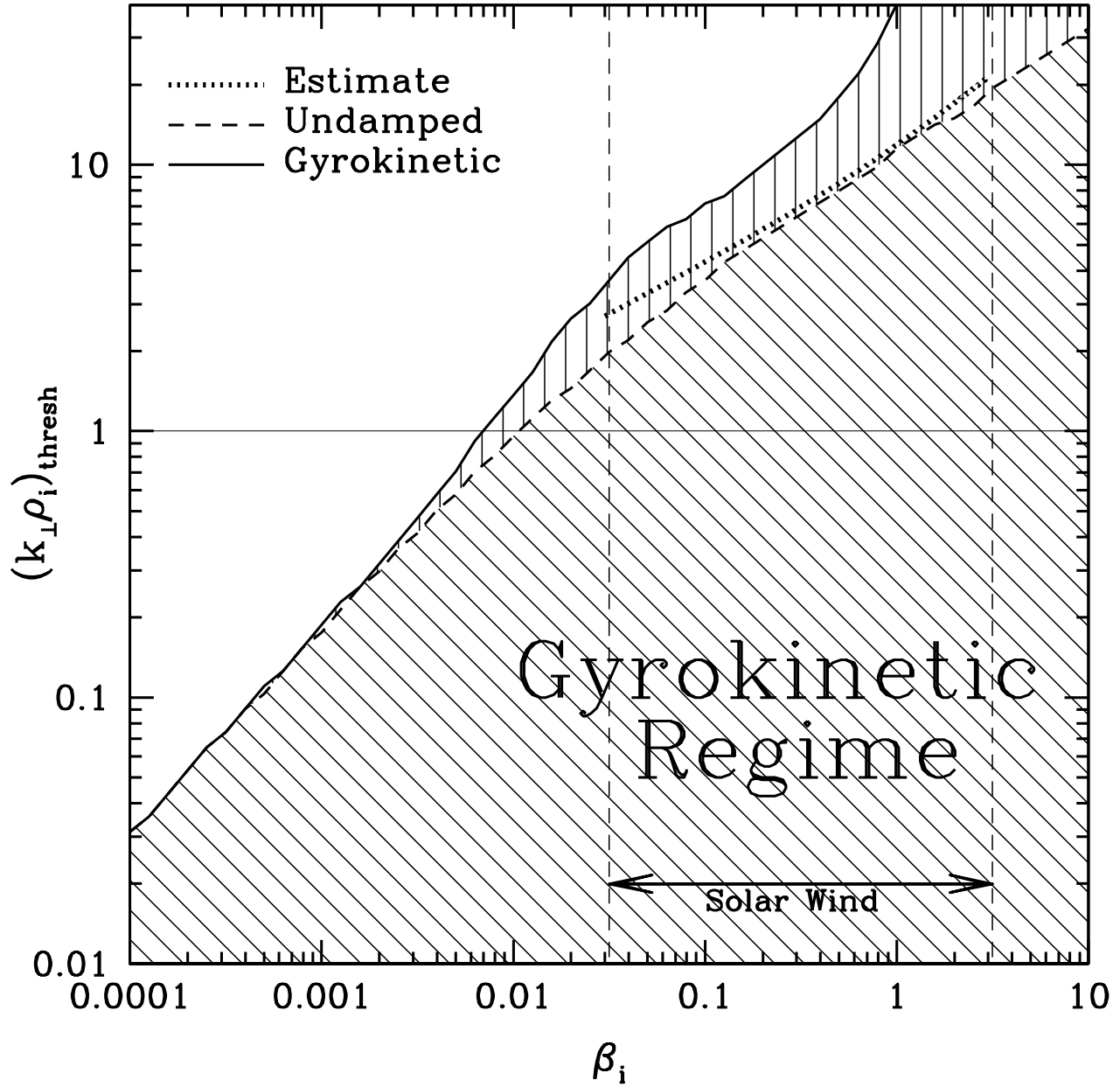


**Figure 9.** The threshold value of  $k_{\perp}\rho_i$  at which the ion cyclotron resonance has an effect on the linear wave modes with  $k_0\rho_i = 10^{-4}$  and  $T_i/T_e = 1$ . The threshold is determined by comparing the solutions of the gyrokinetic and hot plasma dispersion relations. The solid and dashed lines correspond to the path in the  $(k_{\perp}, k_{\parallel})$  plane calculated from the gyrokinetic model with and without damping, respectively; the dotted line is the analytical estimate given by equation (16) (only plotted for the typical range of  $\beta_i$  in the solar wind near Earth).

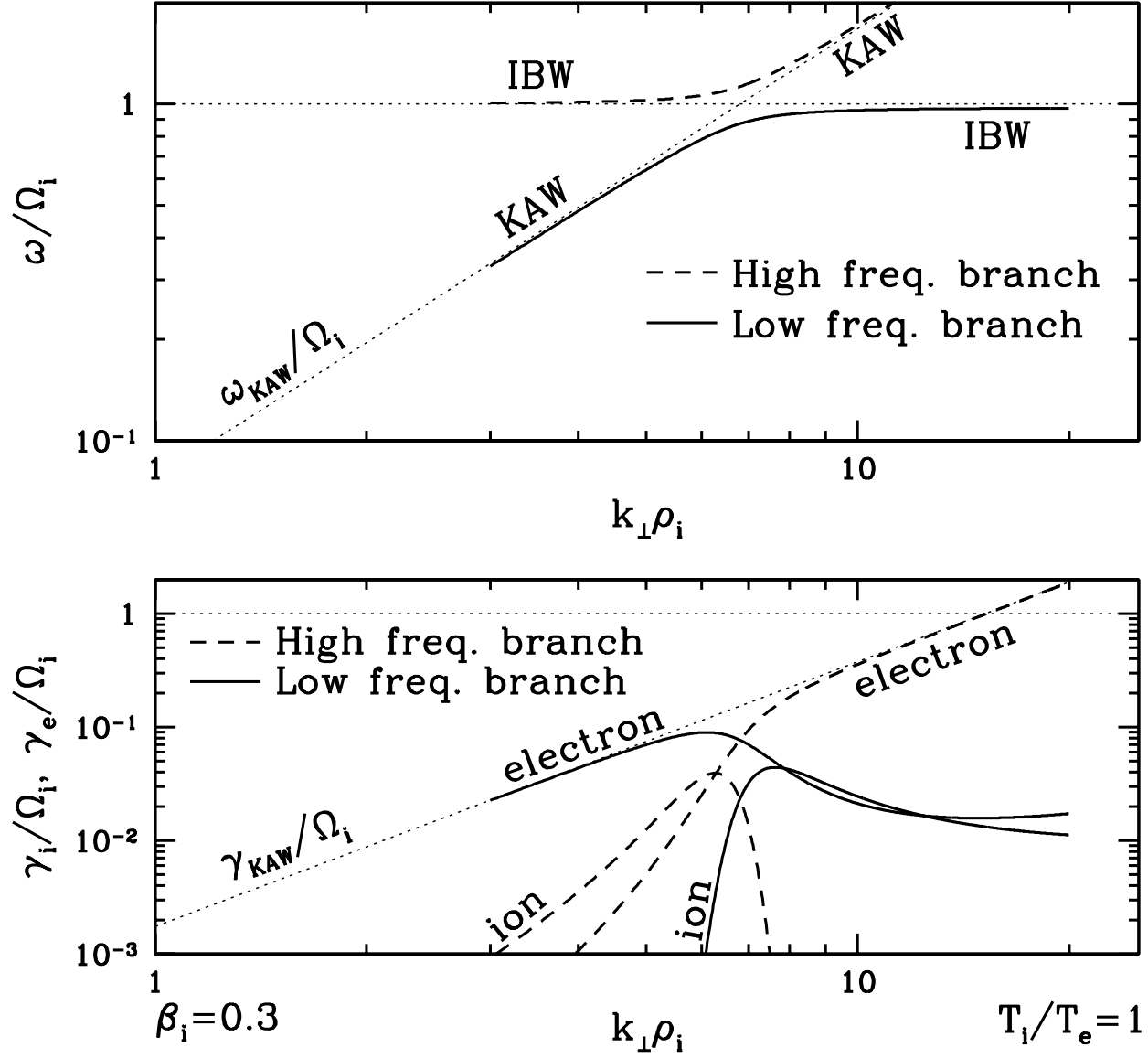


**Figure 10.** Approximate solution of the hot plasma dispersion relation illustrating the conversion between kinetic Alfvén and ion Bernstein waves (see Appendix A). Plotted in the upper panel are frequencies  $\omega/\Omega_i$  [equation (A23)] of the low- (solid) and high-frequency (dashed) branches. The characteristic wave modes along each branch are labeled as kinetic Alfvén wave (KAW) and ion Bernstein wave (IBW). Shown in the lower panel are the electron Landau damping (electron)  $\gamma_e/\Omega_i$  and ion cyclotron damping (ion)  $\gamma_i/\Omega_i$ , given by the first and second terms in equation (A26), respectively. The plasma parameters are  $\beta_i = 0.3$  and  $T_i/T_e = 1$ . The solutions are plotted along the critically balanced cascade path with  $k_{\parallel}(k_{\perp})$  given by equation (11), where  $k_0\rho_i = 10^{-4}$  and  $\bar{\omega} = \alpha$  is given by the second expression in equation (4).

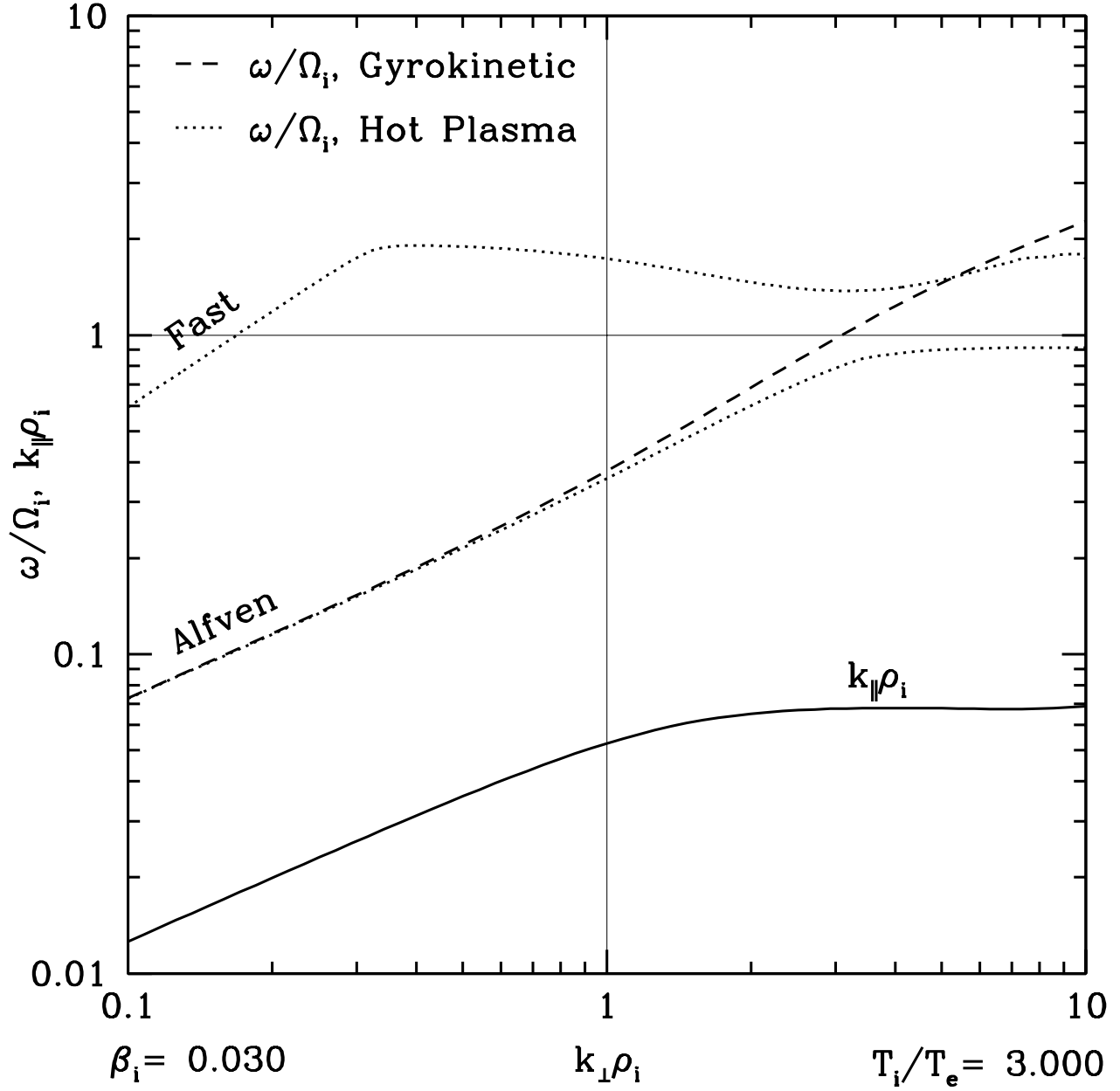


**Figure 11.** Real frequencies from the solutions of the linear gyrokinetic dispersion relation (dashed line) and the hot plasma dispersion relation (dotted line) for  $\beta_i = 0.03$ ,  $T_i/T_e = 3$ , and  $k_0\rho_i = 2 \times 10^{-4}$ . The solid line shows the path in the  $(k_{\perp}, k_{\parallel})$  plane implied by critical balance. Two branches of the hot plasma solution are shown, corresponding, in the  $k_{\perp}\rho_i \ll 1$  limit, to the MHD Alfvén wave and the MHD fast wave.

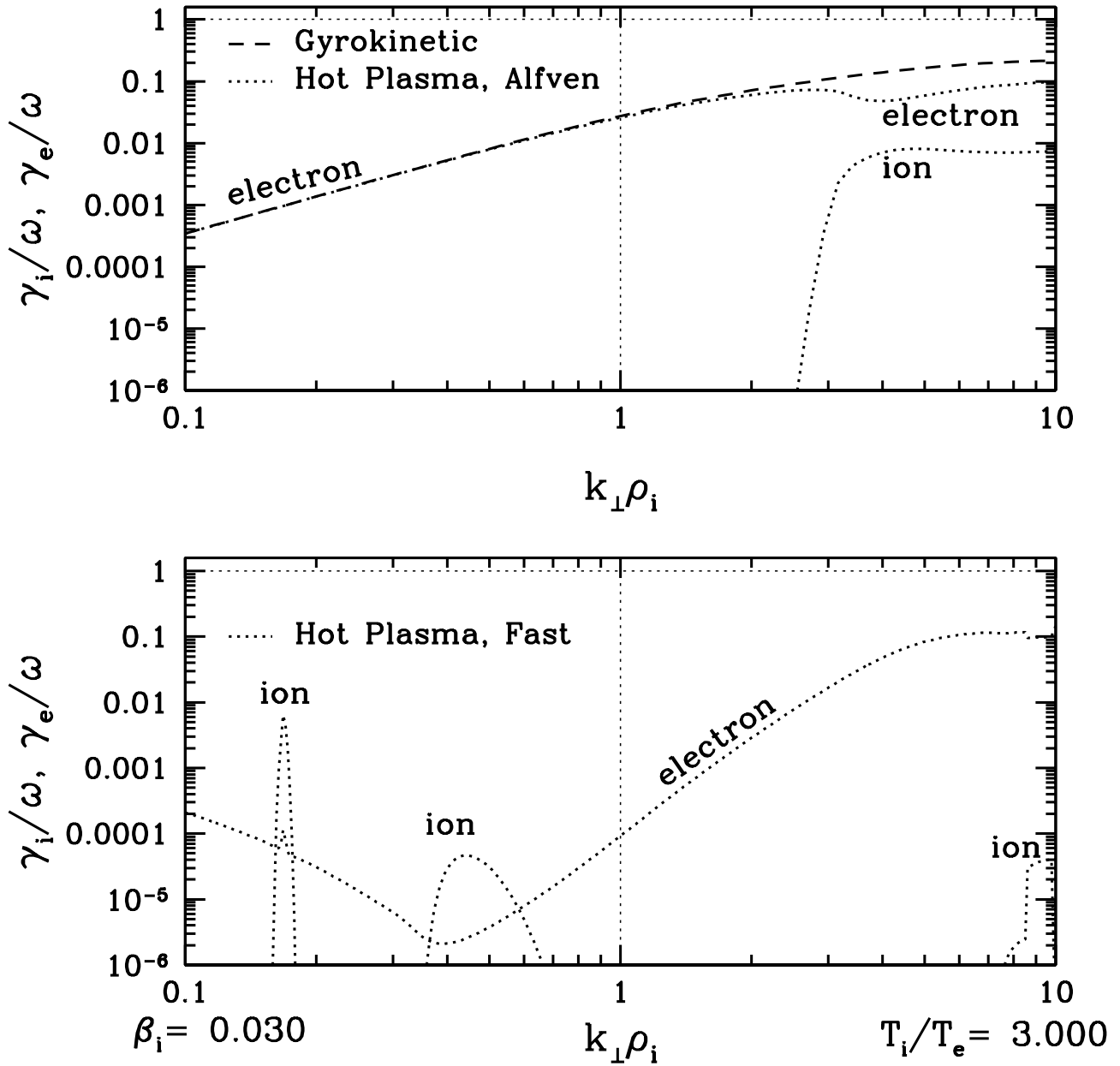


**Figure 12.** Normalized ion and electron damping rates,  $\gamma_i/\omega$  and  $\gamma_e/\omega$ , from the solutions of the linear gyrokinetic dispersion relation (dashed line) and the hot plasma dispersion relation (dotted line). In the upper panel we show the low-frequency (Alfvén) branch solutions; in the lower panel, high-frequency (fast) branch. The gyrokinetic solution shows only the electron damping—the ion damping rates are below the plotted range. For the hot plasma solutions, the contributions from ion and electron damping are labeled accordingly. These solutions are for  $\beta_i = 0.03$ ,  $T_i/T_e = 3$ , and  $k_0 \rho_i = 2 \times 10^{-4}$  and the cascade path in the  $(k_{\perp}, k_{\parallel})$  plane shown in Figure 11.

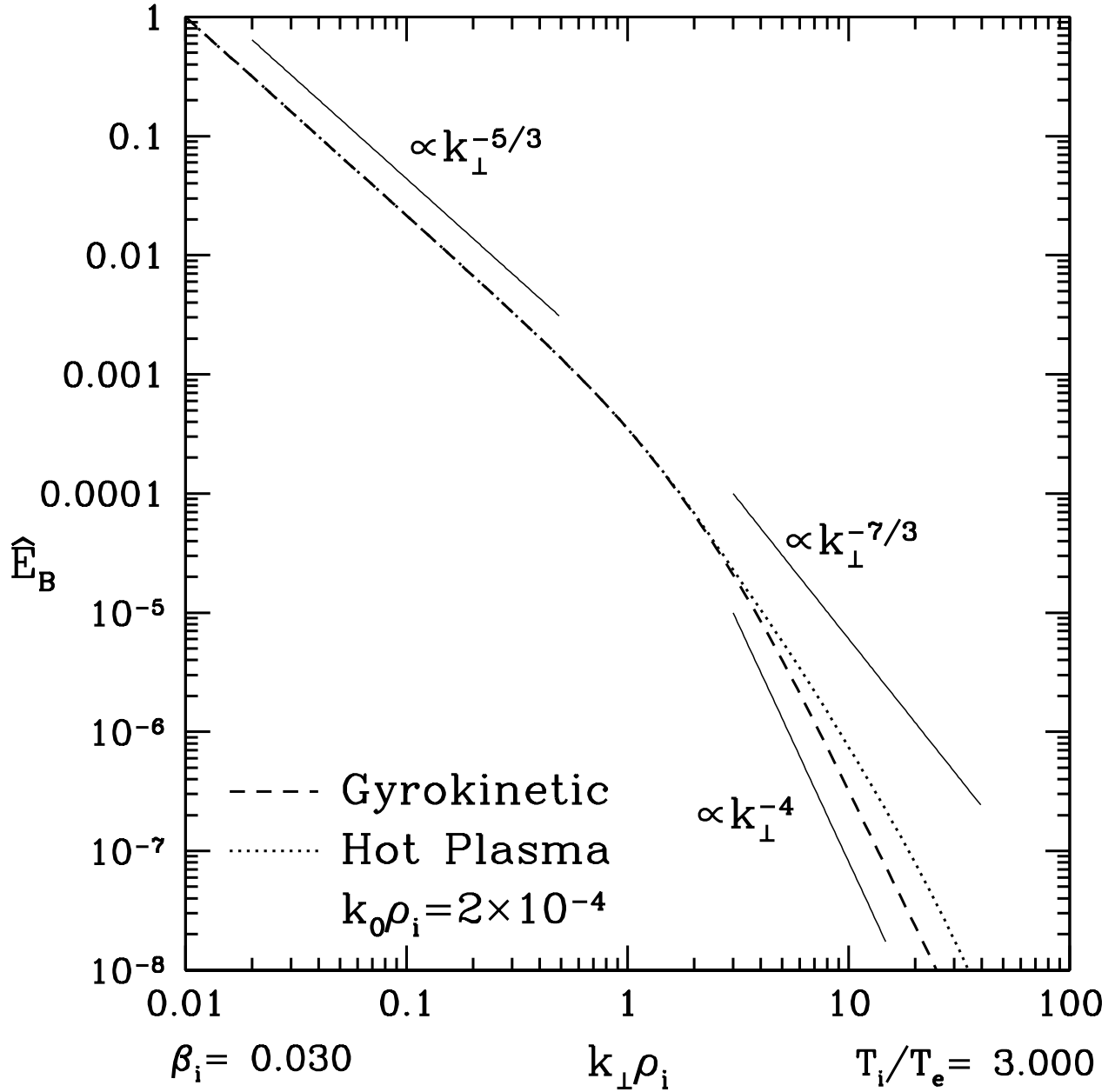


**Figure 13.** One-dimensional magnetic energy spectra for  $\beta_i = 0.03$ ,  $T_i/T_e = 3$ , and  $k_0 \rho_i = 2 \times 10^{-4}$ . Gyrokinetic and hot plasma cascade models are compared; both models show similar spectra in the kinetic regime with the effective spectral index in the dissipation range of approximately  $-4$ .

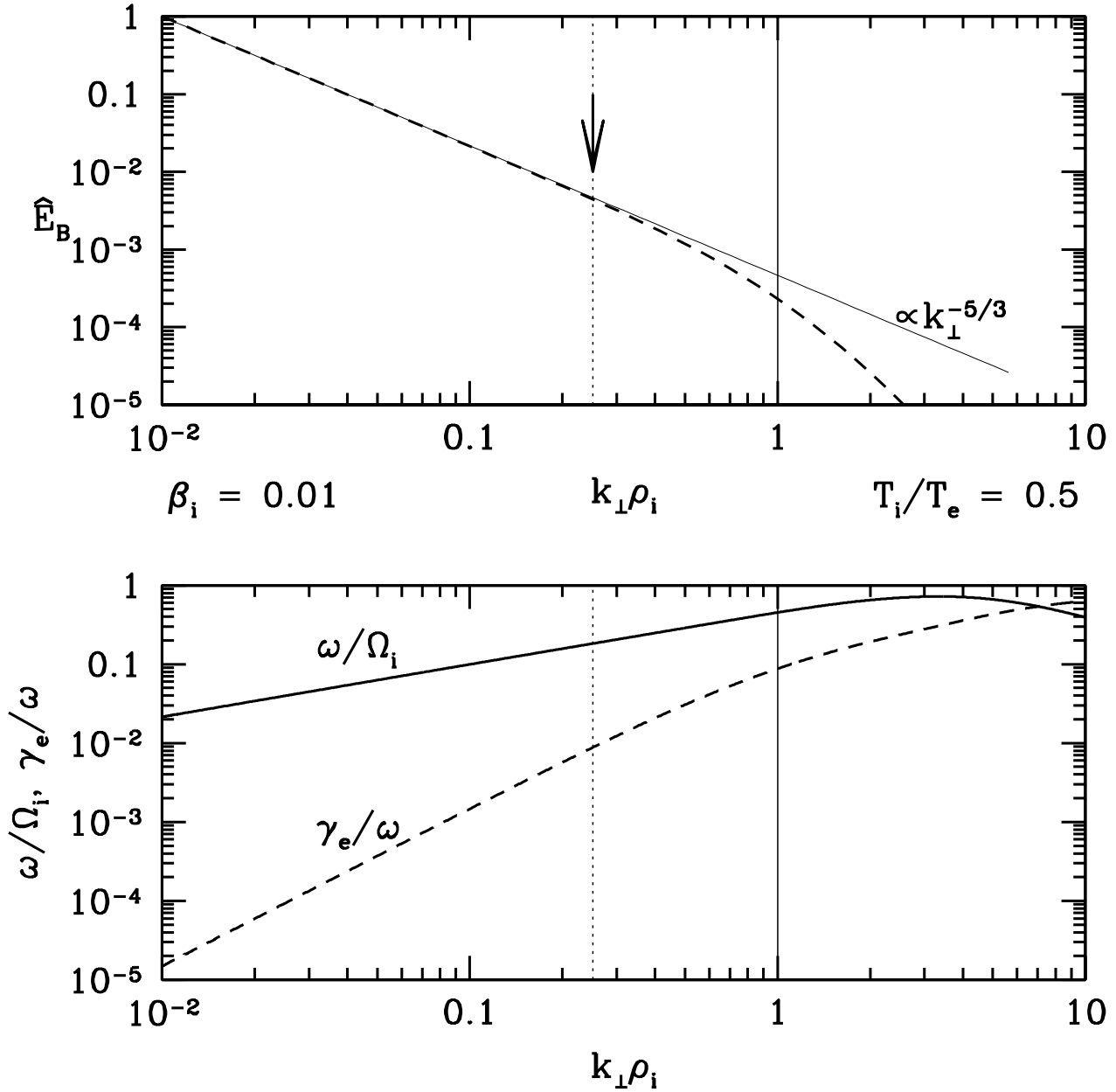


**Figure 14.** The upper panel presents the normalized one-dimensional magnetic energy spectrum using the hot plasma cascade model for  $\beta_i = 0.01$ ,  $T_i/T_e = 0.5$ , and  $k_0\rho_i = 10^{-4}$ , the parameters suitable for modeling the interval of solar wind studied by *Smith et al.* [2001]. The spectrum breaks from the  $k_{\perp}^{-5/3}$  behavior at  $k_{\perp}\rho_i \simeq 0.25$ , as indicated by the arrow. The lower panel shows the frequency of the turbulent fluctuations  $\omega/\Omega_i$  and the normalized electron damping rate  $\gamma_e/\omega$  vs.  $k_{\perp}\rho_i$ . The damping is sufficient to prevent the cascade from reaching the ion cyclotron frequency  $\Omega_i$ ; therefore, the break in the spectrum at  $k_{\perp}\rho_i \simeq 0.25$  is due to damping via the Landau resonance with the electrons.

**Table 1.** Definitions

Species	$s$
Speed of light	$c$
Mass	$m_s$
Charge	$q_s$
Number Density	$n_s$
Temperature <sup>a</sup>	$T_s$
Species Plasma Beta	$\beta_s = 8\pi n_s T_s / B_0^2$
Plasma Frequency	$\omega_{ps} = \sqrt{4\pi n_s q_s^2 / m_s}$
Cyclotron Frequency	$\Omega_s = q_s B_0 / (m_s c)$
Thermal Velocity	$v_{ths} = \sqrt{2T_s / m_s}$
Alfven Velocity	$v_A = B_0 \sqrt{4\pi n_i m_i}$
Mean Free Path	$\lambda_{mfps}$
Larmor Radius	$\rho_s = v_{ths} / \Omega_s$
Inertial Length	$d_s = c / \omega_{ps}$

<sup>a</sup> Temperature is given in energy units, absorbing the Boltzmann constant.